Higher excited states in aromatic hydrocarbon crystals

Ionization and relaxation processes

RYUZI KATOH

Higher excited states in aromatic hydrocarbon crystals
Ionization and relaxation processes

Thesis for the degree of Doctor of Science
submitted to Gakushuin University

by

RYUZI KATOH

1992

Acknowledgements

The author wishes to express his deep gratitude to Professor Masahiro Kotani in Gakushuin University for his helpful guidance, encouragement and exciting discussion throughout this work.

The author would also like to thank Professor Kikujiro Ishii in Gakushuin University and Professor Naoki Sato in Kyoto University for their encouragement and helpful discussion through this work. The author is also greatly indebted to Professor Naoki Sato for making the results of the ultraviolet photoemission measurements of trans-stilbene crystal available to me prior to publication.

The author thanks to Dr. Eizi Morikawa for his collaboration and exciting discussion in the early stage of this work and also thanks to Miss Makiko Ogiu for collaboration in measurements of external photoelectron emission.

The author is greatly indebted to Messrs. Hiroshi Miyagi, Yuji Shimokawa, Takeshi Shimazaki and Masayoshi Hamano of the machine shop of Gakushuin University for their help in constructing vacuum chambers and many small appratus used in this work.

Some of the measurements were performed at the Instrument Center in the Institute for Molecular Science (IMS). The author is obliged to the staff of the Center for their technical help.

This thesis was written principally based on the papers already published as listed below.

(1) "Observation of singlet exciton photoionization in anthracene single crystl at 2.95 eV"
R. Katoh and M. Kotani,
Chem. Phys. Lett. 166 (1990) 258.

(2) "Photoionization of singlet exciton in anthracene single crystal"
R. Katoh and M. Kotani,
Mol. Cryst. Liq. Cryst. 183 (1990) 447.

(3) "Photoemission by singlet-exciton fusion in an anthracene crystal"
R. Katoh, M. Ogiu and M. Kotani,
Chem. Phys. Lett. 174 (1990) 531.

(4) "External photoemission by singlet-exciton photoionization in an anthracene single crystal"
R. Katoh and M. Kotani,
Chem. Phys. Lett. 174 (1990) 537.

(5) "Photoionization and optical absorption of singlet excitons in a t-stilbene crystal: excitation energy dependence of the ionization efficiency"
R. Katoh and M. Kotani,
Chem. Phys. Lett. 174 (1990) 541.

(6) "Photoionization of singlet exciton in an anthracene single crystal through two-color, two-step excitation"
R. Katoh and M. Kotani,
J. Chem. Phys. 94 (1991) 5954.

(7) "Geminate electron-hole pair in an anthracene crystal. Its size and generation yield estimated from high-field measurements"
R. Katoh and M. Kotani,
Chem. Phys. Lett. 186 (1991) 210.

(8) "Photoionization of excitons in aromatic hydrocarbon crystals"
M. Kotani and R. Katoh,
in "Dynamics and Mechanisms of photoinduced transfer and related phenomena" eds. N. Mataga, T. Okada and H. Masuhara. (Elsevier, 1992) p425.

(9) "Autoionization of higher excited states generated by two-photon absorption in p-terphenyl crystal"
R. Katoh and M. Kotani,
Chem. Phys. Lett. 188 (1992) 80.

(10) "Excitonic photoemission in organic crystals"
R. Katoh and M. Kotani,
Mol. Cryst. Liq. Cryst. 218 (1992) 91.

(11) "Time profiles and action spectra of double-quantum photoemission in perylene and naphthacene films"
R. Katoh and M. Kotani,
Chem. Phys. Lett. 196 (1992) 103.

(12) "Fission of higher excited state generated by singlet exciton fusion in an anthracene crystal"
R. Katoh and M. Kotani,
Chem. Phys. Lett. 196 (1992) 108.

(13) "Observation of fluorescence from higher excited states in an anthracene crystal"
R. Katoh and M. Kotani,
Chem. Phys. Lett. 201 (1993) 141.

Contents

1 Introduction

When aromatic hydrocarbon crystal are irradiated with light, various phenomena, such as conversion to heat, emission of fluorescence, photoconduction and external electron emission, can be observed. In this work such a relaxation processes from higher excited states will be discussed in detail.

Figure 1.1 shows a kinetic scheme for the states which are discussed in this work. Higher excited states are generated by fusion of two singlet excitons or photoionization of singlet exciton. External photoemission by singlet exciton fusion is observed (§ 3.3). Two relaxation processes from higher excited state generated by fusion are observed, i.e., fiision into two triplet excitons (§ 7.2) and fluorescence emission from higher excited states (§ 7.3). Photoabsorption of singlet and triplet excitons can be measured by means of pump-and-probe method (§ 4.3). External photoelectron emission (§ 3.4) and photoconductivity (§ 5) due to photoionization of singlet exciton can be observed. External photoemission from conduction band can also be observed (§ 3.5).

Both external photoelectron emission and photoconduction can be deeply related with photoionization processes in a condensed phase. Ionization efficiency can be obtained as a function of excitation energy. Photoionization of a molecule in aromatic hydrocarbon crystals can be discussed (§ 6).

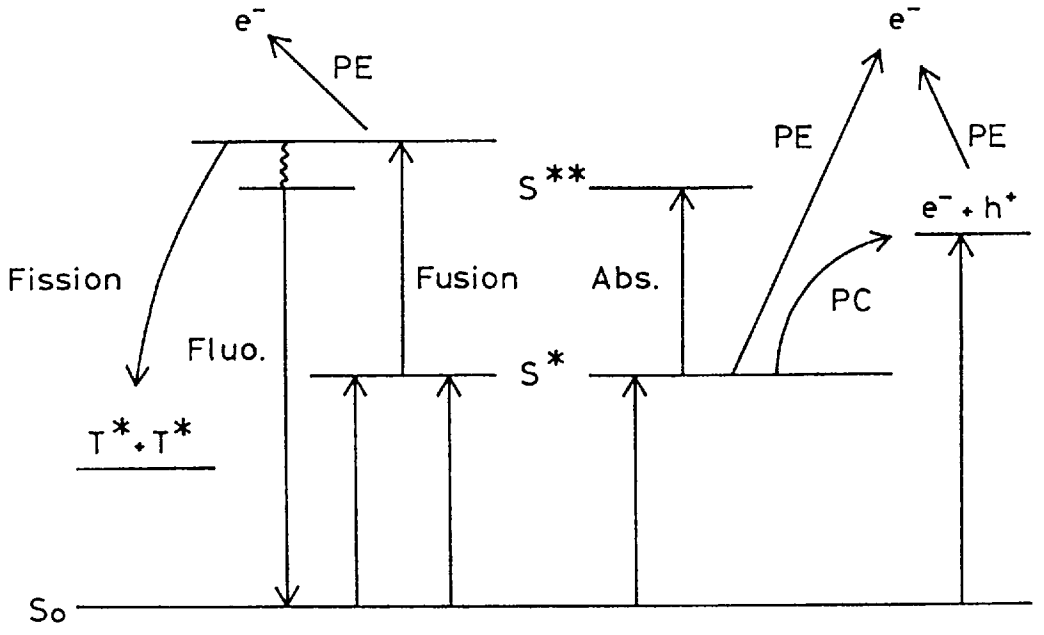

Fig. 1.1 Kinetic scheme for the states which are discussed in this work. S*: singlet exciton, T*: triplet exciton, S**: higher excited state, PE: photoelectron emission, PC: photoconductivity.

1.1 Higher excited states in aromatic hydrocarbon crystals

Higher excited states play an important role in ionization and photochemical processes. Recently, higher excited states of a molecules in a gas phase have been actively studied using synchrotron radiation and high-power lasers. However, only a few studies have been made with organic crystals.

It can be expected that the behavior of higher excited states in organic crystals is very different from that in the gas phase. The excited states can migrate and, as a result, they react with other elementary excitations, such as singlet and triplet excitons, phonon and charge carriers.

Ionization process may be also different in different phases, because inelastic scattering and electron capture can occur by surrounding molecules. Stabilization of ionic species by electronic polarization is also important. Ionization processes of molecules in a condensed phase cannot be understood. To clarify the processes is a fundamental problem for photochemistry and radiation chemistry.

Charge carrier generation in organic crystals is closely related to the primary processes of photosynthesis. Organic photoconductors are widely used as photosensitive materials in recording and copying. Understanding the mechanism of photoconductivity in organic crystals is important not only as a basic science, but also in application.

1.2 Generation and decay kinetics of higher excited states in aromatic hydrocarbon crystals

Figure 1.2 shows absorption spectra of anthracene in solution and in crystal [1.1]. The spectra in both phases are similar to each other. This similarity indicates that electronic states of a molecule are essentially preserved in the crystalline state. A small energy shift present is due to the difference in solvation energy between the solution and the crystal. Absorption spectrum in crystal depends on the light polarization. The splitting, which is known as the Davydov splitting [1.1], is due to the interaction between molecules at different sites within the same unit cell of the crystal. The lowest singlet excited state has a lifetime of the order of 10^{-8} sec and returns to the ground state by emission of fluorescence. Figure 1.3 shows the scheme for the optical transition from the ground state S_0 to the lowest singlet excited state S_1 using a molecular orbital of π -electron.

Excited states can move in a crystal as an exciton. In organic crystals this can be confirmed by studying sensitized luminescence. When a small amount of a guest compound is doped in a host crystal which has higher energy than the guest compound, an efficient fluorescence emission from the guest molecule can be observed. This can be understood in terms of an energy transfer from the host molecules to the guest molecules. Sensitized fluorescence has been studied in numerous systems, such including naphthalene [1.2].

Excitons can interact with each other within their lifetime.

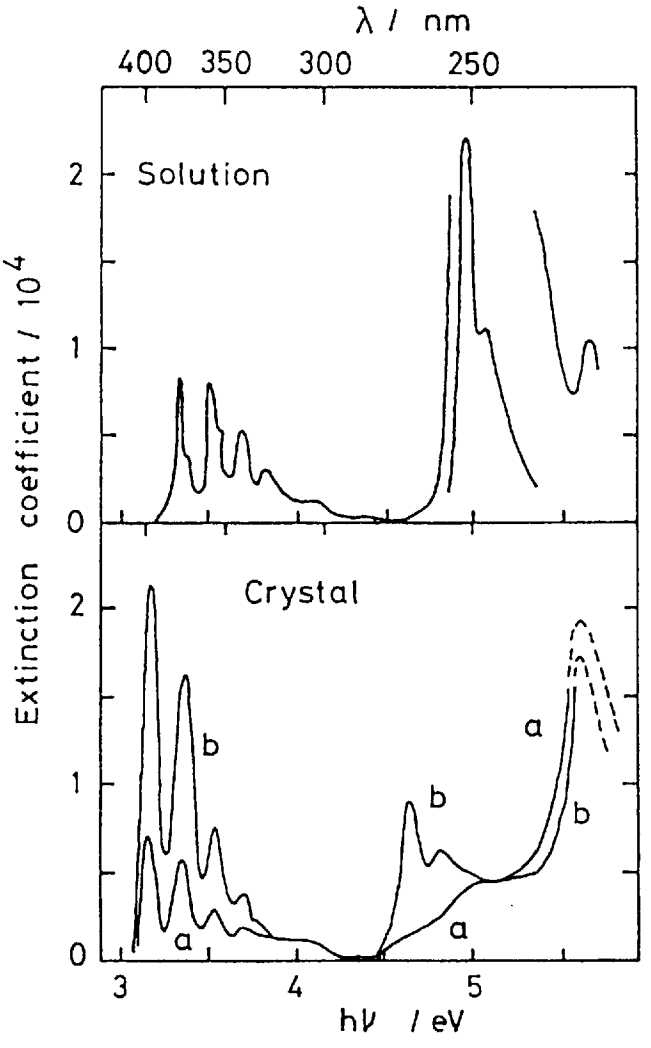

Fig. 1.2 Absorption spectra of anthracene in solution and in crystal.

This process is called exciton fusion (annihilation). When two excitons encounter, one exciton is promoted to a higher excited state, which has twice the energy of the original exciton, and the other returns to the ground state. Fusion of two singlet excitons in the crystal has been studied with many compounds, such as anthracene [1.3]. Fusion of triplet excitons has been studied through measurements of delayed fluorescence [1.4].

Energy levels of higher excited states can be determined by optical absorption. Number density of molecules in organic crystals is very high so that ultra-thin flakes are needed to measure the optical absorption when the transmission is to be measured. In spite of the experimental difficulties optical absorption has been measured with many organic crystals up to 6 eV [1.5-7]. In the energy range of VUV only a few studies have been made. Hino et al. have measured the absorption spectra of some aromatic hydrocarbon crystals [1.8]. Koch and Otto have measured the reflection spectra in an anthracene crystal by using synchrotron radiation [1.9]. Higher excited states exhibit larger Davydov splitting than the lowest excited state. Relaxation from higher excited states is very fast.

1.3 Energy levels of ionized states (Polarization model)

According to the Koopmans theorem, the orbital energy of the highest occupied molecular orbital (HOMO) is equal in magnitude and opposite in sign to the ionization potential $I_P(g)$. In the same way the electron affinity $E_A(g)$ can be evaluated from the orbital energy of the lowest unoccupied molecular orbital (LUMO)

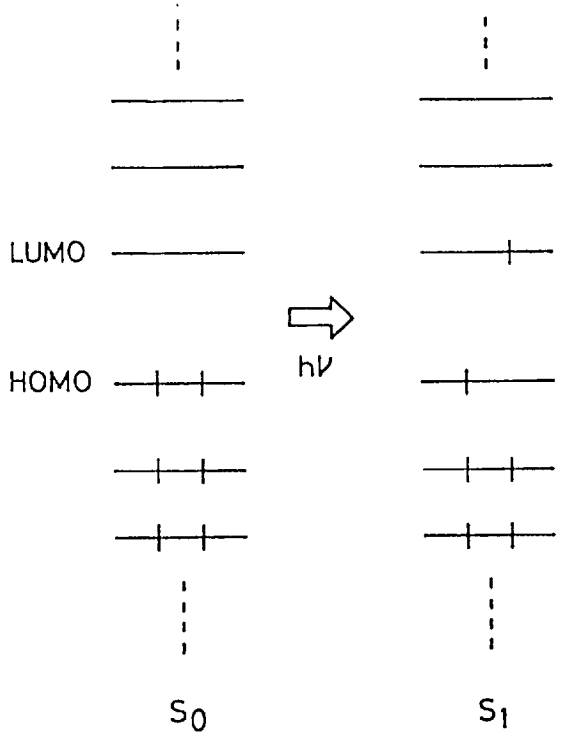

Fig. 1.3 Transition from the ground state (S_0) to the lowest excited state (S_1).

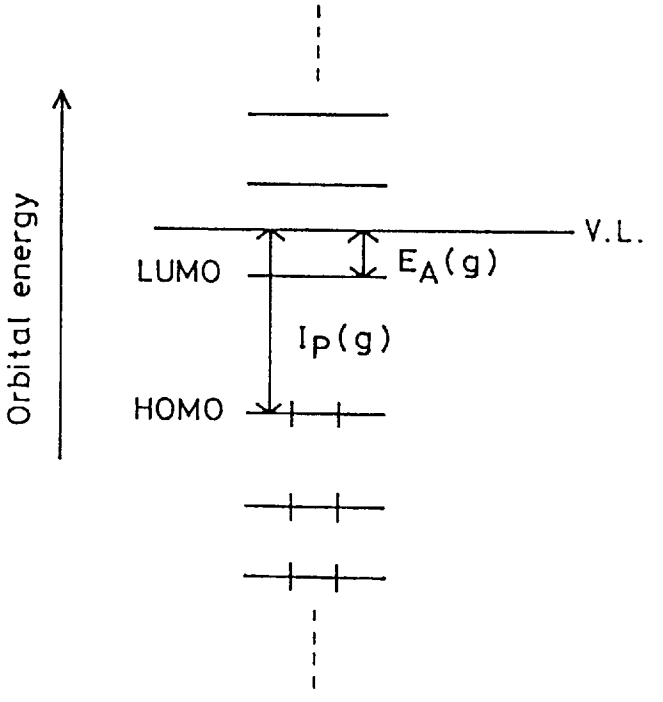

Fig. 1.4 Ionization potential ($I_P(g)$) and electron affinity ($E_a(g)$).

(Fig.1.4). The ionization potential of a gas molecule can be determined precisely through photoelectron spectroscopy and absorption spectroscopy in the Rydberg range. On the other hand, determination of electron affinity of a gas molecules is generally more difficult [1.10-11].

Photoionization in a solid can be regarded as a transition from the valence band to the conduction band. This band model is widely used in solid state physics and is valid for many inorganic semiconductors, where electrons are delocalized. On the other hand, molecular crystals, such as many organic crystals and rare gas solids, are insulators and electrons are tightly bounded within molecules. For this class of materials the band model is not a good approximation and photoconductivity can be explained better as photoionization of a molecule in the medium which consists of the same kind of molecules as the ionized one.

Ionization potential in a condensed phase can be estimated using the polarization energy induced by a cation and an anion and electron affinity of the surrounding molecule. Lyons introduced this consideration to explain the ionization potential of organic crystals, which is called polarization model [1.12]. Silinsh et al. modified this model [1.13]. Recently, Sato et al. discussed the polarization model in detail based on the experimental findings [1.14]. The polarization energies were calculated theoretically by the methods of self-consistent polarization field [1.13] and the Fourier-transformed lattice multipole sums [1.15]. Figure 1.5 shows ionization potential and electron affinity in a solid using the polarization model, compared with those of an isolated molecule.

External photoelectron emission occurs above an energy E_{th}. In this case only the polarization energy for a cation can contribute to the decrease in the ionization potential. Hence, this energy can be expressed by

$$E_{th} = I_P(g) - P_+, \qquad (1.1)$$

where $I_P(g)$ is the ionization potential of the molecule in the gas phase and P_+ is the energy due to electronic polarization induced in the medium surrounding a cation. Threshold energies E_{th} for external photoemission can be determined from ultra-violet photoelectron spectroscopy (UPS) and P_+ can be evaluated by comparing the ionization potential of a molecule in the gas phase with that in the crystal. Sato et al. have made a systematic study of polarization energy due to a positive charge in an organic crystal through UPS study [1.17]. Polarization energies P_+ determined experimentally are in good agreement with the calculated values.

Ionization potential of a crystal E_G, which is sometimes referred to as the band gap, can be expressed by

$$E_G = I_P(g) - P_+ - P_- - E_A(g), \qquad (1.2)$$

where $E_A(g)$ is the electron affinity of the molecule in the gas phase. The band gap can be estimated through photoconductivity study. However, only a few studies have been made in aromatic hydrocarbon crystals [1.13]. The band gap can be also estimated through measurements of electronic absorption to charge transfer states [1.17]. Threshold energies observed for the external photoemission and band gaps agree roughly with the value expected from the polarization model. This indicates that the polarization model is valid for this class of materials.

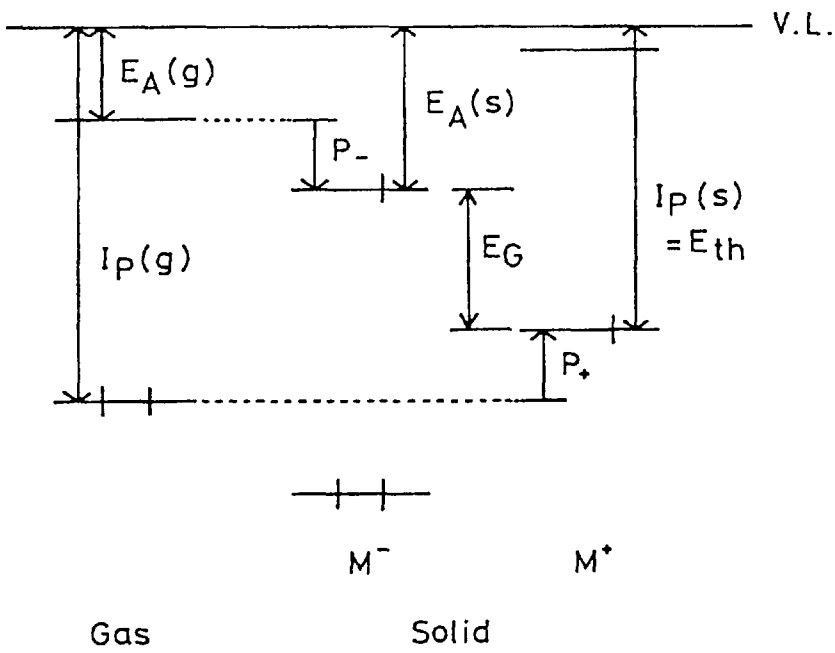

Fig. 1.5 Polarization model.

E_A: electron affinity in gas phase (g) and in solid (s), I_P: ionization potential in gas phase (g) and in solid (s), P_+, P_-: polarization energy, E_G: band gap, E_{th}: threshold energy for external photoemission.

In organic crystals ion pair states can also exsist. They are called charge transfer (CT) excitons. A CT exciton is a neutral state formed between a cation and an anion in a crystal, which are bound by the Coulomb interaction. Figure 1.6 shows CT transitions from a π -electron orbital of a molecule. This is analogous to a Rydberg state in the gas phase. The energy to which the energy of the CT states converges gives the optical band gap. According to electrostatics, energy of a CT state, in which the separation between a cation and an anion is r_{CT}, can be written as

$$E_{CT}=E_G-(e^2/4\pi\ \varepsilon\ \varepsilon_0\ r_{CT}), \qquad (1.3)$$

where ε is the dielectric constant of the medium. Absorption coefficient of a CT transition is small in aromatic hydrocarbon crystals (10^{-4} cm^{-1}), and accordingly CT states have been detected only with a sensitive modulation technique. The CT state has a much larger dipole moment compared to the ground state and, accordingly, a CT absorption is expected to be sensitive to an external electric fields. Abbi and Hanson demonstrated that this was indeed the case with 9,10-dichroloanthracene [1.18]. Sebastian et al. have measured transitions to CT states in anthracene [1.17] and in naphthacene and pentacene [1.19] using the same technique. Tokura et al. have observed CT states in Copper phthalocyanine [1.20]. They could observe the CT bands directly in reflection, and detected a change of these bands by applying an electric field. Takase and Kotani have also reported a direct observations of CT absorption in a phenothiazine crystal at 15K, which is very sensitive to an electric field [1.21]. In naphthacene absorption coefficient of a CT transition is small [1.19]. However, under a pressure of

>10kbar the CT absorption becomes much stronger and can be observed clearly [1.22]. The relation between photoconductivity and charge transfer absorption has been discussed by Bounds and Siebrand [1.23] and Petelenz and Mucha [1.24].

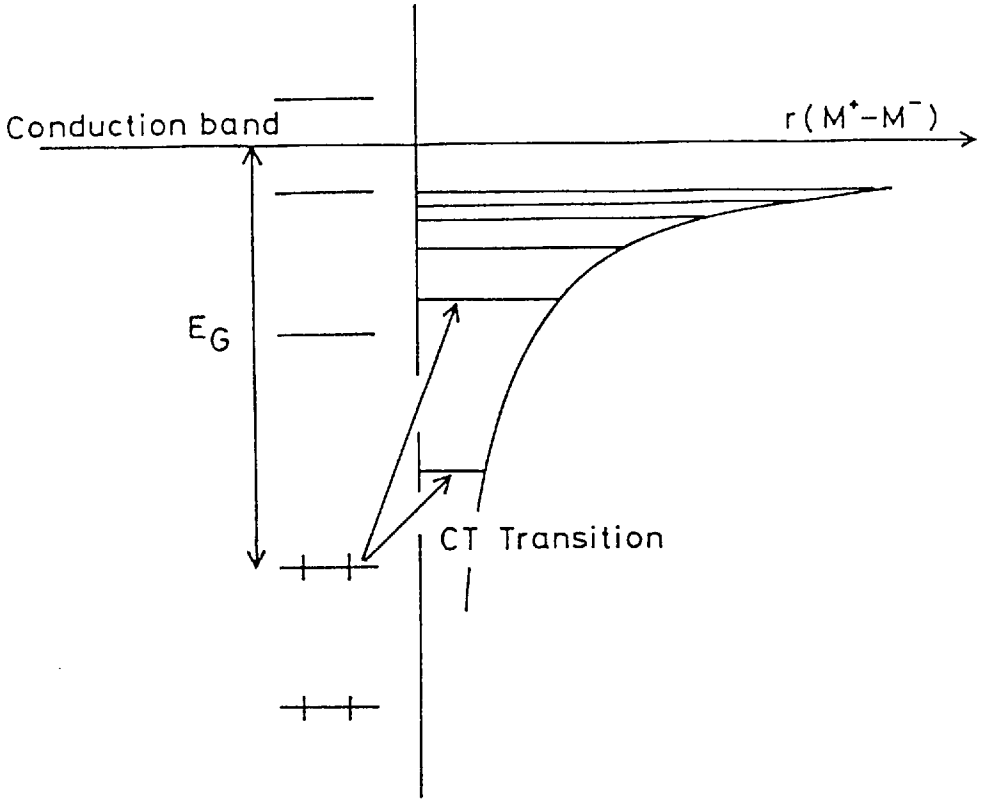

Fig. 1.6 Charge transfer transition.

References

[1.1] W.J.Moore,
"Seven Solid States" (W.A.Benjamin Inc., New York, 1967).

[1.2] H.Auweter, U.Mayer and D.Schmidt,
Z. Naturforsch 33a (1978) 651.

[1.3] A.Braun, U.Mayer, H.Auweter, H.C.Wolf and D.Schmidt,
Z. Naturforsch 37a (1982) 1013.

[1.4] R.C.Johnson and R.E.Merrifield,
Phys. Rev. B1 (1970) 896.

[1.5] D.P.Craig and P.C.Hobbins,
J. Chem. Soc. (1955) 539.

[1.6] L.B.Clark and M.R.Philpott,
J. Chem. Phys. 53 (1970) 3790.

[1.7] J.Tanaka,
Bull. Chem. Soc. Jpn. 38 (1964) 86.

[1.8] S.Hino, T.Veszpremi, K.Ohno, H.Inokuchi and K.Seki,
Chem. Phys. 71 (1982) 135.

[1.9] E.E.Koch and A.O.Otto,
Chem. Phys. 3 (1974) 370.

[1.10] E.C.M.Chen and W.E.Wentworth,
Mol.Cryst.Liq.Cryst. 171 (1989) 271.

[1.11] P.Kebarle and S.Chowdhury,
Chem. Rev. 87 (1987) 513.

[1.12] L.E.Lyons,
J.Chem.Soc. (1957) 5001.

[1.13] E.A.Silinsh,
"Organic Molecular Crystals. Their electronic properties"
(Springer, Berlin, 1980).

[1.14] N.Sato, H.Inokuchi and E.A.Silinsh,
Chem.Phys. 115 (1987) 269.

[1.15] P.J.Bounds and R.W.Munn,
Chem.Phys. 44 (1979) 103.

[1.16] N.Sato, K.Seki and H.Inokuchi,
J.Chem.Soc.Faraday Trans 2 77 (1981) 1621.

[1.17] L.Sebastian, G.Weiser, G.Peter and H.Baessler
Chem.Phys. 75 (1983) 103.

[1.18] S.C.Abbi and D.M.Hanson,
J.Chem.Phys. 60 (1974) 319.

[1.19] L.Sebastian, G.Weiser and H.Baessler,
Chem.Phys. 61 (1981) 125.

[1.20] Y.Tokura, T.Koda, Y.Iyechika and H.Kuroda,
Chem.Phys.Lett. 102 (1983) 174.

[1.21] T.Takase and M.Kotani,
J.Chem.Phys. 90 (1989) 2134.

[1.22] K.Mizuno, A.Matsui and G.J.Sloan,
Chem.Phys. 131 (1989) 423.

[1.23] P.J.Bounds and W.Siebrand,
Chem.Phys.Lett. 75 (1980) 414.

[1.24] P.Petelenz and D.Mucha,
Chem.Phys. 154 (1991) 145.

2. Sample preparation

2.1 Introduction

Optical and electronic properties of a solid are sensitive to the presence of inpurities and structural defects. Purification and characterization of purity are important for measuring such properties. In organic crystals dielectric properties are very often anisotropic and a proper orientation should be maintained when a measurement is to be made of a crystal.

2.2 Purification of crystals and crystal growth

Commercial materials of anthracene, p-terphenyl, trans-stilbene and α -perylene were purified by extensive zone refining. A pyrex tube containing the material to be purified was sealed off with 200 Torr argon. After $\sim$ 200 zone passes, the middle portion of the material was transferred to a new tube for futher zone refining. The final zone refining step was done using a zone refining tube equipped with a breakable seal. After the final zone refining step, the breakable seal was opened under vacuum and the middle part of the purified material was transferred by sublimation to a connected ampoule for the Bridgman crystal growth. Single crystals were grown from the melt by the Bridgman method. Cleaved ingots were used as sample specimens without polishing. Naphthacene was purified by vacuum sublimation and evaporated films, $\sim$ 100Å thick, were used for measurements.

2.3 Orientation of sample specimens

Three methods, i.e. double refraction, fluorescence polarization and x-ray diffraction, were used to orient sample specimens. Double refraction was used for determination of crystal axes of anthracene and p-terphenyl. In the case of anthracene polarization ratio of fluorescence was also used [2.1]. The Laue X-ray diffraction, aided by computer simulation, was used to orient sample specimens of trans-stilbene. The crystal structure data of trans-stilbene are found in Ref. 2.2.

2.4 Characterization of purity

Characterization of purity was made by inspection of fluorescence spectra and current shape of pulsed photoconductivity. Both are very sensitive to the presence of inpurities and defects [2.3]. When singlet excited state of an impurity molecule has a lower energy than that of a host crystal, singlet excitons of the host crystal are captured effectively by impurities. Hence, fluorescence of the host crystal is reduced and guest molecules emit fluorescence efficiently. The lifetime of the host fluorescence is also reduced. Such a sensitized fluorescence has been studied extensively. Figure 2.1 shows part of fluorescence spectrum of p-terphenyl crystal where a small (1×10^{-6} mol/mol) concentration of a dopant (naphthacene) can be seen. Figure 2.2 shows the temporal behaviour of the fluorescence. The decay time of the host fluorescence decreases

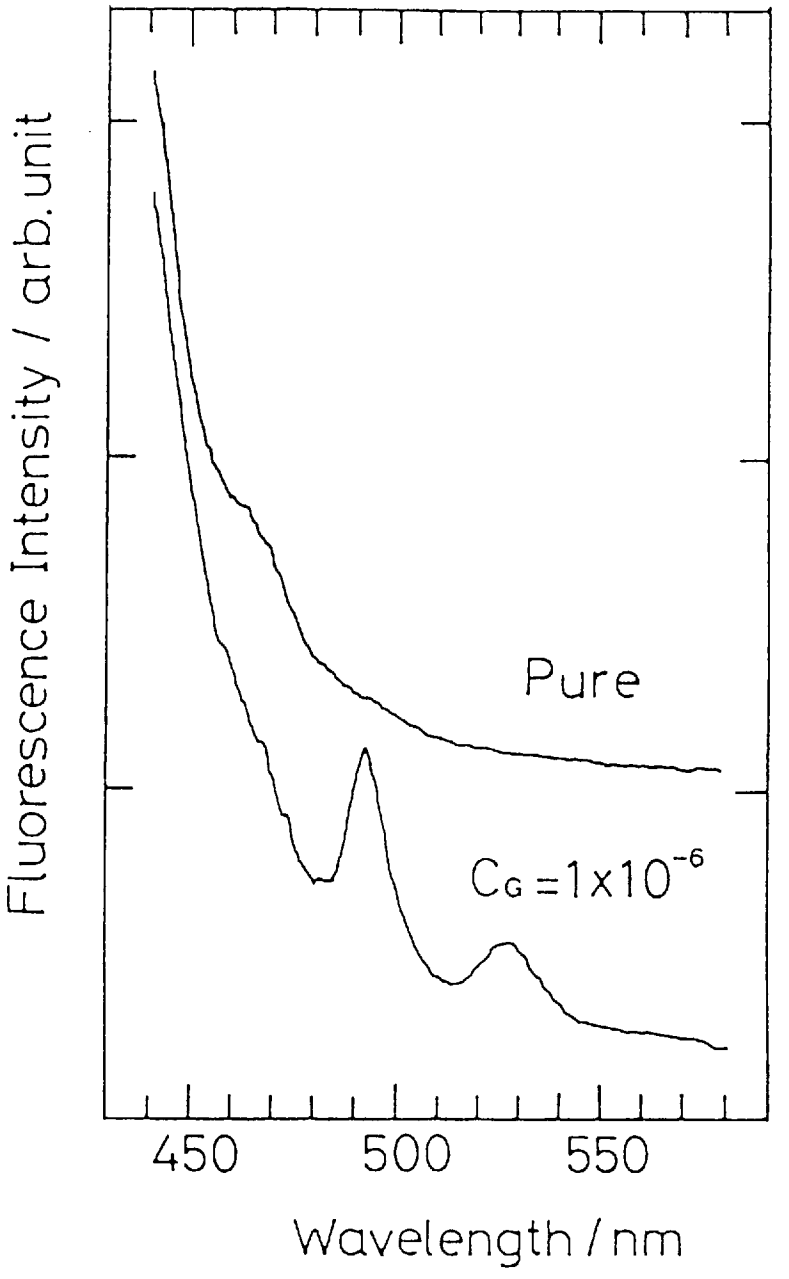

Fig. 2.1 Fluorescence spectra of doped (naphthacene) and undoped p-terphenyl crystal in the range of guest fluorescene.

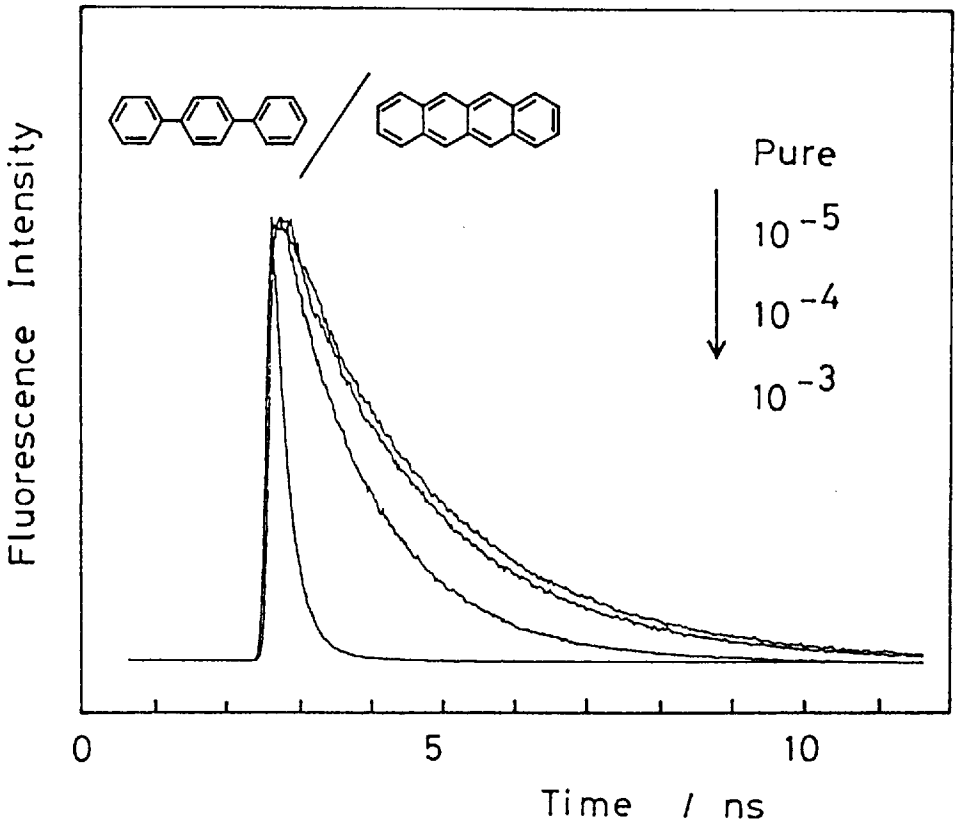

Fig. 2.2 Temporal behavior of the fluorescence of p-terphenyl crystal undoped (pure) and doped with naphthacene (10^{-3}, 10^{-4} and 10^{-5} mol/mol).

with increasing guest concentration.

When charge carriers are generated near the surface of a sample specimen of a high purity, the current pulse exhibits a rectangular form (Fig. 2.3(a)). When deep traps which capture charge carriers are in the crystal, the photocurrent decreases gradually during the drift of the charge carriers across the sample (Fig. 2.3(b)). Photocurrent waveforms observed with anthracene, p-terphenyl and trans-stilbene crystals, used throughout this work, are shown in Fig. 2.4. They do not indicate the presence of any detectable impurities except for trans-stilbene. In the case of trans-stilbene a photocurrent due to mobile electrons could not be measured. This may be due to the efficient trapping of electrons by impurities.

X-ray diffraction has been used extensively to determine the crystal structure and the crystal axis. Defects produced by X-ray irradiation may affect some electric and optical properties. Such a radiation damage has been studied through optical absorption [2.4], lifetime of delayed fluorescence [2.5] and ESR [2.6]. Figure 2.5 shows a change in the waveforms of photocurrent by irradiation with X-ray of an anthracene crystal. This indicates that many deep traps can be generated in the bulk of a crystal by X-ray irradiation. To avoid such the damage by radiation X-ray diffraction was not used before electrical measurements. The defects can act as traps not only for charge carriers, but also for singlet and triplet excitons.

The surface of an organic crystal is inactive compared with that of an inorganic semiconductor. Hence, influence of the

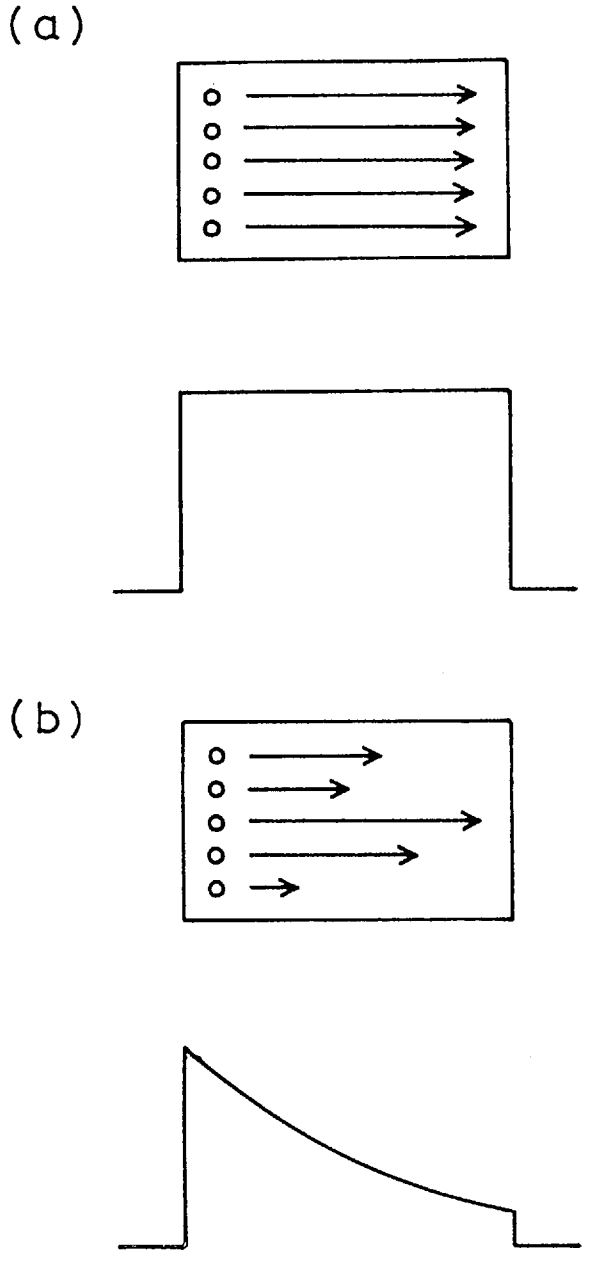

Fig. 2.3 Expected photocurrent waveforms. (a) No traps (b) Deep trapping case.

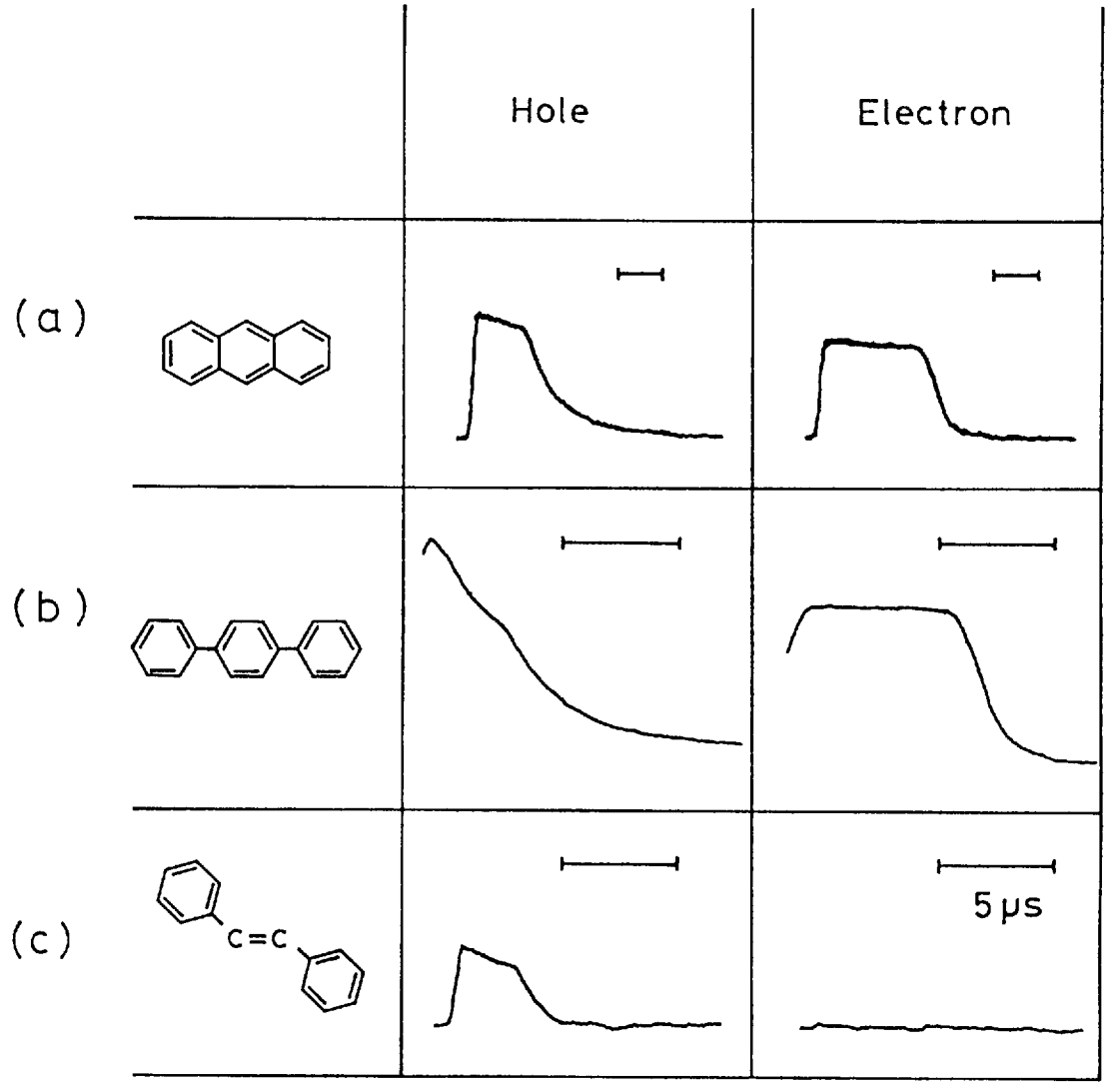

Fig. 2.4 Typical waveforms of photocurrent in (a) anthracene, (b) p-terphenyl and (c) trans-stilbene crystals.

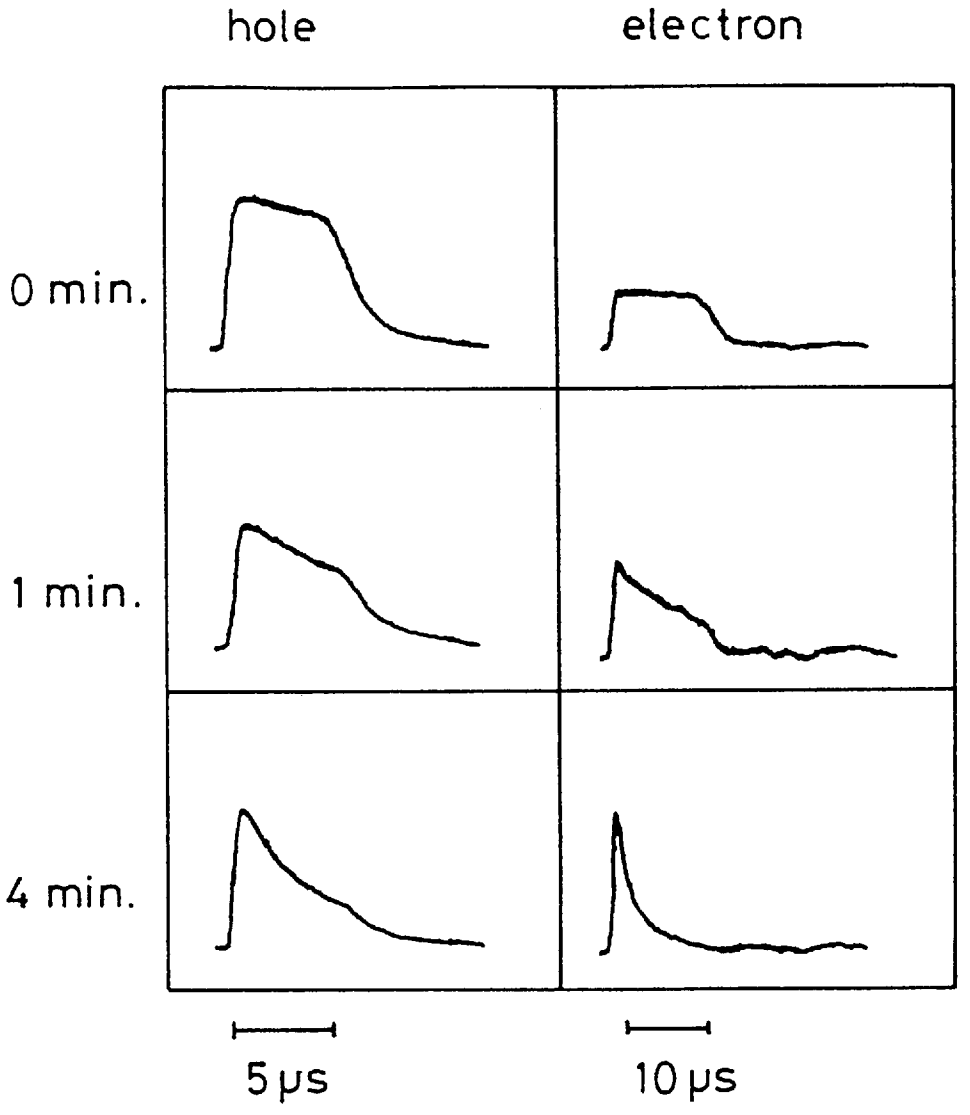

Fig. 2.5 The damage by X-ray irradiation detected by photocurrent waveforms.

surface on electrical properties is usually not a serious problem. Only a small effect can be detected. When an anthracene crystal is exposed to air for several weeks, charge carrier (hole) generation at the surface can be observed by excitation with a visible light. This photocurrent is proportional to the intensity of the exciting light. When the sample specimen is cleaved again, this photocurrent can be reduced. This suggests that the current is due to the hole injection from an oxidation layer formed at the surface [2.7].

References

[2.1] C.D.Akon and D.P.Craig,
Trans. Faraday Soc.62 (1966) 1673.

[2.2] C.J.Finder, M.G.Newton and N.L.Allinger,
Acta Cryst.B 30 (1974) 411.

[2.3] N.Karl,
J. Cryst. Growth 51 (1981) 509.

[2.4] K.Nakagawa and N.Itoh,
Chem. Phys. 16 (1976) 461.

[2.5] K.Yokoi and Y.Ohba,
Oyo Butsuri 47 (1978) 649.

[2.6] N.Itoh and T.Okuba,
Mol. Cryst. Liq. Cryst. 17 (1972) 303.

[2.7] G.Dietrich, H.Pick and H.Bauser.
Chem. Phys. Lett. 33 (1975) 257.

3. External photoelectron emission via excited state

3.1 Introduction

External photoelectron emission via excited states has proved to be useful in understanding the dynamics of excited states of molecules in the gas phase. This technique may be also applicable to solid state. Several studies have been reported on inorganic semiconductors [3.1-2] and metals [3.3]. With organic solids only a few studies have been made on photoemission involving excited states.

Pope et al. made the first observation of the double-quantum photoelectron emission from an anthracene micro-crystal using the Millikan chamber technique [3.4]. Pott and Williams [3.5], and Haarer and Castro [3.6] measured the double-quantum photoemission from anthracene crystals using a conventional vacuum chamber with a steady state light source. From the similarity between the action spectrum of the photoemission and the absorption spectrum such double-quantum photoemission was ascribed to singlet exciton fusion. In an anthracene crystal the energy of a higher excited state generated by singlet exciton fusion, which has twice the energy of an original singlet exciton, exceeds the threshold energy for external photoemission. Hence, the photoemission by singlet exciton fusion is energetically possible.

External photoemission by photoionization of some excited states, such as singlet and triplet excited states and ionized states, has been reported. Salaneck et al. measured the photoemission through excited states in trans-polyacetylene

[3.7]. In this study a steady-state light source was used combined with a pulsed laser. Koch used synchrotron radiation instead of a discharge lamp. He obtained a photoelectron spectrum through triplet excited states in a Cu-phthalocyanine film [3.8]. Munakata and Kasuya have used two lasers, one in the VUV and the other in the visible, and observed photoemission from triplet excited state in Cu-phthalocyanine films [3.9]. Wautelet et al. have reported photoemission of conduction electrons in a β -carotene crystal [3.10]. Photoemission involving a charge transfer state as an intermediate state has been reported by Pope and co-workers [3.11].

In this chapter external photoemission via excited states will be presented. Three types of photoemission are studied;
(a) Photoemission by photoionization of singlet exciton,
(b) Photoemission by singlet exciton fusion (annihilation),
(c) Photoemission of conduction electron.
Energy scheme for these modes are shown in Fig. 3.1. Mode (a) was observed in anthracene, p-terphenyl and naphthacene crystals and mode (b) was observed in anthracene and α -perylene crystals. In the case of perylene and naphthacene crystals the photoemission of conduction electrons (mode (c)) could be observed.

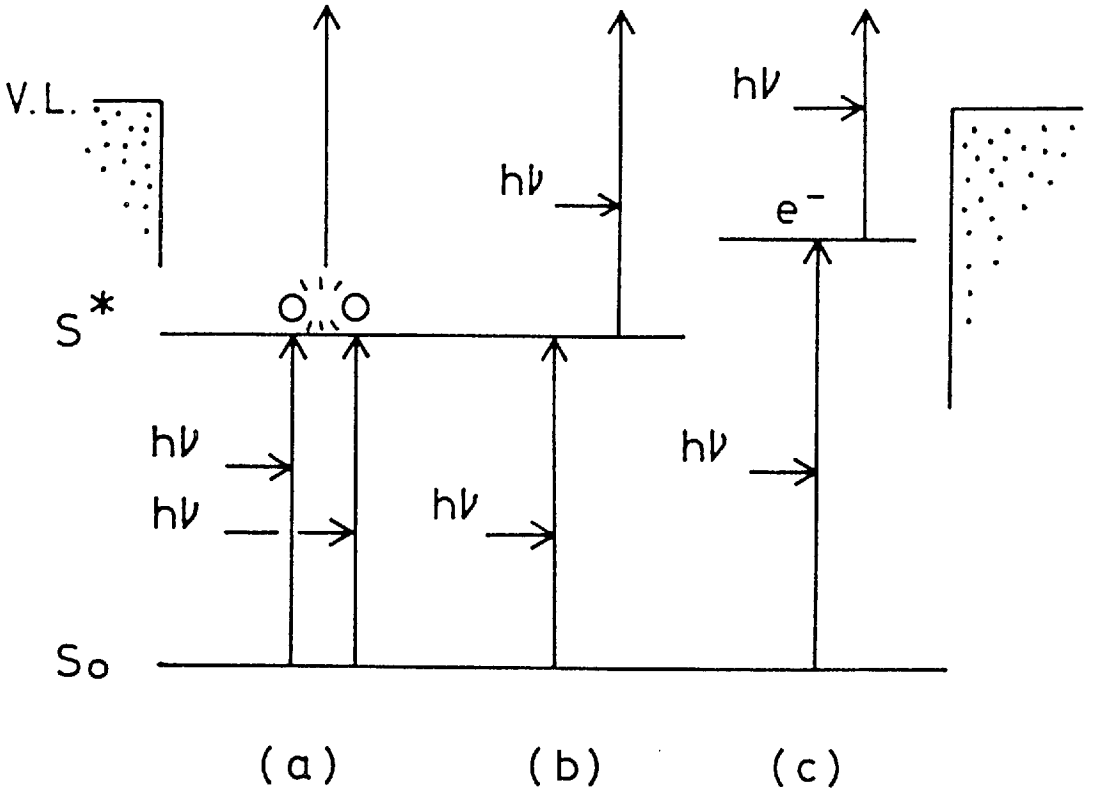

Fig. 3.1 Modes for external photoemission via excites state and ionized state. (a) singlet exciton fusion (b) photoionization of singlet exciton (c) photoemission of conduction electron.

3.2 Apparatus for measurements of excitonic photoemission

The vacuum chamber constructed for the present work is shown in Fig. 3.2. The vacuum chamber was pumped by a turbo-molecular pump (Shimadzu, TMP-150). The pressure in the chamber was $<3\times 10^{-7}$ Torr without the sample and was $<1\times 10^{-6}$ Torr during the measurements.

The sample specimen was a single crystal, typically 0.5 mm thick, and was attached to a stainless steel substrate with silver paste. The vapour pressure of organic crystals is relatively high (the vapour pressure of anthracene at 300 K is 1×10^{-5} Torr estimated from reported data [3.12]). Accordingly, the surface of the sample specimen may be kept clean due to vapourization (self-cleaning effect).

There is a disturbing charging effect when the light intensity, or the repetition rate of the laser, is too high. This charging which was induced by a UV pulse could be erased by irradiating the crystal with a few light pulses in the visible range. When the exciting light of the wavelength at the absorption edge was used, charging effect was not severe and the photocurrent did not change during the measurement. It seems that light pulses at the absorption edge do not only generate photoelectrons, but also erase the charging, through photoinjection of carriers from the substrate (the penetration depth of the light is larger than the thickness of the sample specimen).

A dye laser (Lambda Physik FL3002) pumped by a XeCl excimer

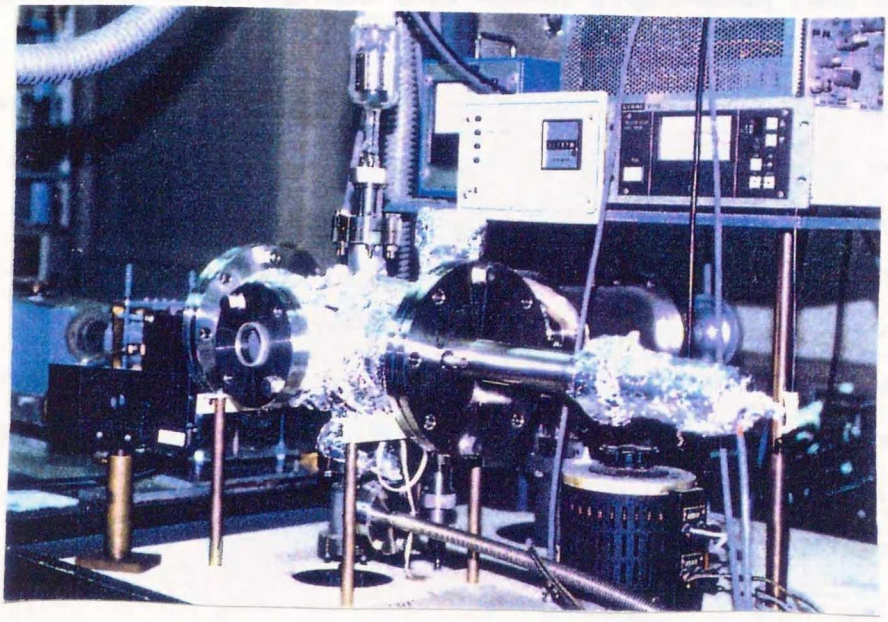

Fig. 3.2 Photograph of vacuum chamber.

laser (Lambda Physik EMG 101 MSC) was used as the exciting light source in one-color experiments. The pulse duration of the laser was 8 ns. The polarization of the exciting light was controlled by a polarizer (Lambda Physik FL50). In two-color, two-step excitation experiments two dye lasers (Lambda Physik, FL-3002 and a homemade one) pumped by a common XeCl excimer laser were used.

Figure 3.3 shows the apparatus for measurements of external photoemission with two-color, two-step excitation. The sample was held at V_b = -200 V and electrons emitted were detected by an electron multiplier (Murata, Ceratron EME-1061B), which was held at the ground potential. In some measurements a multichannel plate (Hamamatsu, F2221-21-S) was used to detect photoelectrons. The photocurrent was monitored on an oscilloscope and processed with a transient digitizer (Autonics, S-210) controlled by a microcomputer (Epson, PC-286VS) using GP-IB interface.

External photoemission by fusion of two singlet excitons is an efficient process, so that a simple detection system could be used (Fig. 3.4). The sample could be rotated around the axis of incidence to control the polarization of excitating light. Electrons emitted were collected by a cylindrical electron collector made by stainless steel. The sample (V_b) was kept at -20 V while the collector was at the ground potential. The photocurrent was observed on an oscilloscope with a load resistor of 1MΩ . The collector was equipped with a mesh window for monitoring the fluorescence from the sample specimen. The fluorescence was observed with a photomultiplier (Hamamatsu, 1P21) through a fused quartz window and filters (HOYA, Y-44 and Y-46).

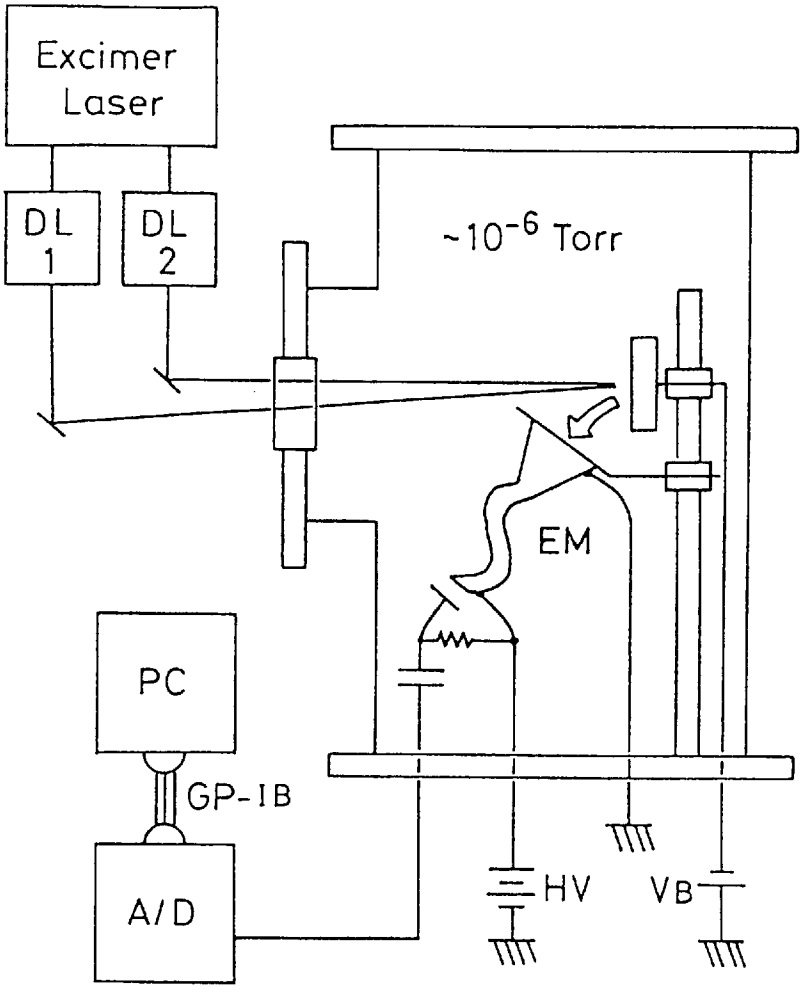

Fig. 3.3 Apparatus for two-color photoemission experiments.

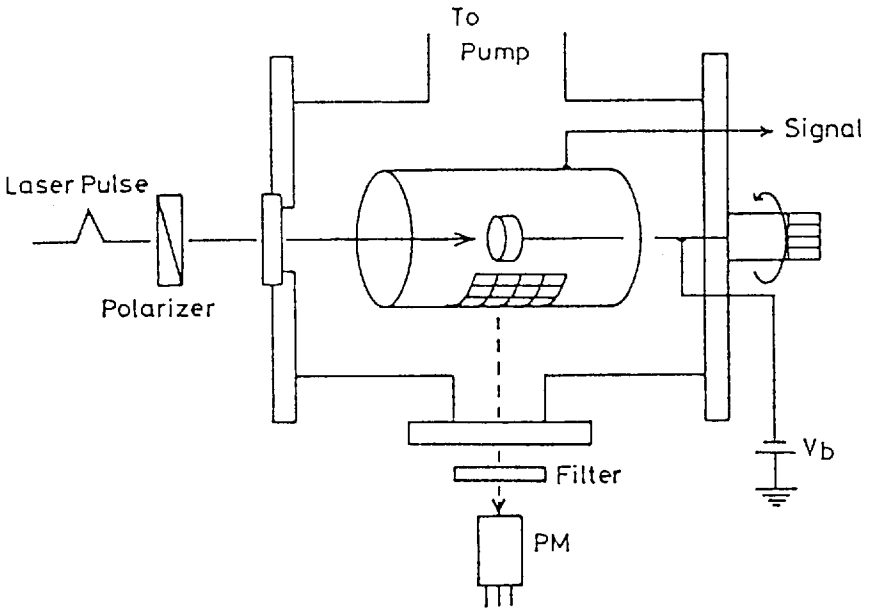

Fig. 3.4 Apparatus for external photoemission by exciton fusion.

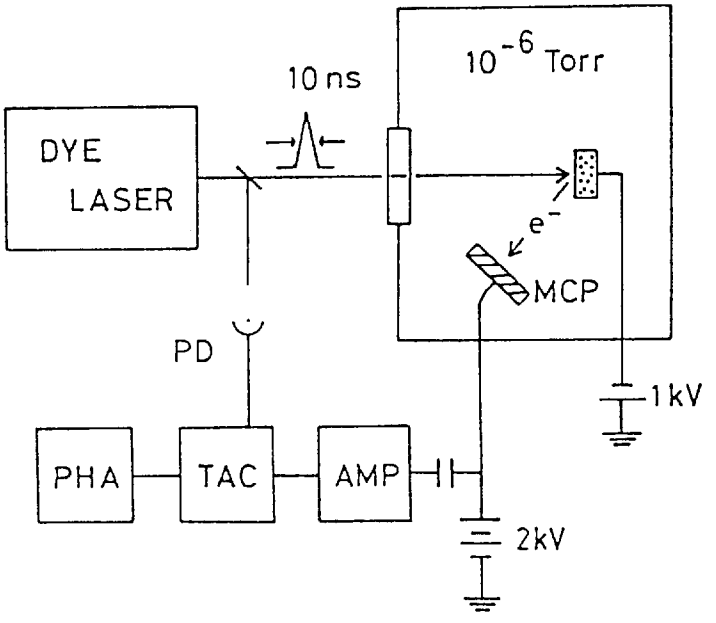

Fig. 3.5 Apparatus for the measurement of time-corrlated single-electron counting.

Time profile of the emitted photoelectrons was measured by time-correlated single-electron counting (Fig. 3.5). Repetition rate of the exciting laser was 50 Hz. The start signal for a time analyzer (TAC, Camberra, Model 1443A) was provided by a fast PIN photodiode (PD, Hamamatsu, S-1211). The signal from the multichannel plate was amplified by a fast amplifier (AMP, Stanford Research, SR440) and was used as the stop signal for the TAC. The count rate of electrons was ~ 0.5 cps. The signal from the TAC was accumulated in a pulse height analyzer (PHA, Camberra, Series 20).

3.3 External photoelectron emission by photoionization of singlet exciton

3.3.1 Introduction

Extrenal photoelectron emission from a paticular excited state gives a new information on the dynamics of this state. External photoemission from triplet exciton has been observed in Cu-phthalocyanine film [3.8-9]. However, external photoemission from a singlet exciton has not been reported. I could measure this type of photoemission in some organic crystals using two-color, two-step excitation technique. Threshold energies of the photoemission were determined in anthracene, p-terphenyl and naphthacene crystals.

3.3.2 Results

[Anthracene]

When a light pulse of λ_2 = 480 nm ($h\nu_2$ = 2.58 eV)irradiated sample specimen simultaneously with a λ_1 = 360 nm ($h\nu_1$ = 3.44 eV) pulse, an enhanced photocurrent was observed in anthracene crystal. Under this condition no photoemission could be observed only with 480 nm pulse. The enhancement of photocurrent $\triangle N_p$ due to the simultaneous irradiation with a 480 nm pulse is proportional to the intensity I_2 of the 480 nm pulse (second-step pulse $h\nu_2$, Fig. 3.6). This indicates that the enhancement of the photocurrent is due to photoionization of singlet exciton:

$$S_0 \xrightarrow[h\nu_1]{} S^* \xrightarrow[h\nu_2]{} e^- .$$

The action spectrum of the external photoemission by photoionization of singlet exciton is shown in Fig. 3.7. Two different wavelengths (360, 420 nm) were used to generate singlet excitons (the first-step excitation $h\nu_1$). The photocurrent seems to increase sharply with the photon energy of the second-step excitation for both first-step excitation photon energies. To determine the threshold energy of the photoemission E_{th} the assumption is made that the photoemission efficiency changes in proportion to $(h\nu_2 - E_{th})^3$.

In Fig. 3.8 $(\triangle N_P)^{1/3}$ is plotted against the energy of the second-step excitation. Observed points could be fitted with straight lines. Such a plot that has been adopted in many papers on conventional one-photon photoemission with vacuum ultraviolet light [3.13]. The threshold energy is found to be 2.36 ± 0.05 eV above the singlet exciton level for the two-color photoemission due to singlet exciton photoionization in anthracene for both photon energies of the first-step excitation.

The same threshold energy has been observed for two different photon energies of the first-step excitation. This indicates that the second-step light is absorbed by vibrationally relaxed singlet excitons. The energy of the relaxed singlet exciton $E(S^*)$ is assumed to be the 0-0 band energy of the absorption spectrum (3.1117 eV [3.14]). The top scale in Fig. 3.8 is the energy above the ground state, defined as $E(S^*) + h\nu_2$. The observed threshold energy of the photoemission via the

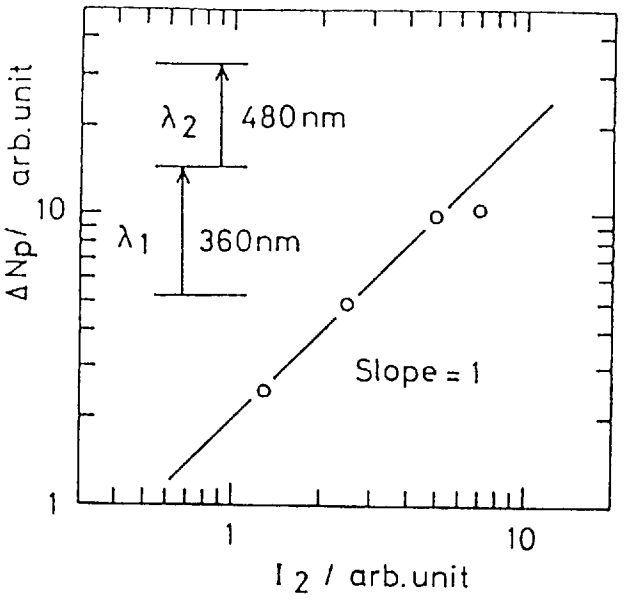

Fig. 3.6 Number of additional photoelectrons ($\triangle N_p$) from anthracene versus the second-step light intensity I_2.

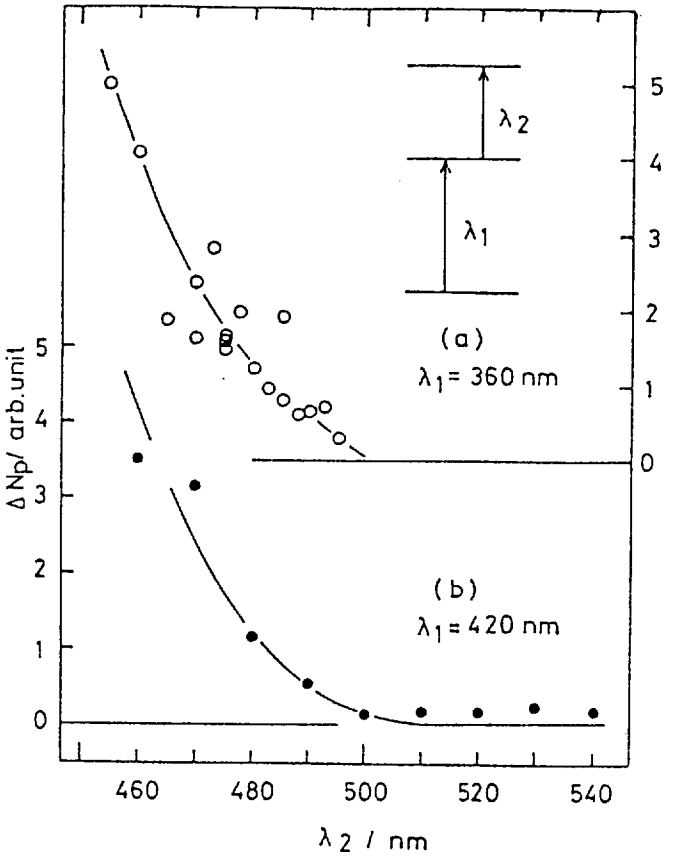

Fig. 3.7 Action spectra of two-color photoemission in an anthracene crystal.

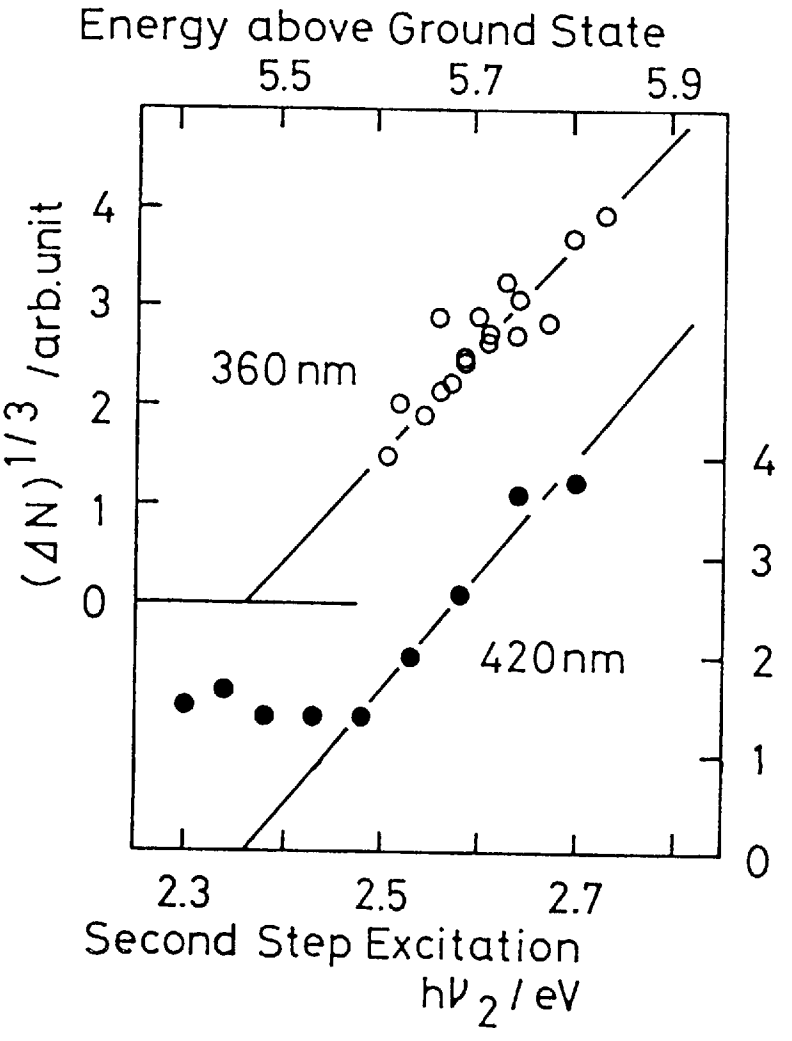

Fig. 3.8 $(\Delta N_p)^{1/3}$ plot of the action spectra in anthracene. Excitation energy above the ground state is defined using the 0-0 band energy in the absorption (3.11 eV).

singlet exciton photoionization, 5.5 eV above the ground state, is smaller than the threshold energy for the conventional photoemission in an anthracene crystal, which has been reported to be 5.67eV [3.15].

[p-Terphenyl]

Photoemission from singlet exciton was also observed in a p-terphenyl crystal. First-step excitation was made by illumination with 340nm light in this case. The action spectra of photoemission from singlet exciton with two-color, two-step excitation are shown in Fig. 3.9. In Fig. 3.9 $(\triangle N_P)^{1/3}$ is also plotted against the second step excitation energy. The threshold photon energy for the external photoemission above singlet exciton is found to be 2.58 eV. Adding the energy of singlet exciton, 3.69 eV in p-terphenyl [3.16], to this value, the threshold energy from the ground state is obtained to be 6.27 eV.

[Naphthacene]

Figure 3.10 shows the photocurrent observed with a naphthacene film as a function of photon energy of the second-step excitation. First-step excitation is made at λ = 505 nm ($h\nu$ = 2.5 eV). Threshold energy from the ground state is found to be 5.30 eV, by adding the energy of the singlet exciton of 2.38 eV [3.17].

3.3.3 Threshold energies for external photoemission by

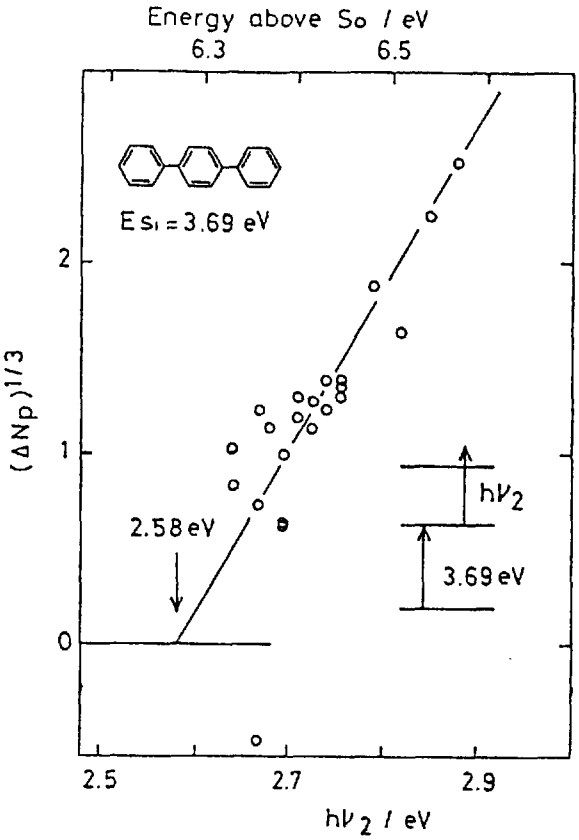

Fig. 3.9 Action spectra of photoemission due to photoionization of the singlet exciton in a p-terphenyl crystal.

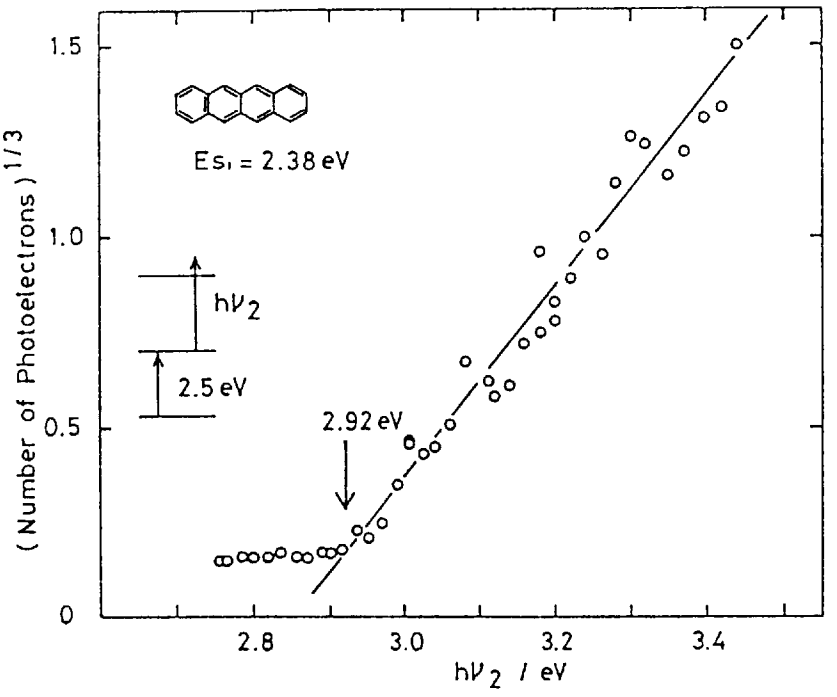

Fig. 3.10 Action spectra of photoemission due to photoionization of the singlet exciton in a naphthacene.

photoionization of singlet exciton

Table 3.1 shows the threshold energies for external photoemission due to photoionization of a singlet exciton in anthracene, p-terphenyl and naphthacene crystals. The threshold energies are different from those obtained by conventional one-photon photoemission, which are also shown in Table 3.1.

The difference in the threshold energy between one-photon excitation and two-step excitation could be due to some geometrical change of the molecule in the excited state or different polarization energy in the excited state. When a change in molecular geometry occurs in a paticular excited state, the threshold energy for the photoemission via the excited state calculated by adding $E(S^*)$ and $h\nu_2$, may be different from that for the one-photon photoemission. In anthracene such a structure change is unlikely, since its molecular structure is rigid and its 0-0 band energy in the absorption spectrum coincides with that in the fluorescence spectrum [3.14]. It is possible that the polarization energy in the excited state (a solvation energy analogue in the solid state) is different from that in the ground state. This difference in the polarization energy could be responsible for the small difference in the ionization thresholds. In the case of a p-terphenyl crystal, the central phenyl ring can be twisted around a long axis of the molecule [3.18]. This geometrical change may occur in the singlet excited state. In a naphthacene crystal molecule has rigid structure, so that geometrical change is unlikely. However, 0-0 band of fluorescence exhibits a red-shift from that of absorption [3.17]. This is due to a lattice deformation induced by singlet exciton.

As a result the threshold energy of photoelectron emission is larger than that obtained by conventional one-photon photoemission.

Table 3.1 Threshold energies for external photoemission due to photoionization of the singlet exciton.

			Threshold energy for photoemission		
	E_{s*}	$E_{th}(h\nu_2)$	via S^*	$1h\nu$	Δ
	eV	eV	eV	eV	eV
Anthracene	3.11	2.36	5.47	5.67	-0.20
p-Terphenyl	3.69	2.58	6.27	6.1	0.17
Naphthacene	2.38	2.92	5.30	5.1	0.20

$\Delta = E_{th}(\text{via } S^*) - E_{th}(1h\nu)$

3.4 External photoelectron emission by singlet exciton fusion

3.4.1 Introduction

Several researchers reported that the double-quantum photoemission from anthracene crystals observed with near-UV light excitation could be due to fusion of two singlet excitons [3.4-6]. However, the possibility that singlet excitons are photoionized has not been seriously considered. In the present study action sepectra for the double-quantum photoemission in anthracene was reinvestigated in more detail. Time profile of photocurrent was also measured in an α -perylene crystal. In these cases I could confirm that the double-quantum photoemission with near-UV excitation was due to singlet exciton fusion. Absolute cross-secton of photoemission could be estimated.

3.4.2 Kinetic analysis for the double quantum photoemission

There are two possible mechanisms for the double quantum photoemission involving a singlet exciton as an intermediate state.

① Double quantum photoemission by photoionization of singlet exciton (PI case)

$$S^* + h\nu \rightarrow M^+ + e^-,$$

② Double quantum photoemission by exciton fusion (collisional ionization; CI case)

$$S^* + S^* \rightarrow S_0 + M^+ + e^-,$$

where S_0 means the ground state molecule, S^* means singlet exciton and M^+ means a molecular cation.

The generation and decay kinetics of the density of singlet excitons [S*] can be expressed by

$$d[S^*]/dt = \alpha I_{ex} - [S^*]/\tau_S - \gamma_{SS}[S^*]^2 \quad (3.1)$$

where α is the absorption coefficient, I_{ex} is the exciting light intensity τ_S is the lifetime of the singlet exciton and γ_{SS} is the rate constant for singlet exciton fusion. When a steady state can be assumed and I_{ex} is relatively low, the concentration of the singlet exciton is given by

$$[S^*] = \alpha \tau_S I_{ex} \quad (3.2)$$

The density of photoelectrons $[N_P]$ can then be written for each mechanism as:

$$[N_P] = \Phi_{PI} \sigma_A [S^*] \tau_P I_{ex} \quad (3.3)$$

for a PI case and

$$[N_P] = \Phi_{CI} \gamma_{SS} [S^*]^2 \tau_P \quad (3.4)$$

for the CI case, where Φ_{PI} and Φ_{CI} are the photoemission efficiencies for the respective mechanisms, σ_A is the absorption cross section of the exciton S*, and τ_P the pulse width of the exciting light.

From the density of photoelectrons $[N_P]$ the number of emitted electrons N_{obs} can be calculated (or estimated) by considering the escape depth of an electron. When the crystal is thick enough and the absorption is complete, the number of photogenerated electrons N (in the interior of the crystal) can be obtained by integrating over the excited volume (= irradiation area × penetration depth of light). However, the photoelectrons that come out into the vacuum are a small fraction of those generated in the bulk. This is due to a small escape depth of the electrons. Hino et al. have estimated the escape depth of electrons in organic crystals to be several angstroms [3.19].

Considering that the volume from which electrons can escape is given by the irradiated area S multiplied by the electron escape depth d, N_{obs} can be written as

$$N_{obs} = \Phi_{PI}\ \sigma_A\ \alpha\ \tau_S\ \tau_P\ I_{ex}^2 Sd \qquad (3.5)$$

for the PI case and

$$N_{obs} = \Phi_{CI}\ \gamma_{SS}\ \alpha^2\ \tau_S^2\ \tau_P I_{ex}^2 Sd \qquad (3.6)$$

for the CI case. These equations predict that the photocurrent observed should be proportional to the square of the excitation intensity. It should also be linearly proportional to the absorption coefficient for the electron generation via photoionization, on the other hand, proportional to the square of the absorption coefficient in the case of collisional ionization (exciton fusion).

When I_{ex} is large, the third term of the right hand side in Eq. (3.1) is important. As a result, density of the singlet exciton can be expressed by

$$[S^*] = (\alpha / \gamma_{ss})^{1/2}\ I_{ex}^{1/2}. \qquad (3.7)$$

This predicts that fluorescence intensity should be proportional to $I_{ex}^{1/2}$ at high density excitation (see Fig. 3.12 and Appendix I). The number of emitted electrons N_{obs} can be written as:

$$N_{obs} = \Phi_{PI}\ \sigma_A\ (\alpha / \gamma_{ss})^{1/2}\ \tau_P\ I_{ex}^2 Sd \qquad (3.8)$$

for the PI case and

$$N_{obs} = \Phi_{CI}\ \alpha\ \tau_P I_{ex}^{3/2}\ Sd \qquad (3.9)$$

for the CI case. These equations indicate that N_{obs} is proportional to $I_{ex}^{3/2}$ for a PI case and I_{ex}^{1} for a CI case.

Another method for distinguishing photoionization from fusion is a measurement of time profile of photoemission. When the photoemission occurs by fusion of two singlet excitons which

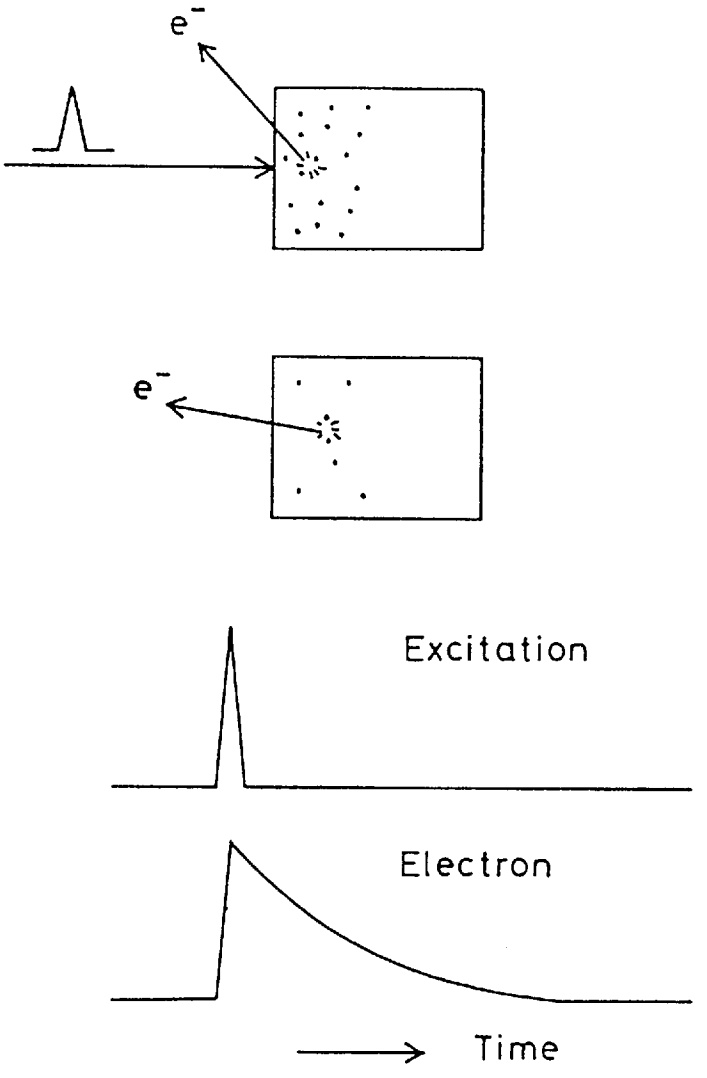

Fig. 3.11 Principle of delayed photoemission. In the case of photoelectron emission by fusion of singlet excitons the photoemission continues during the lifetime of the singlet exciton.

have lifetimes longer than the exciting pulse width, photoemission should continue during the lifetime of the excited state (Fig. 3.11).

3.4.3 Double-quantum photoemission with near-UV excitation

[Anthracene]

When an anthracene crystal was excited with a near UV light (330-420 nm) while negatively biased, a photocurrent could be observed. No photocurrent was observed when the sample was held at a positive potential. This shows that the photocurrent is indeed due to photoelectrons from the anthracene crystal.

In Fig. 3.12 the fluorescence intensity (I_F) and the number of electrons emitted (N) are plotted against the exciting light intensity (I_{ex}, λ_{ex}= 385 nm). It may be seen that the intensity of the fluorescence is proportional to that of the exciting light for low excitation intensities. The dependence changes from I_{ex}^{1} to $I_{ex}^{1/2}$ when intensity of the exciting light increases (Eq. (3.7)). This is due to the fusion of two singlet excitons. The number of electrons emitted, N_{obs}, is proportional to I_{ex}^{2} with weak excitations and gradually saturates for stronger excitations. This may be also due to singlet exciton fusion (Eq. (3.8)). However, there is also an additional space charge effect which could be suppressed in part by applying a large bias voltage between the sample and the collector.

Figure 3.13 shows the action spectra of the double-quantum

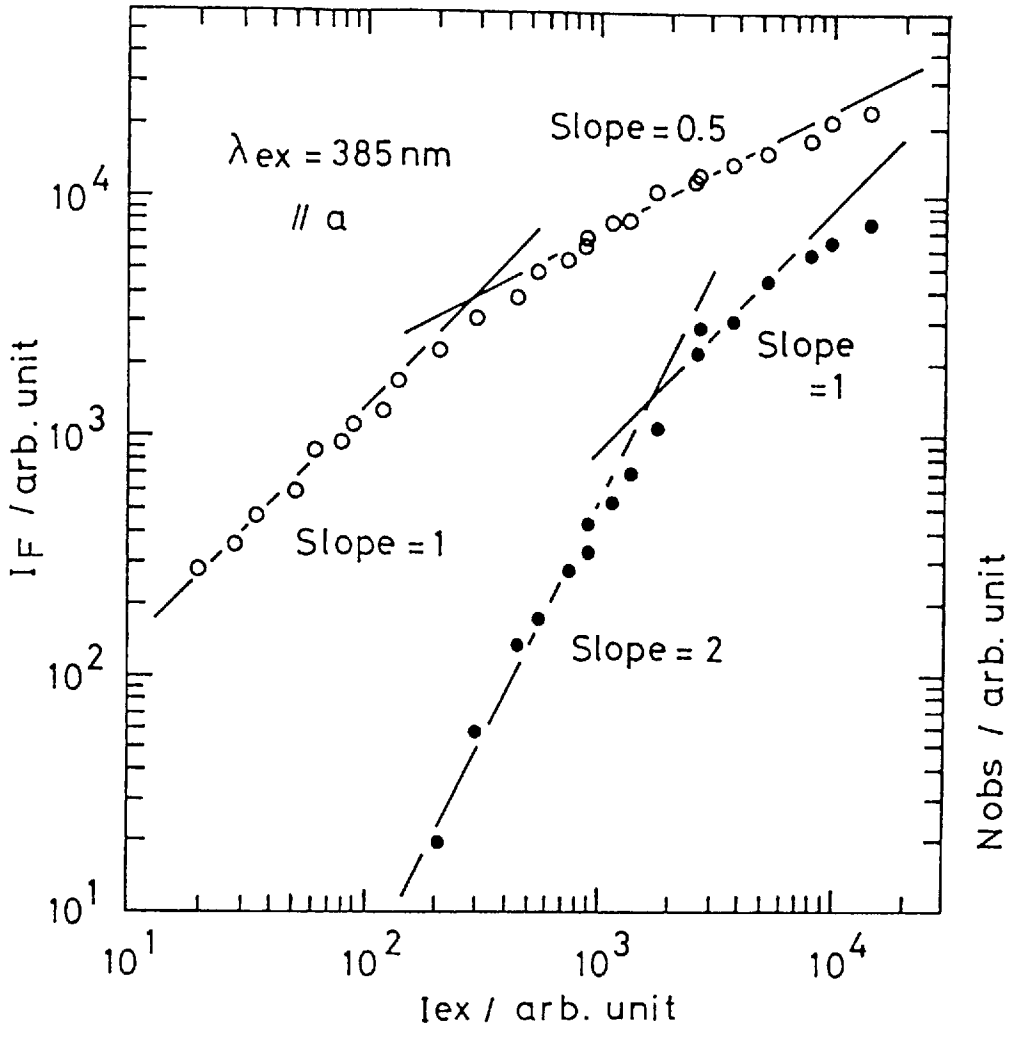

Fig. 3.12 Number of photoelectrons emitted N and fluorescence intensity plotted against exciting light intensity I_{ex} in anthracene.

photoemission for E//a and for E//b. The observed points are normalized to I_{ex}^2. The photoemission is strongly polarization dependent. The maxima and minima correspond well to those of the absorption spectra [3.20]. The close similarity of the spectra to the absorption spectrum clearly indicates that singlet excitons are involved in the double quantum photoemission.

Solid lines in Fig.3.13 are the square of the absorption coefficients normalized at 380nm. It may be seen that the action spectra of the double quantum photoemission are in good agreement with α^2. In Fig. 3.14 the same data are rearranged so that the number of electrons emitted is plotted against the absorption coefficient. It clearly shows that the number of electrons emitted is proportional to the square of the absorption coefficient. This provides clear evidence that the double quantum photoemission is due to the exciton fusion and not due to exciton photoionization.

The ionization efficiency Φ_{CI} in Eq. (3.6) can be estimated from the yield of the excitonic photoemission. I tentatively assume the escape depth of the photoelectrons to be 10Å . This estimate could be in error by an order of magnitude at most. The ionization efficinecy for λ = 385nm (E//a) is then calculated to be $\Phi_{CI} = 10^{-8}$ when using values $\gamma_{SS} = 1\times 10^{-8}$ cm^3 s^{-1} [3.21], $I_{ex} = 4.2\times 10^{22}$ photons/cm^{2}s, $\alpha = 5\times 10^4$ cm^{-1} [3.23], τ_S = 20ns [3.22], τ_P = 8ns, S = 0.07cm^2 and $N_{obs} = 1.1\times 10^5$ electrons. The result means that one out of 10^8 fusion events which occur in the surface layer of thickness d gives rise to photoemission.

Braun has studied photoconductivity through singlet exciton

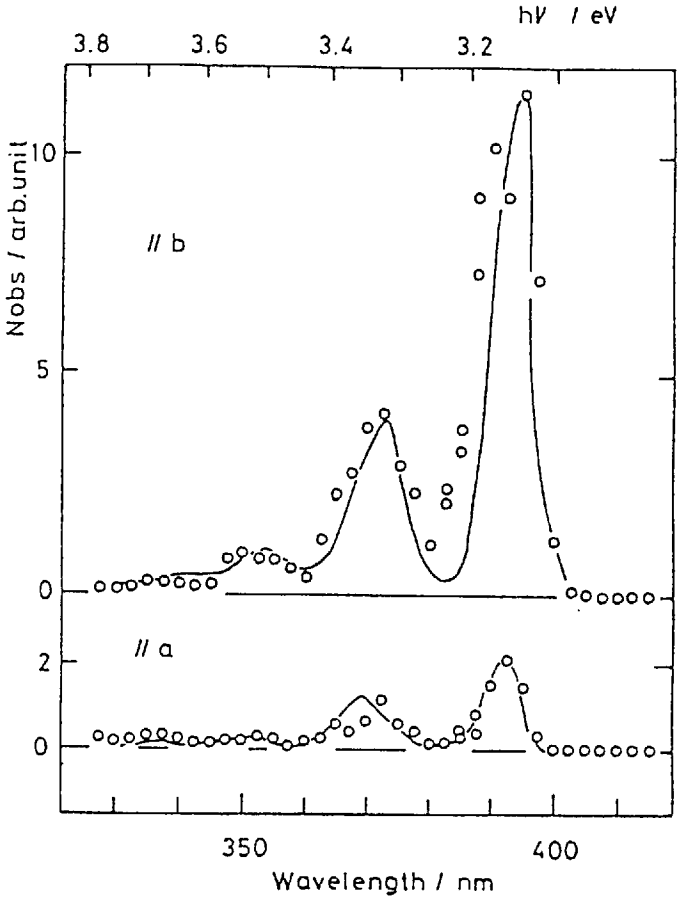

Fig. 3.13 The action spectra for the excitonic photoemission in anthracene for polarization E//b (top) and E//a (bottom). The solid line is the square of the absorption coefficient.

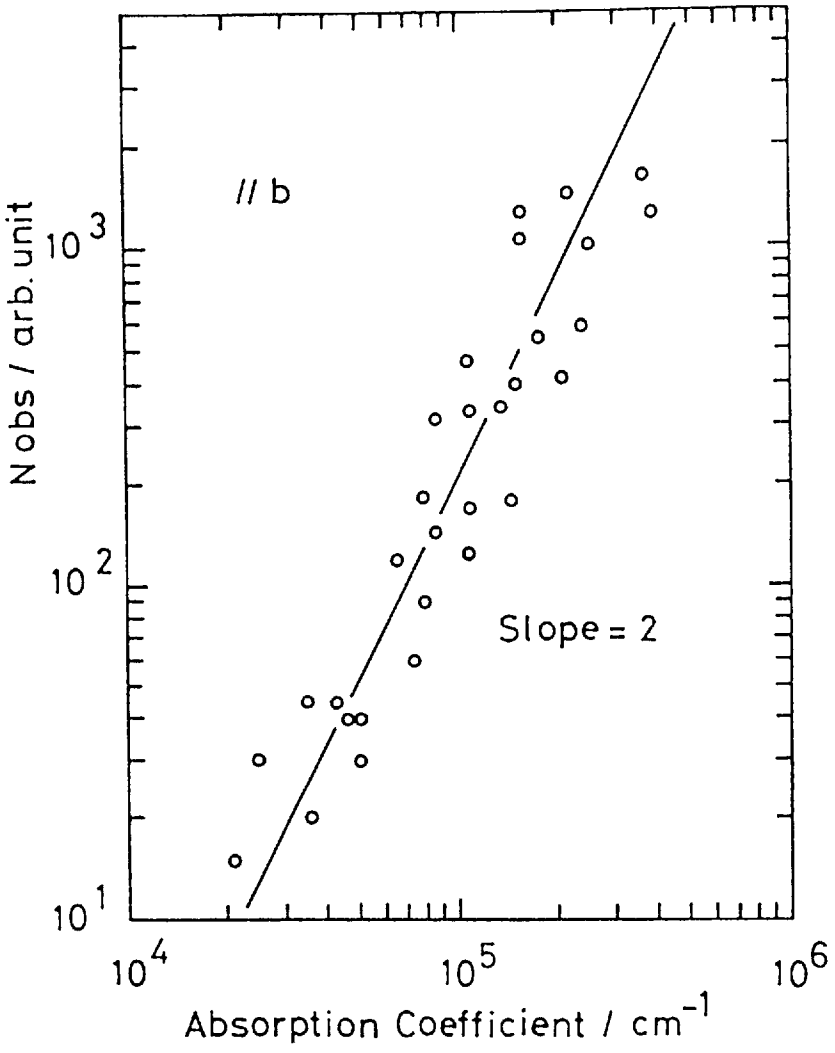

Fig. 3.14 The number of photoelectrons N_{obs} in an anthracene plotted against the absorption coefficient α .

fusion and found the ionization efficiency to be $\Phi_{IPE} = 10^{-4}$ (IPE stands for internal photoemission) [3.23]. This is four orders of magnitude larger than the ionzation efficiency for external photoemission Φ_{CI}. One possible reason for the difference is the relaxation which intervenes. In the study of photoconductivity, a rapid relaxation which precedes carrier generation has been observed [see § 6]. External photoemission occurs from a higher excited state which has a short lifetime. It is possible that the relaxed excited state contributes to the photoconductivity through photoionization, while it cannot contribute to the external photoemission.

Another reason may be sought in the spatial distribution of excitons near the surface and probably also its temporal development. Actually the escape depth of photoelectrons is much smaller than the penetration depth of light. The change in the slope for the number of photoelectrons N_{obs} in Fig.3.12 occurrs changes at a higher intensity as compared to that for the fluorescence intensity I_F. It is possible that the density of singlet exciton at the surface, which can contribute to the photoemission, is lower than that in the bulk of the crystal. Quenching of the singlet excitons at the surface and diffusion of the singlet excitons into the bulk of the crystal may cause such a difference.

It is generally recoginized that, in the conventional one-photon photoemission, the efficiency of external photoemission increases with photon energy. In the present case, the action spectrum of the external photoemission agrees well with the square of the absorption spectrum over the energy range

studied (Fig. 3.13). This may imply that the efficiency of the external photoemission does not depend on the photon energy between 3.0-3.8 eV. The energy in excess of the bottom of the singlet exciton band, which lies at 3.1117 eV [3.14], seems to have no effect to the photoemission. This indicates that excitons which undergo fusion are in the relaxed singlet state.

[α -Perylene]

Figure 3.15 shows the action spectrum for double quantum photoemission for different polarizations from an α -perylene single crystal. The solid line in the Figure is the square of the absorption coefficient in an α -perylene crystal [3.24]. The similarity of both spectra indicates that the photoemission is due to the fusion of two singlet excitons.

Figure 3.16 shows a time profile of the photoemission with 480 nm pulse. Duration of exciting light pulse is τ_P = 1ns. The light of this wavelength can excite the lowest singlet exciton only. The emission persists after the excitation is over and decays with a time constant of 7.5 ns. This strongly indicates that the external photoemission is due to the fusion of singlet excitons. However, the observed decay is much faster (7.5 ns) than the expected decay constant (singlet lifetime/2 = 40 ns [3.25]). The reason of this discrepancy is unclear. One possiblity is the quenching of the singlet exciton at the crystal surface.

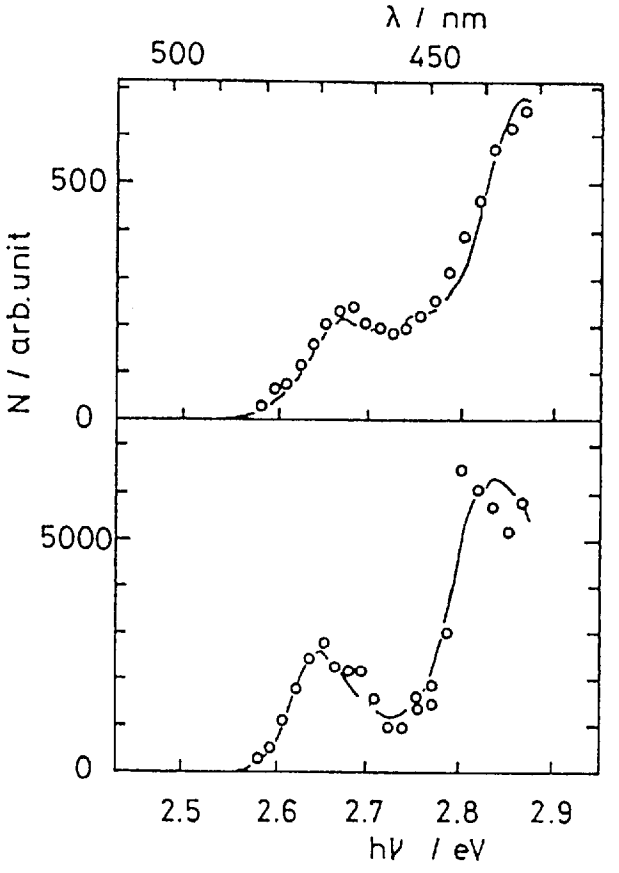

Fig. 3.15 The action spectra for the excitonic photoemission in α -perylene for polarization E//a (top) and E//b (bottom). The solid line is the square of the absorption coefficient.

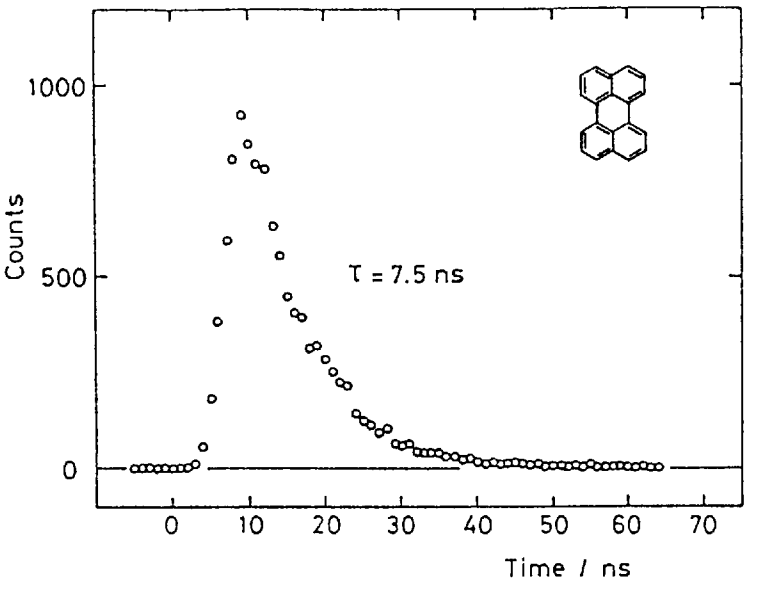

Fig. 3.16 Time profile of the emitted photoelectrons from α -perylene single crystal.

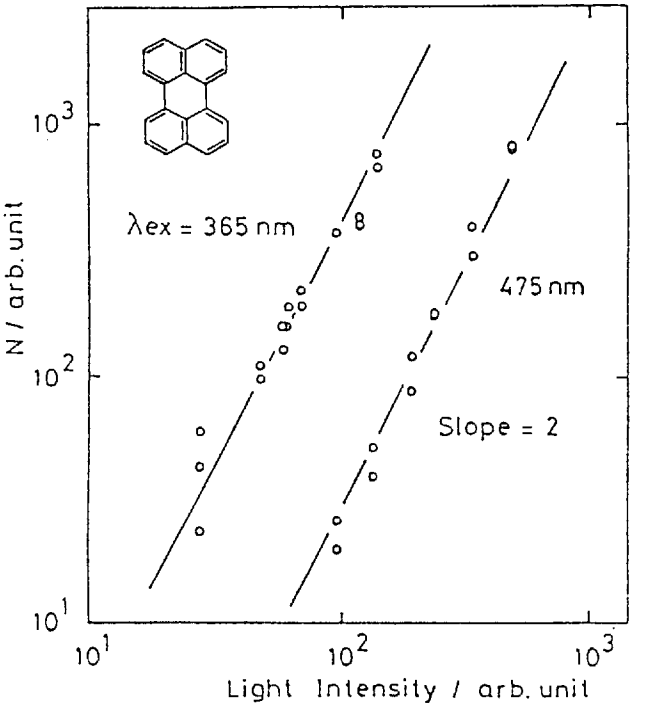

Fig. 3.17 The number of photoelectrons (N) emitted from an α -perylene film is plotted as a function of the exciting light intensity.

3.5 External photoelectron emission from conduction band

3.5.1 Introduction

When photon energy of exciting light exceeds the band gap, i.e. the ionization threshold in a crystal, free charge carriers can be generated. Double-quantum photoemission via such an ionized state may be possible. In this section double-quantum photoelectron emission (DQPE) from α -perylene and naphthacene crystal will be presented. Action spectra and time profiles of the photoemission indicate that conduction electrons are being photoemitted above 3.2 eV, while, below 3.2eV, photoemission occurs by fusion of two singlet excitons in α -perylene and by photoionization of singlet exciton in naphthacene.

3.5.2 Results and discussion

[Perylene]

Vacuum evaporated films on stainless steel substrate, $\sim$ 100 Å thick, were used as samples. Judged from their fluorescence spectrum, the films of perylene studied were in dimeric crystal structure (α -form). When a perylene film is excited at 475 nm or at 365 nm, a photocurrent is observed which is proportional to the square of the exciting light intensity I_{ex} (Fig. 3.17). Figure 3.18 shows the action spectrum for the double-quantum photoemission from a perylene film, normalized to I_{ex}^2. The DQPE starts at the photon energy of $\sim$ 2.5 eV and has a shoulder at 2.9 eV (λ = 430nm).

The action spectrum for the DQPE in Fig. 3.18 is similar to the absorption spectrum of the crystal in that it has the same onset energy and a common structure at 2.9eV. Accordingly, I conclude that the DQPE occurs via an intermediate state which is the lowest excited singlet state.

The square of the absorption coefficient is also shown in Fig. 3.18 by a solid line. The absorption spectrum, which is averaged in polarization (//a + //b), is obtained using the results with a single crystal [3.24]. Below 3.2eV, the action spectrum for the external photoemission agrees with the square of the absorption spectrum. This indicates that the DQPE is due to fusion of two singlet excitons below 3.2eV (see § 3.4). Above that energy a new channel for the DQPE seems to open.

It has been known that the majority of singlet excitons in an α -perylene crystal are formed as excimer excitons [3.26] and they migrate in the crystal. The energy of the relaxed excimer exciton (2.52 eV) is lower, by 0.08 eV [3.26], than that of the monomer exciton (2.6 eV [3.26]), which can be recognized through a weak monomer exciton fluorescence. It is to be noted that twice the energy of the relaxed excimer exciton in α -perylene crystal (5.04 eV) is lower than the threshold energy for external photoemission (5.2 eV), determined by conventional VUV photoelectron spectroscopy [3.27]. It seems that the threshold energy for external photoemission via excimer exciton is different from that determined by photoelectron spectroscopy with (single photon) VUV excitation. It is possible that the polarization energy, which corresponds to solvation energy in solution, is larger in the excited state than in the ground

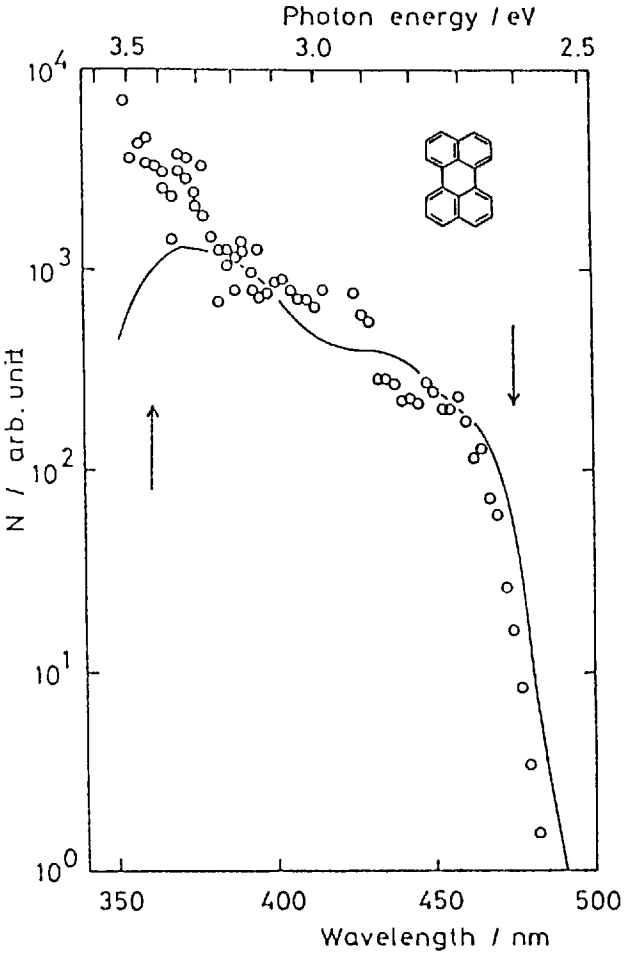

Fig. 3.18 The action spectrum of double-quantum photoemission from α -perylene film. The solid line indicates the square of the absorption coefficient. Arrows indicate the wavelengths at which the time profiles of photoelectrons emitted are measured (see Fig. 3.19).

state, so that the intermediate state in the DQPE is stabilized. This has been observed in anthracene.

Figure 3.19 shows the time profiles of electrons emitted with 475 and 360 nm excitations from a perylene film. Duration of the exciting light pulse is $\sim$ 10ns. A relatively high bias voltage (-1 kV) is applied to the sample specimen, so that the flight time of electrons is short ($\sim$ 2.5 ns). Hence, the time profile of electrons observed is not the time-of-flight of electrons but does show the time characteristics of electron emission. It may be seen that, when excitation is made with 475nm, the photoemission persists after the excitation, while the time profile reproduces the exciting pulse in the case of 360nm excitation. The photocurrent decays exponentially with a time constant of τ = 6.5ns with 475 nm excitation. It corresponds fairly well to a previous result with a single crystal (τ = 7.5ns) (see § 3.4). The time profile with 475 nm excitation can be ascribed to the photoemission due to fusion of two singlet excitons. In the case of 360 nm excitation the electron emission has no observable lifetime and its mechanism seems to be different. The photoelectrons may arise from photoionization of an excited state. Possible interpretation will be presented below.

[Naphthacene]

A singlet exciton in a naphthacene crystal has an energy of 2.38 eV [3.17]. Twice that energy is less than the threshold energy for photoemission via singlet exciton (see § 3.3 5.30 eV). Hence, external photoemission by fusion of two singlet excitons

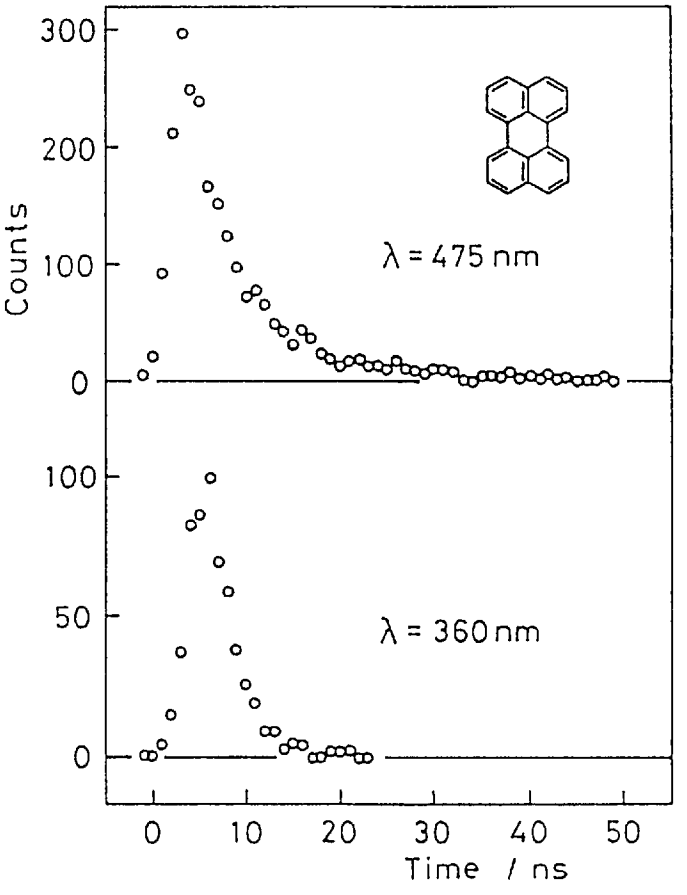

Fig. 3.19 The time profiles of photoelectrons emitted from an α -perylene film with λ = 475 nm and with 360 nm excitation.

is energetically impossible. However, when a naphthacene film was excited with 370 nm light, a photocurrent was observed which was proportional to the square of the exciting light intensity. Figure 3.20(a) shows the action spectrum for the external photoemission, normalized to I_{ex}^2. It is obvious that the photocurrent increases steeply with the photon energy. Cube root of the number of emitted photoelectrons, $N^{1/3}$, is also shown in Fig. 3.20(b). The signal below 2.95 eV may be the background, and the break at 2.95 eV can be ascribed to the threshold energy for the photoemission. This energy (2.95 eV) is close to the threshold photon energy for external photoemission from singlet exciton (2.92 eV; see § 3.3). Hence, it seems probable that one photon generates a singlet exciton and another photon releases an electron from the exciton:

$$S_0 \xrightarrow{h\nu} S^* \xrightarrow{h\nu} M^+ + e^-.$$

The slope in Fig. 3.20 (b) changes at 3.2 eV. Above this energy another mechanism seems to be operating.

A notable change is observed in the behavior of the action spectrum for external photoemission at 3.2 eV in both in α -perylene and in naphthacene. This indicates that the mechanism of generating an electron for the DQPE changes at the same energy of 3.2 eV. This energy is close to the threshold energies for the intrinsic photoconduction in both materials (so-called band gap; 3.1eV in α -perylene [3.28] and 3.13eV in naphthacene crystals [3.29]). In the case of perylene the time profile of the electron emission excited with 360nm (3.44eV) is essentially identical to that of the exciting pulse. This suggests that electrons are generated by photoionization, and not

by fusion, of some excited states. I propose that the increase observed in the photoemission efficiency above 3.2 eV is brought about by the photoemission of conduction electrons (free charge carriers):

$$S_0 \xrightarrow{h\nu} M^+ + [e^-] \xrightarrow{h\nu} M^+ + e^-,$$

where $[e^-]$ means a conduction electron (free charge carrier). Band gap is an important parameter for understanding the mechanism of photoconductivity. However, it has been determined with only a few organic materials because of experimental difficulties [3.30]. DQPE can be a useful technique to detect the appearance of conduction electrons and hence to determine the location of the conduction band.

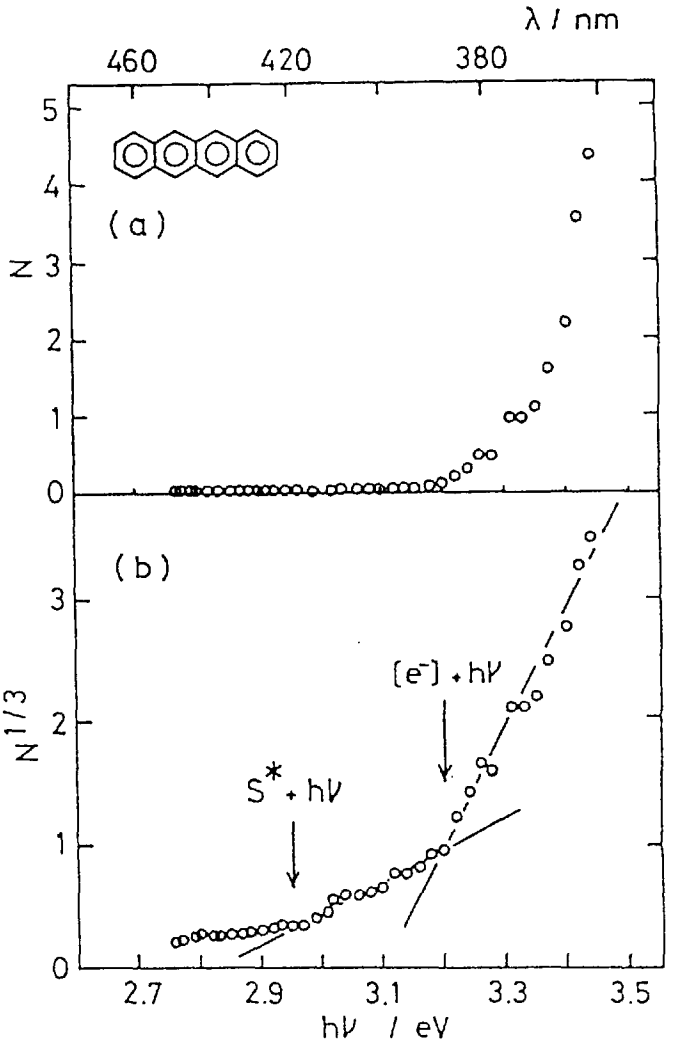

Fig. 3.20 (a) The number of photoelectrons (N) emitted from a naphthacene film is plotted as a function of the exciting photon energy. (b) The same as (a), with $N^{1/3}$ as ordinate. Arrows indiccate photon energies at which processes indicated start.

References

[3.1] J.M.Moison and M.Bensoussan,
Phys. Rev. B35 (1987) 914.

[3.2] R.Haight, J.A.Silberman and M.I Lilie,
Rev. Sci. Instrum 59 (1988) 1941.

[3.3] W.S.Fann, R.Storz and J.Bokor,
Phys. Rev. B49 (1991) 10980.

[3.4] M.Pope, H.Kallmann and J.Giachino,
J. Chem. Phys. 42 (1965) 2540.

[3.5] G.T.Pott and D.F.Williams,
J. Chem. Phys. 51 (1969) 203.

[3.6] D.Haarer and G.Castro,
Chem. Phys. Lett. 12 (1971) 277.

[3.7] E.R.Salaneck, H.W.Gibson, E.W.Plummer and B.H.Tommer,
Phys. Rev. Lett. 49 (1982) 801.

[3.8] E.E.Koch,
Physica Scripta T17 (1987) 120.

[3.9] T.Munakata and T.Kasuya,
J. Appl. Phys. 28 (1989) 1677.

[3.10] M.Wautelet, L.D.Laude and A.H.Madjid,
Chem. Phys. Lett. 51 (1977) 530.

[3.11] S.Arnold, M.Pope and T.K.T.Hsieh,
Phys. Stat. Sol. (b) 94 (1979) 263.

[3.12] L.Malaspina, R.Gigli and G.Bardi,
J. Chem. Phys. 59 (1973) 387.

[3.13] M.Kochi, Y.Harada, T.Hirooka and H.Inokuchi,
Bull. Chem. Soc. Jpn. 43 (1970) 2690.

[3.14] N.Karl,
in: Landort-Burnstein numerical data and fundamental

relationships in science and technology, New series, Vol.17, Eds. O.Madelung, M.Schulz and H.Weiss (Springer, Berlin, 1985).

[3.15] N.Sato, H.Inokuchi B.M.Schmid and N.Karl, J. Chem. Phys. 83 (1985) 5413.

[3.16] C.Kryschi, W.Klufer and H.Kupka, Chem. Phys. 146 (1990) 231.

[3.17] K.Mizuno, A.Matsui and G.J.Sloan, Chem. Phys. 131 (1989) 423.

[3.18] J.L.Baudour, H.Cailleau and W.B.Yelon. Acta. Cryst. B33 (1977) 1773.

[3.19] S.Hina, N.Sato and H.Inokuchi, Chem. Phys. Lett. 37 (1976) 494.

[3.20] A.Matsui, J. Phys. Soc. Japan 23 (1967) 581.

[3.21] J.Fourny, M.Schott and G.Delacote, Chem. Phys. Lett. 20 (1973) 559.

[3.22] H.Nishimura, T.Yamaoka, K.Hattori, A.Maysui and M.Mizuno, J. Phys. Soc. Japan 54 (1985) 4370.

[3.23] C.L.Braun, Phys. Rev. Lett. 21 (1968) 215.

[3.24] J.Tanaka, Bull. Chem. Soc. Jpn. 36 (1963) 1237.

[3.25] B.Walker, H.Port and H.C.Wolf, Chem. Phys. 92 (1985) 177.

[3.26] H.Nishimura, A.Matsui and M.Iemura, J. Phys. Soc. Jpn. 51 (1982) 1341.

[3.27] N.Sato, K.Seli and H.Inokuchi, J. Chem. Soc. Faraday Trans. 2,77 (1981) 1621.

[3.28] V.V.Aleksandrov, A.I.Belkind, I.Ya.Muzinkante, E.A.Silinsh

and L.F.Taure,
Sov. Phys. Soc. Phys. Solid. State. 18 (1976) 1405.
[3.29] N.Sato, H.Inokuchi and E.A.Silinsh,
Chem. Phys. 115 (1987) 269.
[3.30] E.A.Silinsh,
"Organic Molecular Crystals. Their electronic properties"
(Springer, Berlin, 1980).

4. Photoabsorption by excited states

4.1 Introduction

Photoabsorption by excited states gives information about dynamics and energy levels of higher excited states. Photoabsorption by excited molecules in solution have been studied extensively. However, only a few studies have been made in organic crystals. This may be mainly due to technical reasons; possible damage by intense exciting light and low optical quality of sample specimens.

Higuchi et al. have observed, using pump-and-probe method, a triplet exciton absorption in a naphthalene single crystal excited with high energy electron pulses [4.1]. Morris and Yoshihara have measured absorption spectrum due to triplet exciton in a benzophenone and a benzil crystals [4.2]. Williams and Nelson have observed of a pyrene crystal with femto-second time resolution and found a channel due to formation of an excimer from Franck-Condon state [4.3]. Zeiri et al. have observed transient photoabsorption by an excimer state of a pyrene crystal [4.4].

Diffuse reflection spectroscopy has been used to measure transient absorption in a powder sample. Wilkinson and Willsher have made the first observation of triplet excitons in a benzophenone micro-crystal by transient diffuse reflection [4.5]. Masuhara and co-workers measured transient reflection spectra of p-terphenyl, benzophenone and benzil crystals [4.6,4.7]. By this method polarization of a spectrum remains unresolved. Also,

spectral line shapes are often deformed.

Ludmer et al. have made use of nonlinear reabsorption effect to deduce photoabsorption by singlet exciton in pyrene and α -perylene crystals [4.8].

In this chapter transient photoabsorption spectra in anthracene, p-terphenyl and trans-stilbene crystals will be presented. Photoabsorption by singlet and triplet excitons inthese materials could be measured with a high S/N ratio using pump-and-probe method. It has been observed that most spectra are strongly polarized. Cross sections for absorption of singlet exciton are estimated in these materials.

An energy scheme for transient photoabsorption is shown in Fig. 4.1. The lowest singlet exciton is populated by the first light pulse (exciting light: $h\nu_1$). The singlet exciton absorbs the second step light (probing light: $h\nu_2$) or relaxes into triplet exciton by intersystem crossing (ISC). The triplet exciton can also absorb the second step light.

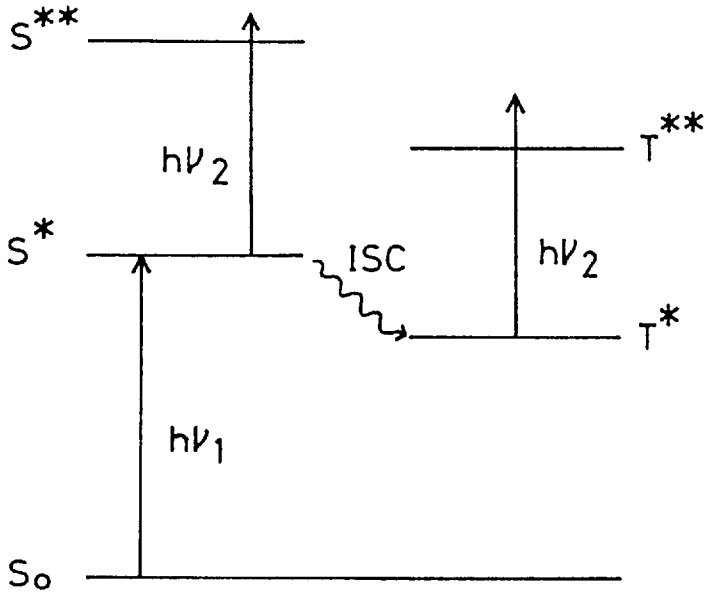

Fig. 4.1 Energy scheme of photoabsorption by singlet and triplet excitons.

4.2 Apparatus for measurements of transient absorption

Experimental arrangement for measurements of transient absorption is shown in Fig. 4.2. Two dye lasers (Lambda Physik, FL-3002, and a home made one), pumped by a common XeCl excimer laser (Lambda Physik, EMG 101 MSC), were used as sources for exciting (pumping) light and for probing light. Polarization of the two laser pulses were controlled with polarizers (Lambda Physik FL50 or Polaroid HN38). In measurements, in which two laser pulses were used with a delay, the homemade dye laser pumped by another XeCl laser (Lumonics TE-860-2) was used. The delay was varied with a pulse generator. The jitter between the pulses typically was $\pm$ 5 ns.

In measurements of transient absorption, intensity of the probe pulse transmitted through a sample crystal was measured with a pyroelectric joulemeter (Molectron J3-02) or with a phototube (Hamamatsu 1P39). The signal from the photodetector was averaged by a boxcar integrator (Molectron LP20) or a transient digitizer (Autonics S-210) which was interfaced (GP-IB) and controlled by a microcomputer (EPSON PC286VS).

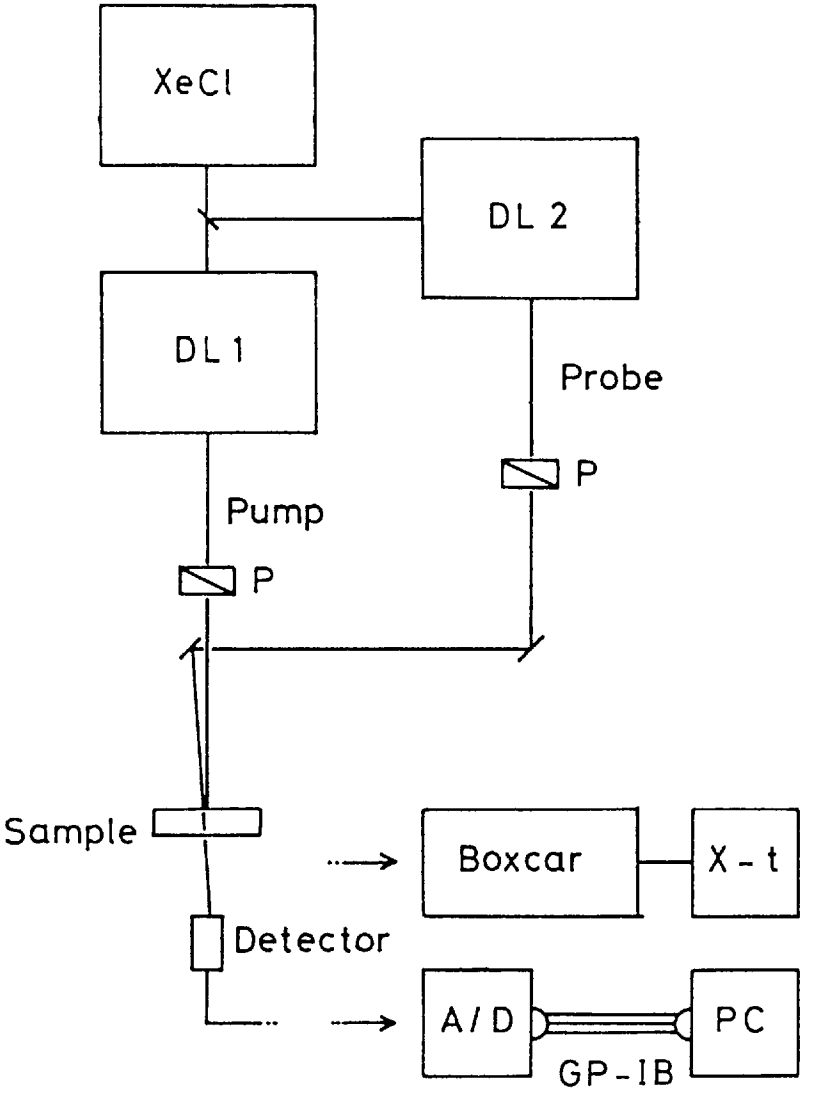

Fig. 4.2 Experimental arrangement for transient absorption measurements.

4.3 Transient absorption spectra in organic crystals

4.3.1 Principle of measurement

When an organic crystal is excited with a UV laser pulse, singlet excitons are generated in the crystal. In the case of strong absorption excitation, the sample specimen is easily damaged by intense laser pulse (Fig. 4.3 (a)). To avoid such a excitation damage multi-pass or multi-sample technique was used [4.9]. In the present study absorption edge excitation technique was used to avoid the sample damage (see Fig. 4.3 (b)). The number of excitons generated in the crystal is independent of the absorption coefficient when the absorption is complete. In anthracene, λ = 420 nm light is used for excitation. The penetration depth of 420 nm light is 270 μ m when polarized parallel to the crystal a-axis, and it is 50 μ m with polarization parallel to the crystal b-axis [4.10]. In this way a known number of excitons can be generated in a crystal at a low density. With these large penetration depths, the damage of a sample by intense laser pulses is not a serious problem, and absorption measurements can be made with a single pass.

The absorbance (A) due to exciton is given by $A = \log(I_0/I)$, where I_0 is the intensity of the probing light pulse recorded without the excitation pulse and I is the intensity with the excitation pulse present.

4.3.2 Anthracene

In anthracene transient absorption could be measured with

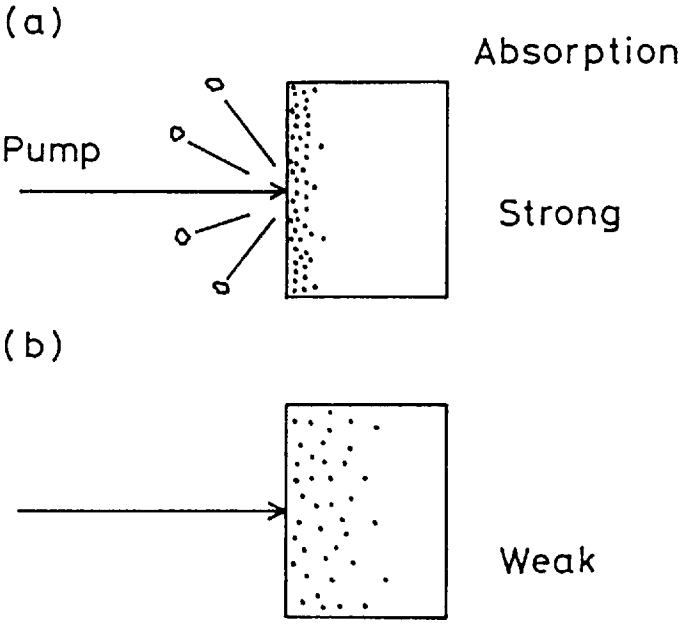

Fig. 4.3 Principle of the absorption edge excitation. (a) Strong absorption condition. Sample specimen is easily damaged. (b) Weak absorption condition.

absortion edge excitation (λ_1 = 420 nm). The decay of the transient absorption in an anthracene crystal at λ_2 = 580nm is shown in Fig. 4.4. The absorption decays with a time constant of 25 ± 10 ns, which agrees with the lifetime of singlet exciton [4.11]. This indicates that the observed absorption is due to the transition from the lowest excited singlet state (S*) to a higher excited singlet state (S**). A slow component can also be seen in the figure. This may be due to transition from the lowest excited triplet state (T*) to a higher triplet excited state (T**).

Figure 4.5 shows the absorbance due to S* as a function of the exciting light intensity I_1. The E vector of the excitation pulse E_1 is parallel to the crystal a-axis and E vector of the probe pulse E_2 (λ =585nm) is parallel to the crystal b-axis. It is observed that the absorbance is proportional to $I_1^{1/2}$. This indicates that fusion of singlet excitons dominates under these experimental conditions (see Eq.3.7).

Transient absorption spectrum in an anthracene crystal is shown in Fig. 4.6 for different polarizations. The excitation and probe pulses irradiated the sample specimen simultaneously. The E_1 (λ_1 = 420nm) is parallel to the crystal a-axis in (a) and (c), and is parallel to the b-axis in (b) and (d) in Fig.4.6. The E_2 (λ_2 = 485-610nm) is parallel to the a-axis in (a) and (b), and is parallel to the b-axis in (c) and (d). The result (a) is similar to (b) and (c) is similar to (d). Obviously the spectrum depends on the E_2 and irreverent on the E_1. This insensitivity to the E_1 indicates that the S* absorption occurs after a vibrational relaxation of the hot singlet exciton state

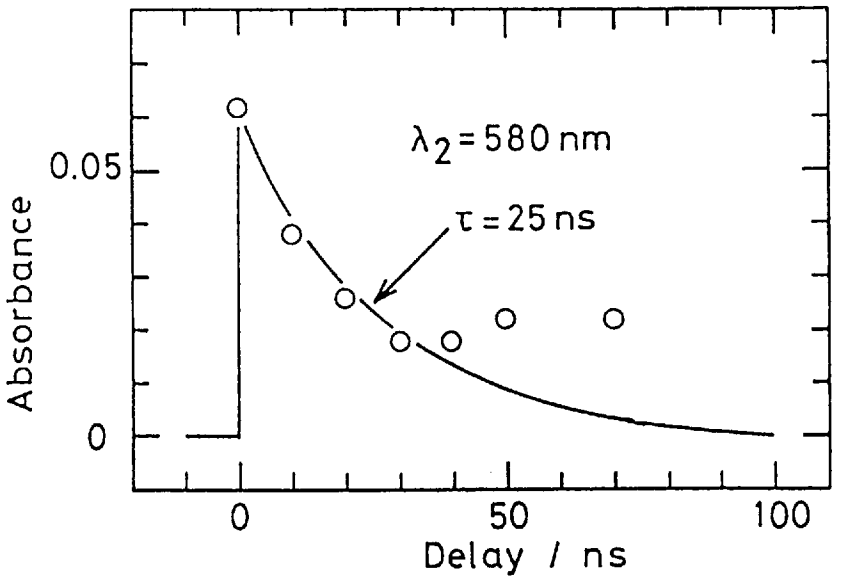

Fig. 4.4 The decay of the transient absorption in an anthracene crystal with λ_2 = 580nm light.

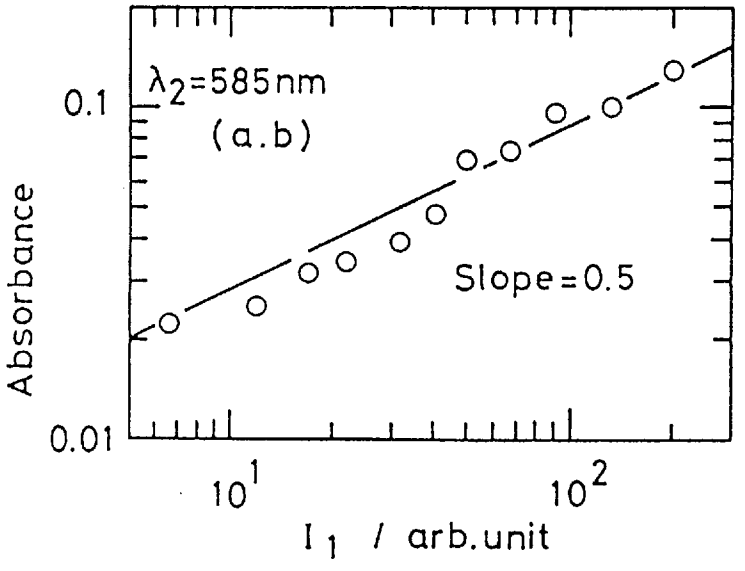

Fig. 4.5 Excitation light intensity (I_1) dependence of the absorption due to the singlet exciton in an anthracene crystal. (a,b): E_1 // a and E_2 // b.

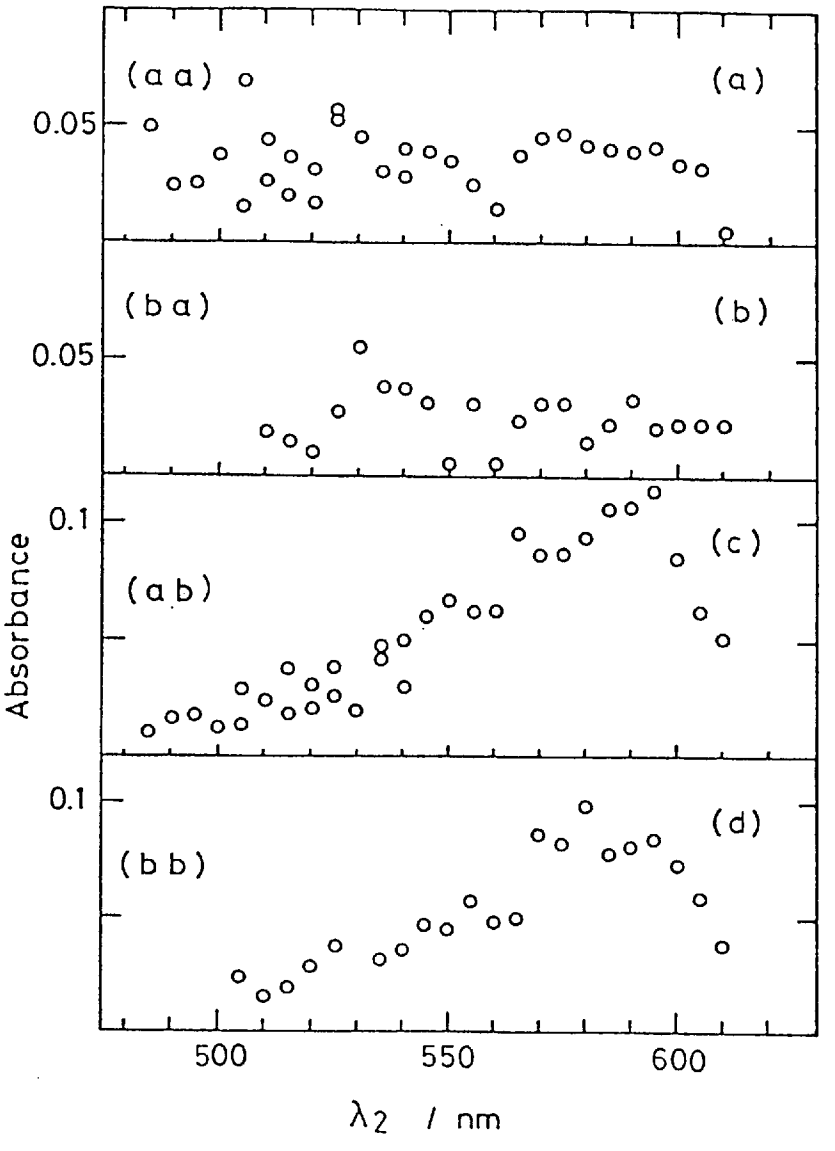

Fig. 4.6 Transient photoabsorption spectra in an anthracene crystal for different polarizations.

reached by the excitation from the ground state. Absorption with E_2//b (i.e., (c) and (d)) is stronger than that with E_2//a (i.e., (a) and (b)). A small difference in the optical density between (a) and (b), and likewise between (c) and (d) may be due to the difference in the reflectivity for the exciton generation pulse (λ_1 = 420nm). Figure 4.7 shows transient absorption in crystal in comparison with that of solution.

4.3.3 p-Terphenyl

To measure the transient absorption in p-terphenyl single crystal, excitation was made with λ_1 = 340nm light. This wavelength is in the absorption edge of this material. Penetration depth of 340nm is 100 μ m (see Appendix 1). Transient absorption spectra in solution and single crystal are shown in Fig. 4.8. The E_1 is parallel to the crystal b-axis and the E_2 is parallel to the crystal a-axis (b,a) and crystal b-axis (b,b). Absorbance is smaller in (b,a) spectrum. There are two peaks at 480 and 550 nm in (b,b) spectrum. The transient absorption spectrum which is delayed by 20 ns after excitation is shown in Fig. 4.9. The strong absorption due to singlet exciton is absent and the peak at 480 nm remain. Koshihara et al. have measured the transient absorption of this material in microcrystals using diffuse reflection spectroscopy [4.7]. They observed a long-lived state in the same wavelength range with the spectrum obtained and assigned the band as the transition from triplet exciton to higher excited state.

Figure 4.10 shows the absorbance as a function of exciting light intensity I_1. It may be seen that the absorbance is

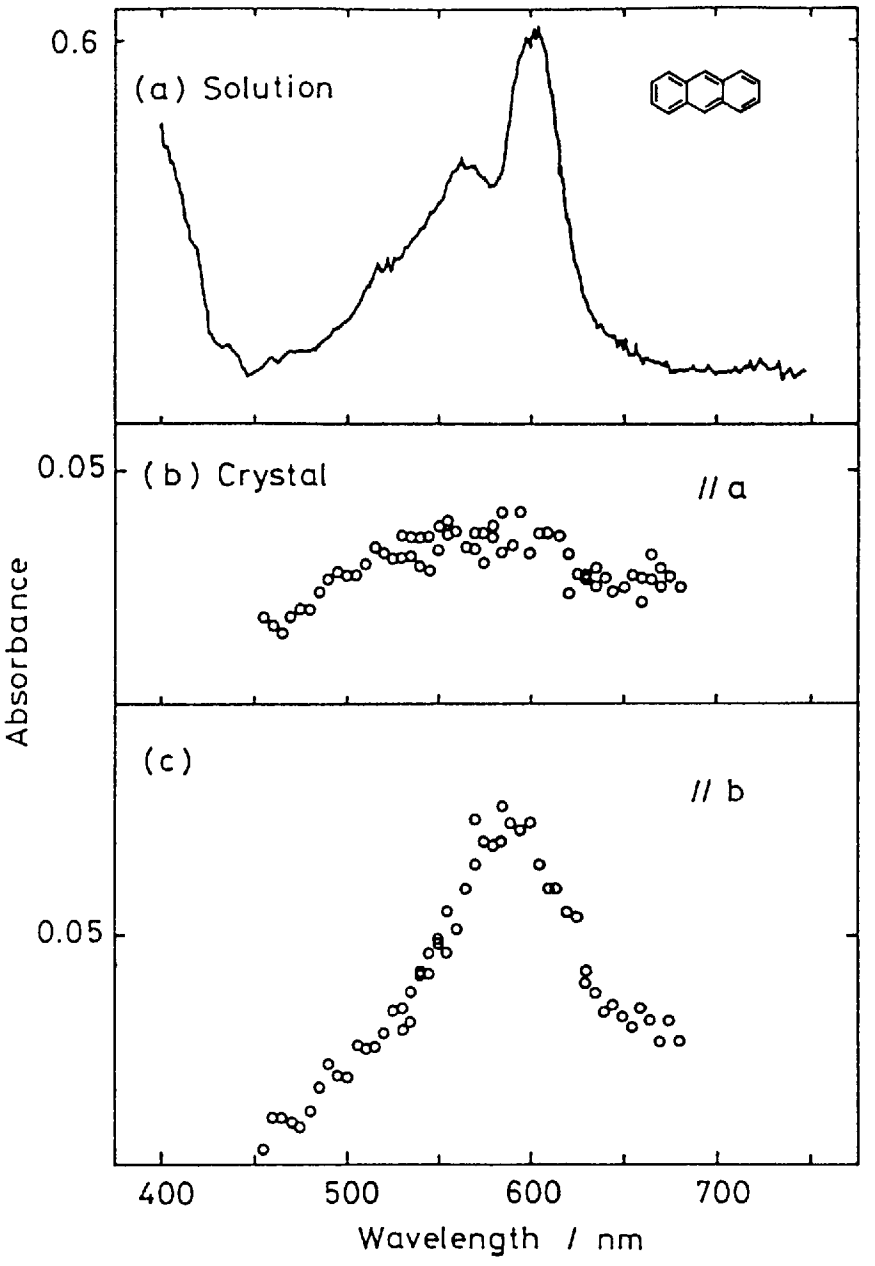

Fig. 4.7 Transient photoabsorption spectra in an anthracene solution (a) and crystal (b), (c).

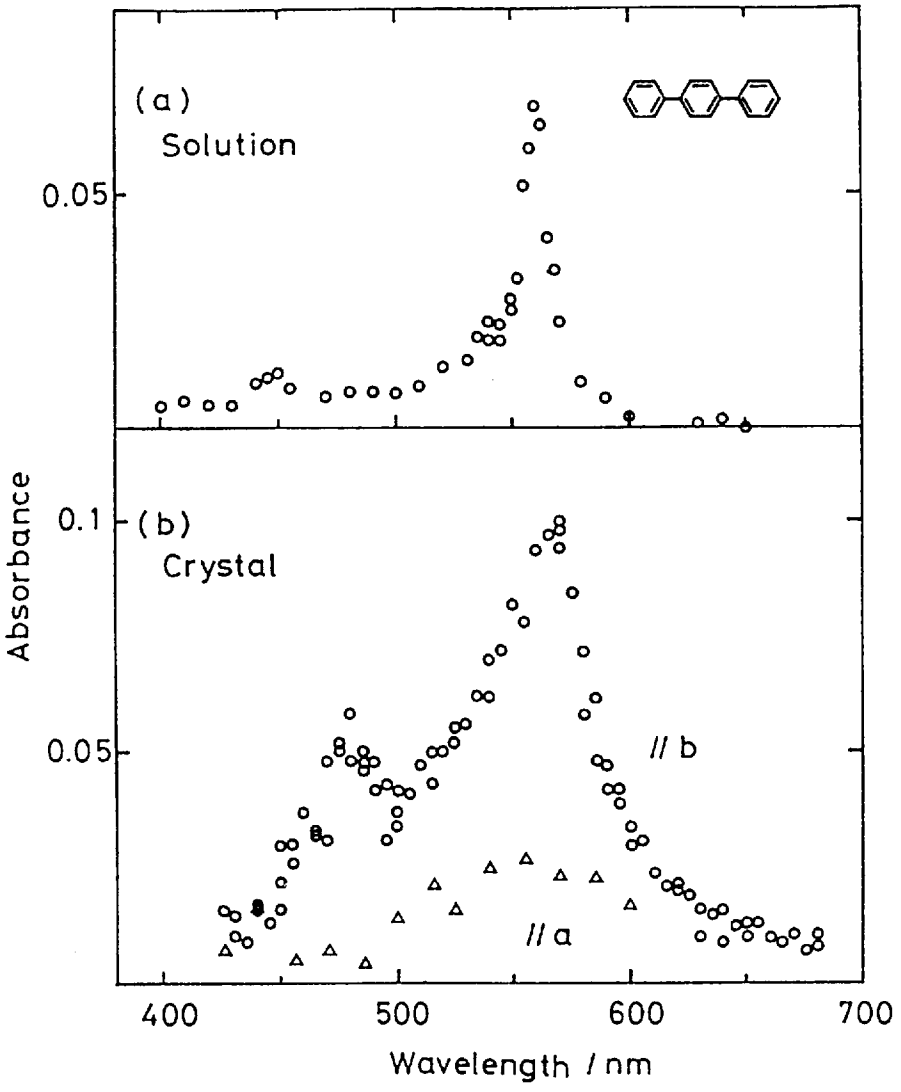

Fig. 4.8 Transient photoabsorption spectra in a p-terphenyl solution (a) and crystal (b). E_1 // b.

proportional to $I_1^{1/2}$. This indicates that annihilation of singlet exciton is the dominant decay route under the excitation conditions.

Transient absorption spectrum in solution [4.9] is also shown in Fig. 4.8. It agrees with that of crystal in a spectral range of absorption by singlet exciton. A slight red-shift was observed in the case of absorption due to the triplet exciton. This is due to different molecular geometries in the triplet excited state between the solution and the solid [4.7].

4.3.4 trans-Stilbene

The wavelength of exciting light was 360 nm, which is in the absorption edge of a trans-stilbene crystal. Transient absoption spectra are shown in Fig. 4.11. The E_1 is parallel to the crystal c-axis and the E_2 is parallel to the crystal b-axis in the (c,b) spectrum and paralell to the crystal c-axis in the (c,c) spectrum. A strong peak was observed at 580nm in (c,b). Its lineshape is similar to that of solution with a slightly narrower spectral width. In (c,c) spectrum absorption of singlet exciton was much weaker. In this material, transient absorption spectrum in the crystalline state is similar to that of solution (Fig. 4.11) [4.12].

Absorbance due to singlet exciton is shown as a function of the exciting light intensity in Fig. 4.12. It may be seen that the absorbance is proportional to $I_1^{1.0}$. This dependence is different from those observed with anthracene and p-terphenyl crystals. This indicates that singlet exciton annhilation is not

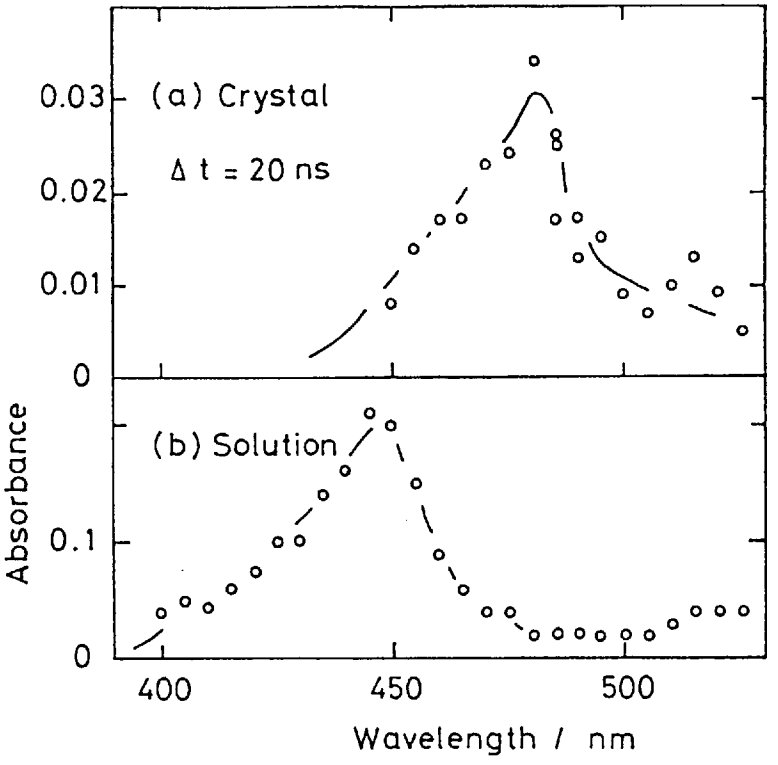

Fig. 4.9 Transient absorption due to triplet exciton in a p-terphenyl crystal (a) and solution (b).

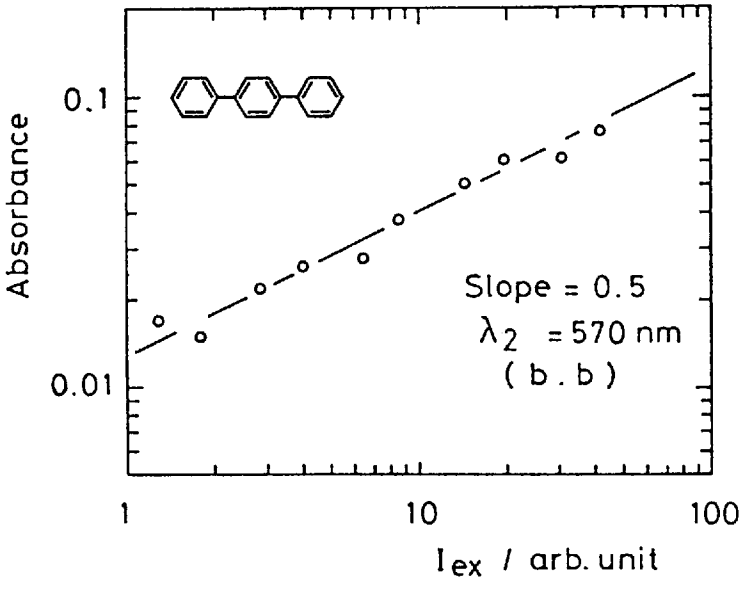

Fig. 4.10 Excitation light intensity (I_1) dependence of the absorption due to the singlet exciton in a p-terphenyl crystal.

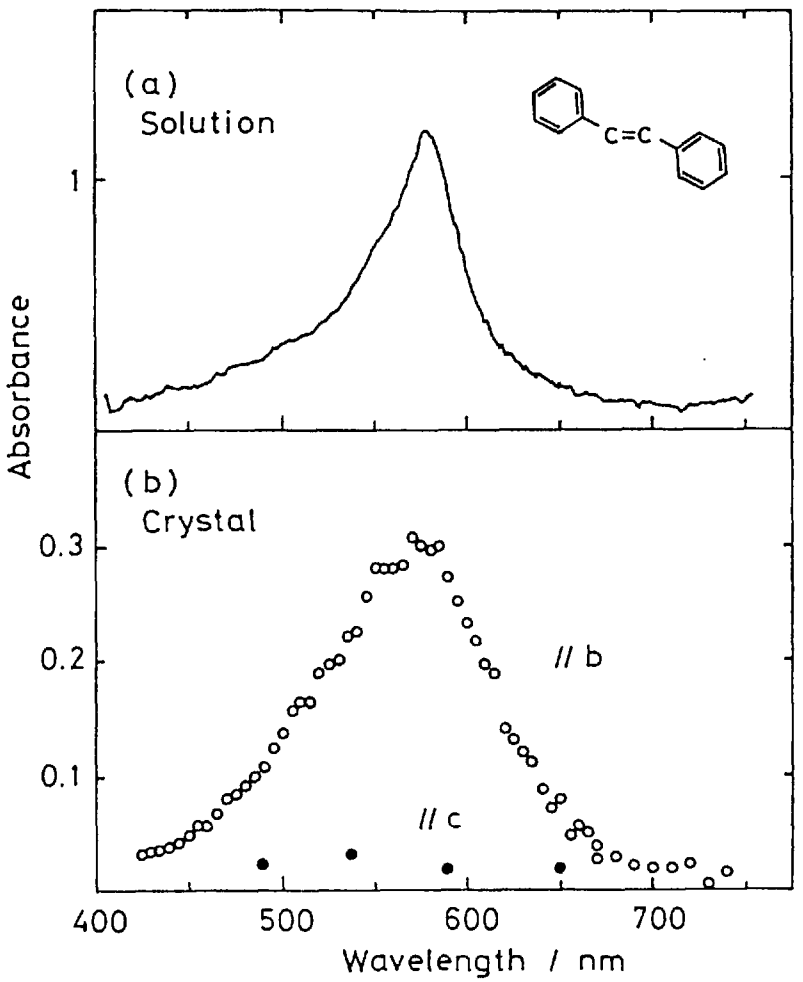

Fig. 4.11 Transient photoabsorption spectra in a trans-stilbene solution (a) and crystal (b). E_1 // c.

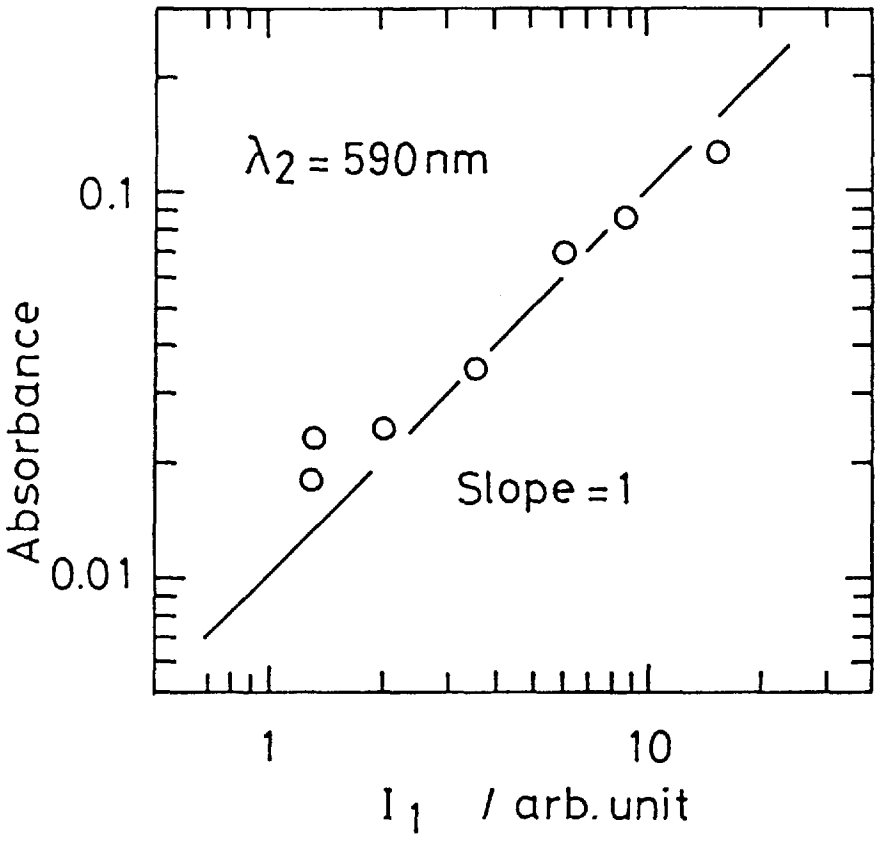

Fig. 4.12 Excitation light intensity (I_1) dependence of the absorption due to the singlet exciton in a trans-stilbene crystal.

efficient in this material under the excitation condition studied.

4.3.6 Some common features of the spectra

Transient absoption spectra in anthracene, p-terphenyl and trans-stilbene crystals are presented in the previous sections. Common features of these spectra are as follows:

(1) The spectra in the crystals are similar to those of the solutions. This similarity indicates that electronic properties of molecules are largely preserved in the crystal. This seems to be resonable when I thisk about intermolecular interaction in organic crystals.

(2) The spectra are strongly polarized. Molecules are oriented in the crystal. Accordingly, transition dipoles are also oriented. Hence, transient absorption should be observed only for polarization along a paticular axis of the crystal.

4.4 Cross sections for transient absorption

The kinetics of generation and decay of singlet excitons S* can be written by Eq. (3.1). The absorbance (A) due to $S^{**} \leftarrow S^{*}$ is given by

$$A = \sigma_A [S^*] x, \tag{4.1}$$

where σ_A is the cross section for $S^{**} \leftarrow S^{*}$ absorption and x is the interaction distance between exciting light and S* with the singlet exciton. The $S^{**} \leftarrow S^{*}$ absorption cross section can be estimated from Eq.(4.1) by using the values of [S*] and x. In the present experimental condition the exciting light is absorbed completely, therefore, penetration depth of exciting light x is given by $1/\alpha$. When annihilation of the singlet excitons is the dominant decay process, density of the S* is given by (cf. Eq. (3.1))

$$[S^*]=[(\alpha / \gamma_{SS}) I_{ex}]^{1/2}. \tag{4.2}$$

In anthracene and trans-stilbene the steady state apporoximation is not valid because the lifetime of singlet exciton (anthracene; 20 ns [4.13], trans-stilbene; 14 ns [4.14]) is longer than pulse duration of exciting light (8 ns). Hence, the singlet exciton concentration [S*] was computed numerically with Eq. (3.1). On the other hand, in p-terphenyl lifetime of singlet exciton (2.1 ns [4.15]) is shorter than pulse duration, therefore, the concentration of the singlet exciton can be caluculated using Eq. (4.2).

Absolute cross sections for transient absorptions in these materials are summarized in Table 4.1.

Table 4.1 Cross sections for the photoabsorption due to the singlet exciton in the materials studied.

	λ_2	Polarization	E_{s_1}	Excitation energy	Cross section σ_A
	nm		eV	eV	cm^2
Anthracene	585	(a,b)	3.11	5.23	1.8×10^{-17}
p-Terphenyl	570	(b,b)	3.69	5.88	1.8×10^{-17}
trans-Stilbene	590	(c,b)	3.60	5.70	7.0×10^{-18}

Excitation energy = $E_{s_1} + h\nu_2$

References

[4.1] M.Higuchi, T.Nakayama and N.Itoh,
J. Phys. Soc. Japan 40 (1976) 250.

[4.2] J.M.Morris and K.Yoshihara,
Mol. Phys. 36 (1978) 993.

[4.3] L.R.Williams and K.A.Nelson,
J. Chem. Phys. 87 (1987) 7346.

[4.4] L.Zeiri, G.Berkovic and Z.Ludmer,
Chem. Phys. Lett. 147 (1988) 279.

[4.5] F.Wilkinson and C.J.Willsher,
Chem. Phys. Lett. 104 (1984) 272.

[4.6] N.Ikeda, M.Koshioka, H.Masuhara and K.Yoshihara,
Chem. Phys. Lett. 150 (1988) 452.

[4.7] M.Koshihara, H.Mizuma, K.Imagi, N.Ikeda, H.Fukumura,
H.Masuhara and C.Kryschi.
Bull. Chem. Soc. Jpn. 63 (1990) 3495.

[4.8] Z.Ludmer, L.Zeiri and S starobinets,
Phys. Rev. Lett. 48 (1982) 341.

[4.9] E.Morikawa, K.Shikichi, R.Katoh and M.Kotani,
Chem. Phys. Lett. 131 (1986) 209.

[4.10] A.Matsui.
J. Phys. Soc. Japan 21 (1966) 2212.

[4.11] N.Karl,
in: Landort-Burnstein numerical data and fundamental relationships in science and technology, New series, Vol.17, eds. O.Madelung, M.Schulz and H.Weiss (Springer, Berlin, 1985).

[4.12] H.Miyasaka,
Ph.D. thesis, Department of Chemistry, Faculty of Engineering Science, Osaka University (1985).

[4.13] H.Nishimura, T.Yamaoka, K.Hattori, A.Maysui and M.Mizuno,
J. Phys. Soc. Japan 54 (1985) 4370.

[4.14] R.Katoh, E.Yamazaki and M.Kotani,
to be published.

[4.15] A.C.Jones, K.J.Styrcz, D.A.Elliott and J.O.Williams,
Chem. Phys. Lett. 80 (1981) 413.

5. Photocarrier generation via excited states

5.1 Introduction

5.1.1 Survey of the studies of photoconductivity in aromatic hydrocarbon crystals

Studies of photoconduction in organic crystals date back to the beginning of this century [5.1]. Photoconductivity depends on surface conditions and kinds of electrodes, and could not be understood easily in early studies. Such photoconduction, which is extrinsic one, can be due to carrier injection from an electrode or impurities on the surface or exciton dissociation at the surface of a crystal. First observation of an intrinsic photoconduction was made in anthracene crystal by Castro and Hornig in 1965 [5.2].

$$S_0 \xrightarrow{h\nu} e^- + h^+ .$$

Geacintov and Pope studied extensively the intrinsic photoconductivity [5.3-4]. They have measured photocarrier yields as a function of the excitation energy and explained the action spectra for photoconductivity based on energy levels of the valence band [5.5]. Kepler [5.6] and LeBlanc [5.7] have established a time-of-flight technique for measuring photocondutivity in organic crystals. The yields of photoelectrons and their drift mobilities can be measured directly by this technique.

When an anthracene crystal is excited with near-UV light, singlet excitons are generated and a photocurrent which is

proportional to the squre of the exciting light intensity can be observed. It is due to the fusion (annihilation) of two singlet excitons S^*.

$$S^* + S^* \rightarrow e^- + h^+ .$$

Jortner observed such a photocurrent in anthracene [5.8] and made a theoretical description [5.9]. Braun have found this type of photoconductivity in anthracene [5.10] and in naphthalene [5.11].

Photoionization of some excited states has also been observed. Kepler observed photoconductivity in an anthracene crystal with three-photon excitation using a ruby laser [5.12]. He concluded that the photocurrent was due to photoionization of singlet exciton generated by two-photon absorption.

$$S_0 \rightarrow S^* \rightarrow e^- + h^+ .$$

$$2h\nu \quad h\nu$$

Bergman and Jortner [5.13] and Schott et al. observed photocurrent due to photoionization of singlet exciton with steady state excitation [5.14]. Morikawa and Kotani found the same type of photoconductivity with two-color, two-step excitation in p-terphenyl [5.15-17] and in naphtalene [5.18].

$$S_0 \rightarrow S^* \rightarrow e^- + h^+ .$$

$$h\nu_1 \quad h\nu_2$$

Holzman et al. reported photoconductivity due to photoionization of triplet excitons [5.19].

Photoconductivity measurements with multi-photon excitation become possible with the development of lasers. Strome et al. made the first observation of photoconductivity with two-photon excitation [5.20].

$S_0 \rightarrow e^- + h^+$.

$2h\nu$

Using a dye laser, Kepler measured an action spectrum for photoconductivity in an anthracene crystal with two-photon excitation [5.21]. By comparing the action spectrum for photoconductivity with excitation spectrum of two-photon-excited fluorescence he obtained ionization efficiency as a function of excitation energy and found that it steeply increased with the photon energy. He concluded that ionization occurred due to band-to-band transition. Bergman and Jortner also found this type of photoconductivity [5.13].

5.1.2 Two-color, two-step excitation method

Photoconductivity is very sensitive to surface conditions. This sensitivity to surface conditions can be reduced when charge carriers are generated in the bulk of a solid. This can be realized by two-color, two-step excitation. Figure 5.1 illustrates the principle of the method. Exciton are generated homogeneously in the bulk of a crystal by a weakly absorbed light (λ_1), and are photoionized with light (λ_2), for which the solid in the ground state is transparent. By changing the photon energy of the ionizing light it is possible to change the excitation energy without introducing difficulties associated with the changing penetration depth.

The nature of the intermediate state can be investigated by observing transient absorption spectrum, as well as its decay kinetics. By comparing the exciton absorption spectrum (Abs) (see § 4) with the photoionization spectrum of the exciton (PI)

it is possible to determine the ionization efficiency (Φ) of the higher excited state. Details of discussion on the ionization efficiency will be presented in § 6.

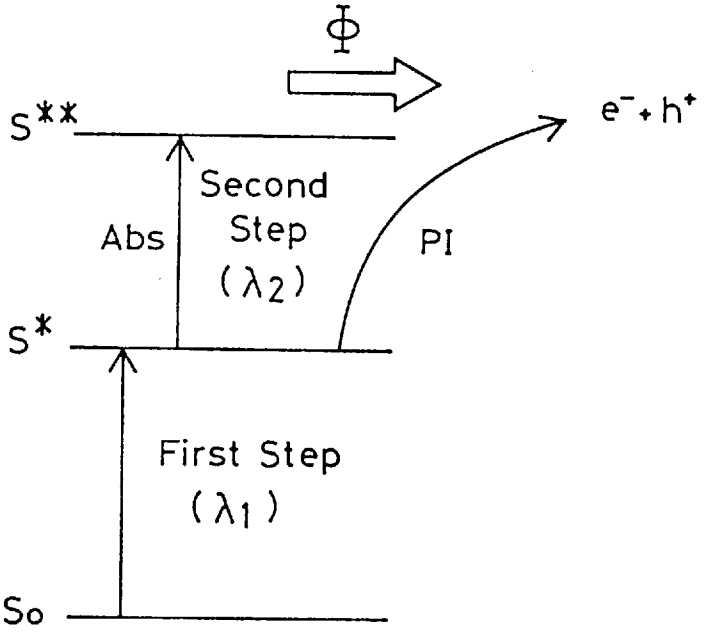

Fig. 5.1 Principle of two-color, two-step excitation.

5.2 Principle of photoconductivity measurements

5.2.1 Introduction

The principle of the time-of-flight method is illustrated in Fig. 5.2. When charge carriers, generated near the surface of a crystal, move along the direction of an electric field, a current is induced in the external circuit. The current can be displayed on an oscilloscope. A typical waveform of the photocurrent pulse with excitation with a strongly absorbed light is shown in Fig. 5.3. The number of carriers generated N can be evaluated using Eq. (5.1).

$$N = (V_i \times R)\tau , \qquad (5.1)$$

where V_i is the initial photovoltage with load resistor R and τ is the transit time of charge carriers. The number of generated carriers N is a function of exciting light intensity, external electric field, temperature and excitation energy.

Mobility of charge carriers μ can be obtained from the transit time τ .

$$\mu = d/(\tau E), \qquad (5.2)$$

where d is the thickness of the sample specimen and E is the electric field applied.

5.2.2 Apparatus for measurement

Experimental arrangement for photoconductivity measurements is shown in Fig. 5.4. Single crystals, cleaved from ingots, were used as sample specimens (typically 5 mm× 5 mm× 0.8 mm in size).

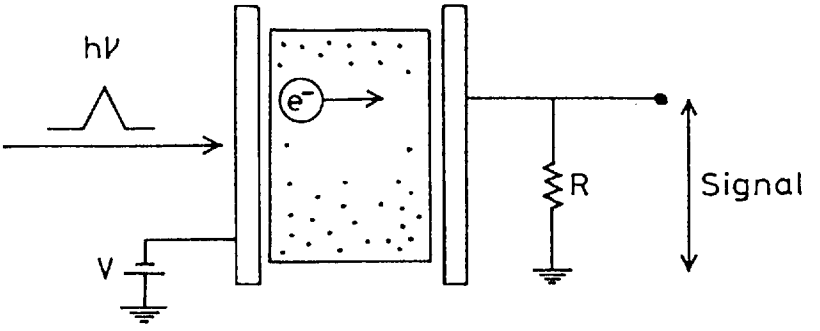

Fig. 5.2 Principle of time-of-flight method.

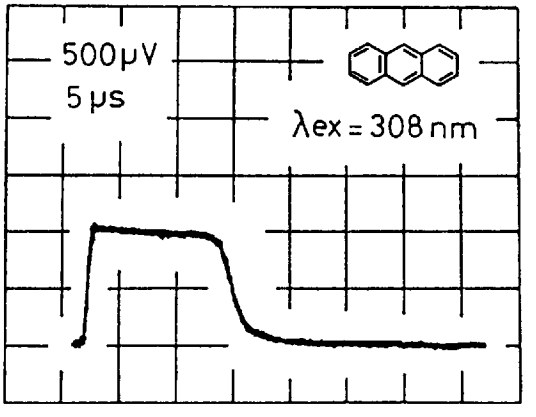

Fig. 5.3 Typical waveforms of plsed photoconductivity (anthracene, with λ = 308 nm excitation).

Electrodes were pressed against the crystal but were not in direct contact with it in order to avoid possible photoinjection of charge carriers from the electrodes. Thin mylar sheet (12 μ m thick) was used as a spacer. A semi-transparent tin oxide on quartz substrate was used as the front and back electrodes. The exciting light was incident normal to the cleavage plane of the sample specimen. Laser beam of about 2 mm diameter irradiated the sample through a pinhole (1 mm diameter) and the front electrode. An electric field was applied normal to the cleavage plane. Photocurrent was measured across a load resistor, typically of 500 Ω , with an oscilloscope (Tektronix, 7623A with plug-in 7A22). This was a very sensitive system and was used when the rise time of this system, about 400 ns, could be tolerated. To measure a fast signal, such as an initial decay due to volume recombination (see Fig. 5.8 (a)), a faster detection system (plug-in 7A16A, load resistance; 50 Ω) with 20ns rise time was used. For measurements of a temperature dependence a stainless steel electrode equipped with an electric heater was used as the back electrode. In this case a thin glass plate (50 μ m thick) was used as a spacer instead of the mylar sheet. Temperature of the sample specimen was measured with a cupper-constantan thermocouple. Temperature could be increased up to 100 ℃ for an anthracene crystal. When photoconductivity was to be measured at high electric fields, the sample and electrodes were housed in a gas cell, which was filled with SF_6 to 5 bar. The SF_6 suppressed efficiently the electric discharge so that it enabled measurements at high fields up to 1.8×10^7 V/m.

For one-color, two-photon measurements (§ 5.4 and 5.6) a

dye laser (Lambda Physik, FL-3002), pumped by a XeCl excimer laser (Lambda Physik, EMG 101 MSC), was used as the exciting light source. Polarization of the laser pulse was controlled with a polarizer (Lambda Physik FL50) . For two-color, two-step excitation measurements (§ 5.5 and 5.6) two dye lasers (Lambda Physik FL-3002, and a home made one), pumped by a common XeCl excimer laser (Lambda Physik EMG 101 MSC) was used. Polarization of the laser pulses were controlled with polarizers (Lambda Physik FL50 and Polaroid HN38). In measurements in which two laser pulses were used with a delay, the homemade dye laser which is pumped by another XeCl laser (Lumonics TE-860-2) or a YAG laser (Quanta Ray DCR-2/2A) were used for generation of the second-step (ionizing) pulse. The jitter between the laser pulses was ± 5 ns.

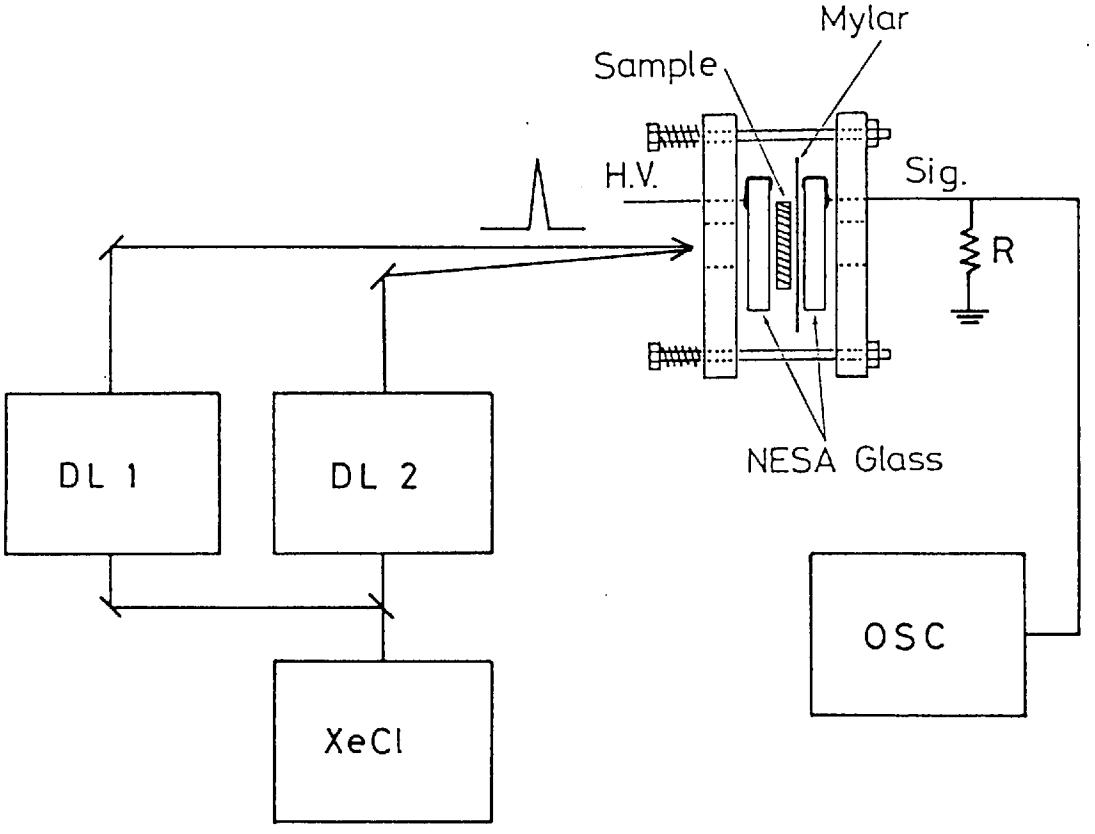

Fig. 5.4 Experimantal arrangement for observing photoconductivity.

5.3 Charge carrier mobility

There have been many studies of mobilities of electrons and holes in organic crystals [5.22-23]. Photocurrnet waveforms are sensitive to the presence of impurities and defects. When these traps are present, the charge carriers are captured during their transit to show a decrease of the photocurrent.

Figure 2.4 shows the waveforms for the electron and the hole in materials studied ((a) anthracene, (b) p-terphenyl and (c) trans-stilbene) with excitation by λ = 308 nm light. Rectangular waveforms indicate that there is no significant impurities in the crystals except for the electrons in trans-stilbene. Figure 5.5 shows reciprocal transit time as a function of the electric field for hole in trans-stilbene. Mobilities can be evaluated using Eq. (5.2) from electric field dependence of the transit time. The mobilities studied are summarized in Table 5.1. These values are in fair agreement with reported values except for the electrons of trans-stilbene [5.22-26]. Figure 5.6 shows the charge carrier mobilities as a function of temperature in an anthracene crystal.

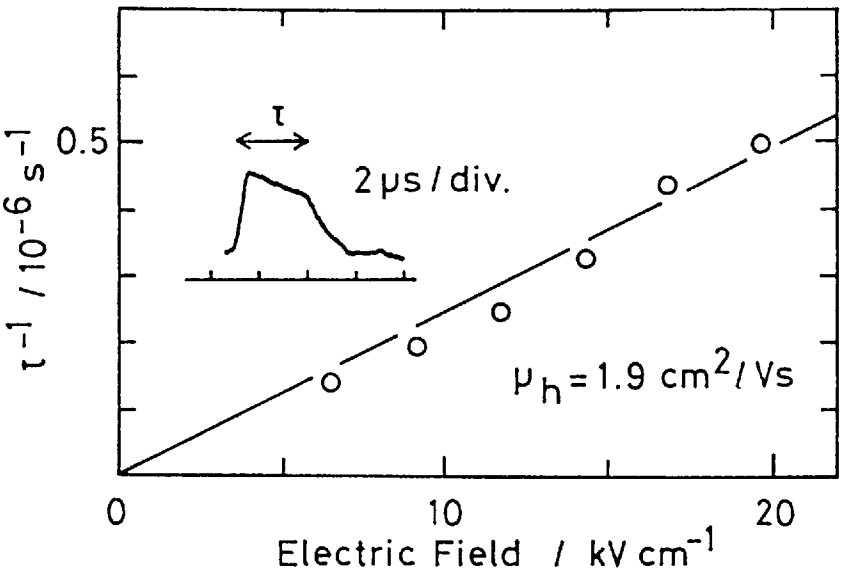

Fig. 5.5 Reciprocal transit time against electric field in trans-stilbene.

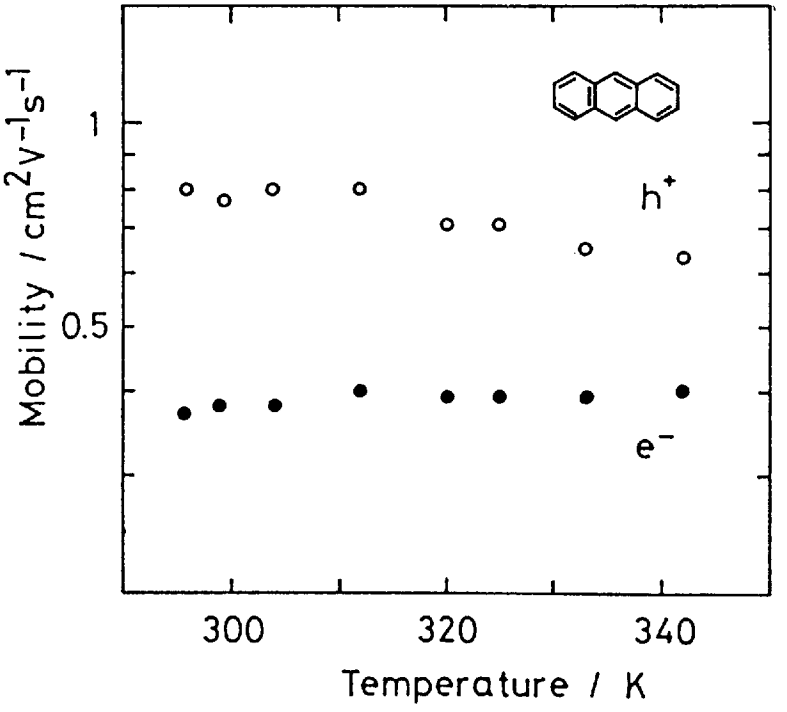

Fig. 5.6 Temperture dependence of the charge carrier mobilities in anthracene.

Table 5.1 Charge carrier mobilities of materials studied.

	Mobility / $cm^2\ V^{-1}\ s^{-1}$	
	Electron	Hole
Anthracene	0.46	0.83
p-Terphenyl	0.38	0.46
trans-Stilbene	———	1.9

2

5.4 Photoionization of singlet exciton through one-color, two-step excitation

5.4.1 Introduction

In this section photoconductivity involving the lowest singlet excited state as an intermediate state will be discussed. There are two possible mechanisms; photoionization of singlet exciton (PI) and collisional ionization of two singlet excitons (CI). Figure 5.7 illustrates a kinetic scheme for two mechanisms. Charge carrier generation is found to be due to photoionization of singlet exciton which is determined by a kinetic analysis for singlet excitons and charge carriers. Cross sections for photoionization of singlet exciton is estimated in antharcene, p-terphenyl and trans-stilbene crystals.

5.4.2 Photocurrent waveforms with 420 nm light excitation

Figure 5.8 shows photocurrent waveforms when an anthracene crystal is excited under various conditions. The time resolution of the measurement system is about 400 ns. In (a) the crystal is excited weakly with 308 nm light which is strongly absorbed. The rectangular waveform indicates that charge carriers are generated close to the irradiated surface. The waveforms (b), (c) and (d) are observed with λ = 420 nm excitation in the absorption edge of the ground state. The trace (b) is observed with excitation light polarized parallel to the crystal b-axis. Both electrons and holes are contributing to the current and, as a result, the waveform deviates from the rectangular shape. The penetration

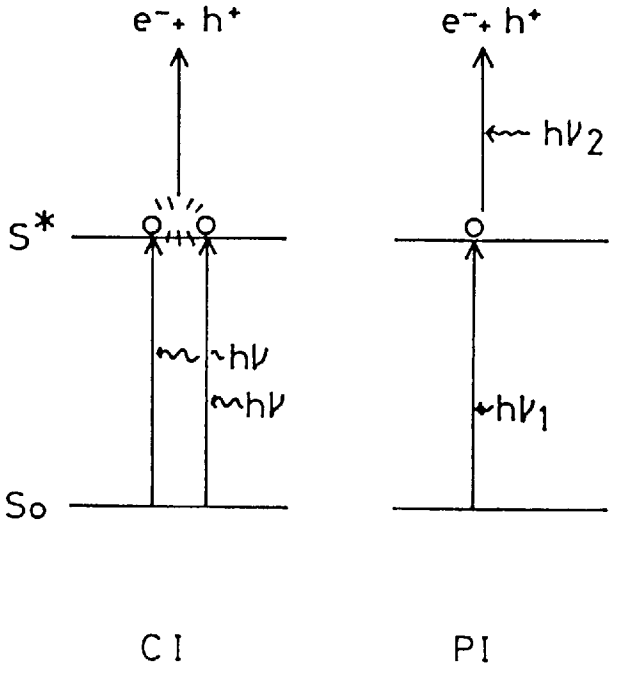

Fig. 5.7 Kinetic scheme for the charge carrier generation; PI: photoionization of singlet exciton, CI: collisional ionization by fusion of two singlet excitons.

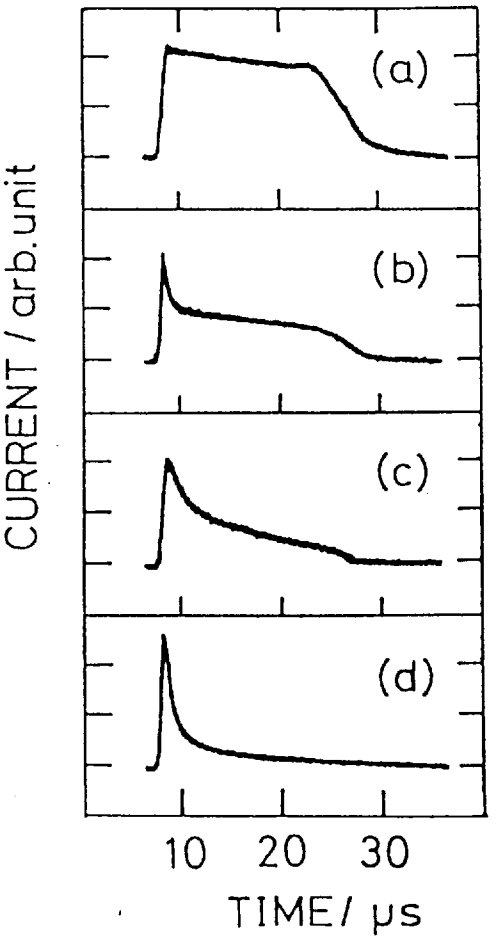

Fig. 5.8 Photocurrent waveform in anthracene. Illuminated side negative. (a) 308 nm excitation, (b) 420 nm excitation, b-polarized, (c) 420 nm excitation, a-polarized, (d) with strong 420 nm excitation, a-polarized.

depth of λ = 420 nm light is 270 μ m when it is polarized parallel to the a-axis and 50 μ m with polarization parallel to the b-axis [5.27]. The difference in the absorption coefficient is reflected in the photocurrent waveforms, as seen in (b) and (c). If direct two-photon ionization occurs, its cross section may be much smaller and accordingly the photocurrent waveform will become triangular in shape. The fact that the spatial distribution of the generated charge carriers corresponds to the penetration profile of the incident light indicates that the singlet exciton is a real intermediate state in charge carrier generation. When the light intensity is increased to $\sim 10^{23}$ photons cm^{-2} s^{-1} the waveform (d) is observed. The fast decay in (d) is caused by the volume recombination of electrons and holes [5.28], as will be described below.

5.4.3 The number of generated charge carriers as a function of exciting light intensity

Figure 5.9 shows the number of generated carriers N as a function of excitation light intensity I_{ex}. The excitation was made at λ = 420 nm (a-polarized) to avoid a high density excitation near the surface. It may be seen that N is proportional to the square of the excitation light intensity when the light intensity is below 2×10^{22} photons cm^{-2} s^{-1}. Above this intensity the exponent gradually decreases unit for $I_{ex}>5\times 10^{23}$ photons cm^{-2} s^{-1} we find $N \propto I_{ex}^{3/4}$. This intensity dependence, with an exponent of 3/4, will prove to be a key to the interpretation to be given.

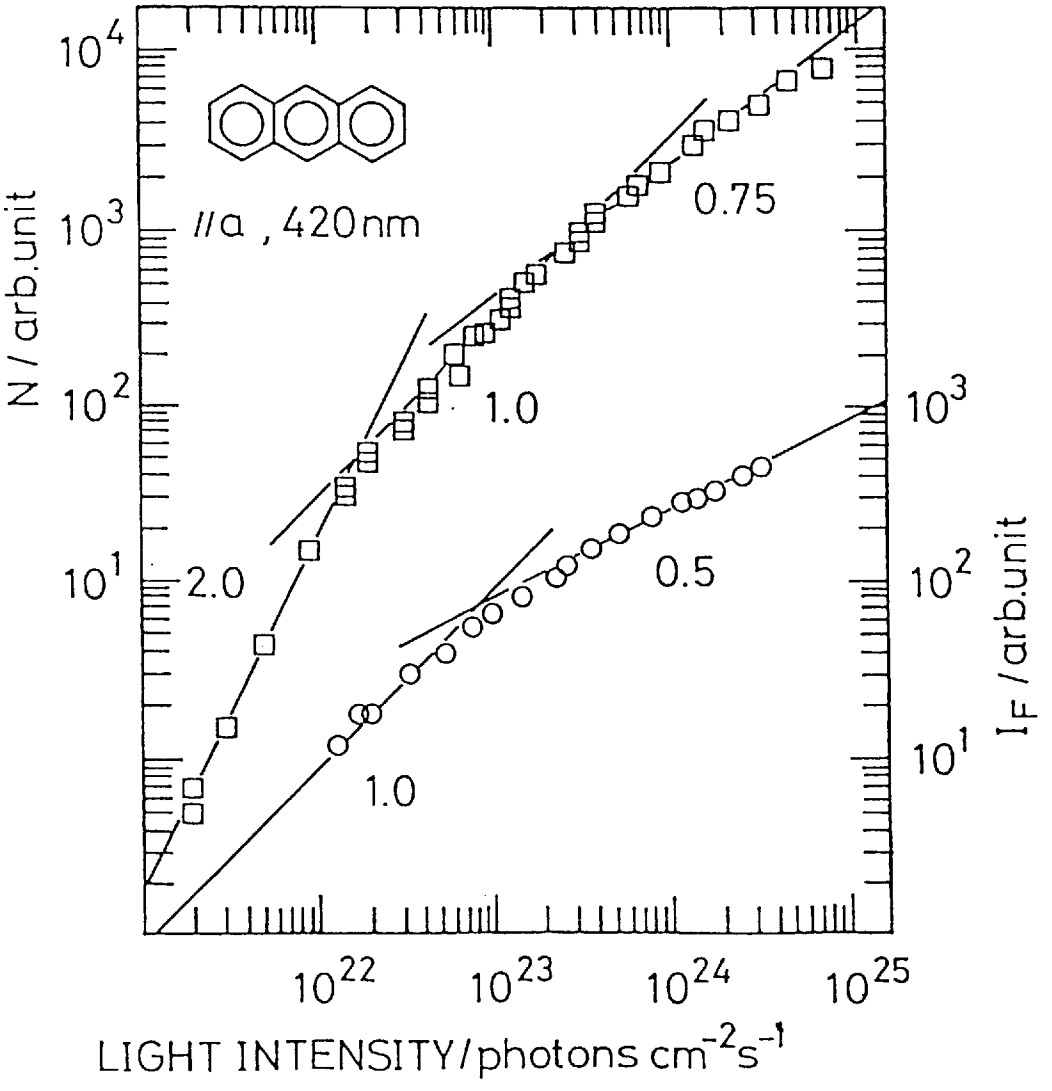

Fig. 5.9 Top: Number of charge carriers versus exciting light intensity I_{ex} (420 nm excitation, a-polarized) in anthracene. Bottom: Fluorescence intensity versus I_{ex}.

In Fig.5.9 is shows the fluorescence intensity I_F monitored under the same condition as that of photoconductivity. It may be seen that the fluorescence intensity is proportional to the intensity of the exciting light below 1×10^{23} photons cm^{-2} s^{-1}, and such a relationship is quite normal. Above this intensity, however, I_F becomes proportional to $I_{ex}^{1/2}$.

5.4.4 Kinetic analysis of the dependence on the exciting light intensity of charge carrier generation

There are two possible mechanisms of charge carrier generation involving a singlet exciton as an intermediate state which show a quadratic relationship to excitation light intensity (Fig. 5.9).

① Photoionization of a singlet exciton (PI case)

$$S^* + h\nu \rightarrow e^- + h^+ .$$

② Collisional ionization of two singlet excitons (CI case)

$$S^* + S^* \rightarrow e^- + h^+ .$$

The kinetics of the charge carriers is given by

$$d[N]/dt = GI_{ex}^2 - \gamma_{eh}[N]^2, \qquad (5.3)$$

where GI_{ex}^2 is the generation term, [N] is the density of the charge carriers and γ_{eh} is the rate constant of the volume recombination. When I_{ex} becomes large, the second term in the right hand side of Eq. (5.3) becomes progressively important. In the limit of high I_{ex} a stationary state is reached during the exciting pulse ($d[N]/dt = 0$) and [N] is proportional to I_{ex}. This is in qualitative agreement with the results in Fig. 5.9. The generation term GI_{ex}^2 can be written as

$$\Phi_{PI}\ \sigma_A\ [S^*]I_{ex}, \qquad (5.4)$$

for the PI case and

$$\Phi_{CI}\ \gamma_{SS}[S^*]^2, \qquad (5.5)$$

for the CI case, where Φ_{PI} and Φ_{CI} are the ionization efficiencies for singlet excitons in the respective cases, and σ_A is the $S^{**} \leftarrow S^*$ absorption cross section. With a strong excitation the singlet exciton concentration is given, from Eq.(3.7), by

$$[S^*] = \{(\alpha/\gamma_{SS})I_{ex}\}^{1/2}, \qquad (5.6)$$

which is, in the present experiment, on the order of 10^{17} cm^{-3} with $I_{ex} \sim 10^{24}$ photons cm^{-2} s^{-1} (see Fig. 5.9). By substituting Eq.(5.6) in Eqs.(5.3), (5.4) and (5.5), the density of charge carriers in the stationary state is given by

$$[N] = (\sigma_A\ \alpha^{1/2}\ \Phi_{PI}/\gamma_{eh}\ \gamma_{SS}^{1/2})^{1/2}\ I_{ex}^{3/4}, \qquad (5.7)$$

in the PI case and

$$[N] = (\alpha\ \Phi_{CI}/\gamma_{eh})I_{ex}^{1/2}, \qquad (5.8)$$

in the CI case. The experimental results ($N \propto I_{ex}^{3/4}$), clearly show that the photoionization of the singlet exciton (Eq. (5.7)) is a dominant process at this photon energy (λ = 420nm, i.e., $h\nu$ = 2.95eV).

5.4.5 Cross section for photoionization of singlet exciton in anthracene crystal with 420 nm (2.95 eV) excitation

In anthracene the stationary state approximation (Eq.(5.6), for example) is not strictly valid under the present experimental condition where the exciton lifetime (20 ns) is longer than the pulse duration τ_P (10 ns). Accordingly concentration of the singlet excitons was computed numerically with Eq. (3.1) to

estimate the photoionization cross section of singlet exciton under weak excitation, with Eq. (5.4),

$$\sigma_{PI} = \Phi_{PI}\sigma_A = [N]/\{[S^*]I_{ex}\tau_P\} \qquad (5.9)$$

It has been found that σ_{PI} is 3.5×10^{-19} cm^2 with an applied electric field of 1.5×10^6 V/m.

In p-terphenyl and trans-stilbene charge carrier generation by a biphotonic process is observed with absorption edge excitation (p-terphenyl: 340 nm, t-stilbene: 360 nm). Morikawa has reported that such a photocurrent in p-terphenyl is due to photoionization of singlet exciton [5.29]. In trans-stilbene the rate constant for fusion of two singlet excitons is small (see § 4.3). Hence, I assume that charge carriers are generated by photoionization of singlet exciton when a trans-stilbene crystal is excited at 360 nm light. The cross section for photoionization of singlet exciton can be estimated in these materials. A steady state apporoximation is valid in p-terphenyl where the lifetime of the singlet exciton is 2.1 ns [5.30]. In trans-stilbene this is not valid (lifetime of the singlet exciton: 14 ns [31]). Accordingly, $[S^*]$ is calculated numerically in Eq.(3.1). The cross sections are summarized in Table 5.2.

Table 5.2 Cross sections for photoionization of singlet exciton with absorption edge excitation.

	Wavelength	$E_{s.}$	Excitation energy	Cross section σ_{PI}
	nm	eV	eV	cm^2
Anthracene	420	3.11	6.1	3.5×10^{-19}
p-Terphenyl	340	3.69	7.35	4.1×10^{-19}
trans-Stilbene	360	3.60	7.04	3.3×10^{-19}

Excitation energy = $E_{s.}$ + photon energy

5.5 Photoionization of singlet exciton through two-color, two-step excitation

5.5.1 Introduction

In this section photoionization of singlet exciton in anthracene, p-terphenyl and trans-stilbene through two-color, two-step excitation will be presented. Action spectra of photoionization of singlet exciton are measured and cross sections for photoionization can be estimated.

5.5.2 Action spectrum for photoionization of singlet exciton

[Anthracene]

Singlet excitons are generated by a λ = 420 nm pulse, which is at the absorption edge of this material, as in the transient absorption measurements. A photocurrent is observed (the lower trace in Fig. 5.10) which is due to photoionization of singlet excitons (see § 5.4). The deviation of the current pulse shape from a square wave is due to the spatial distribution of singlet excitons which are to be photoionized. Both electrons and holes contribute to the current and the waveform deviates from the rectangular shape [5.15].

When a λ = 580 nm pulse (exciton-ionizing light: λ_2) irradiates a sample specimen simultaneously with the 420 nm pulse, an enhancement of the photocurrent is observed (the upper

trace in Fig. 5.10). The increase of the photocurrent is proportional to intensity I_2 of the 580 nm pulse. This is also the case when the wavelength of the exciton-ionizing pulse is 490 nm (Fig. 5.11).

This extra photocurrent decreases when the time interval between the exciton generating pulse (λ_1 = 420 nm) and the exciton-ionizing pulse (λ_2 = 580 nm) increases, as shown in Fig. 5.12. The decay has a time constant of 25 $\pm$ 10 ns. This time constant clearly indicates that singlet excitons are photoionized. A similar decay is also observed by irradiation of 1064 nm light (Fig. 5.13). In this case excitation energy ($E_{S^*} + h\nu_2$ = 3.11 + 1.17 [5.23]) is 4.28eV. Photoionization of singlet exciton is energetically possible in this excitation condition, because the excitation energy exceeds the proposed band gap of this material (4.1 eV [5.32-33]).

No photocurrent is observed when the crystal was excited with a λ = 580 nm pulse only. However, when the intensity of the 580nm pulse is much higher than normally used in the experiment, a triangular photocurrent signal is observed. This shape of the signal indicates that the carrier are generated homogeneously in the crystal. Figure 5.14 shows the fluorescence intensity as a function of intensity I_{ex} for two excitation wavelengths (λ_{ex}= 490, 580 nm). The quadratic intensity dependence indicates that singlet excitons can be populated only through two-photon absorption at this photon energy and supports the view that the visible light at λ = 490 nm or 580 nm is not absorbed with one photon absorption.

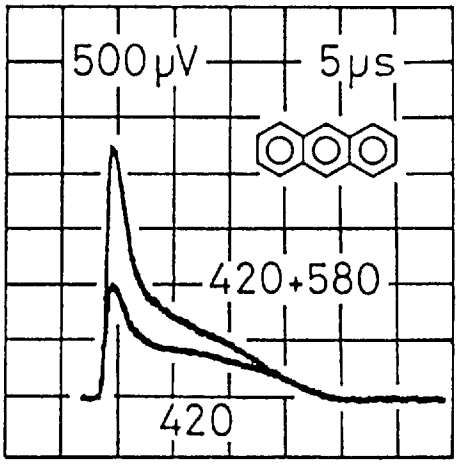

Fig. 5.10 Photocurrent waveform in anthracene. The lower trace is the photocurrent pulse with 420 nm light only. The upper part trace is the photocurrent pulse with simultaneous irradiation at 580 nm.

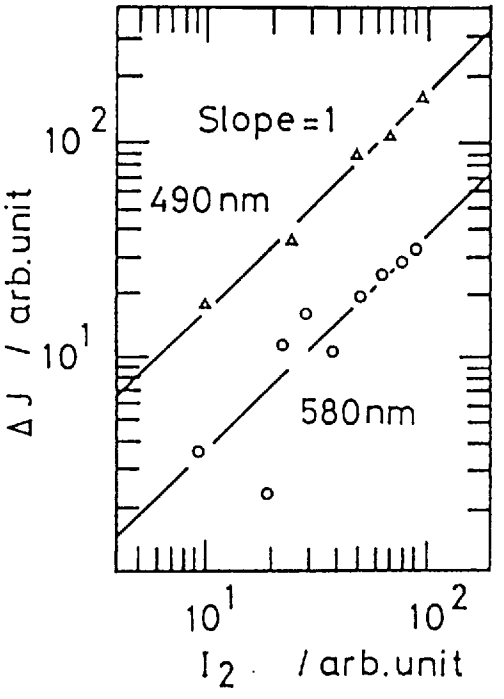

Fig. 5.11 Dependence of the excess photocurrent (△ j) on the ionizing pulse intensity (I_2) in anthracene.

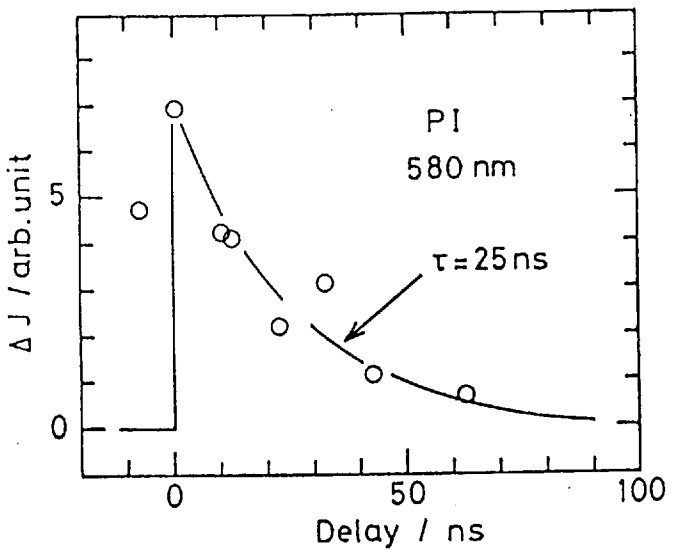

Fig. 5.12 The time dependence of the excess photocurrent on the delay between the two pulses (λ_2 = 580nm) in anthracene. The solid line indicates a decay curve with a time constant 25ns.

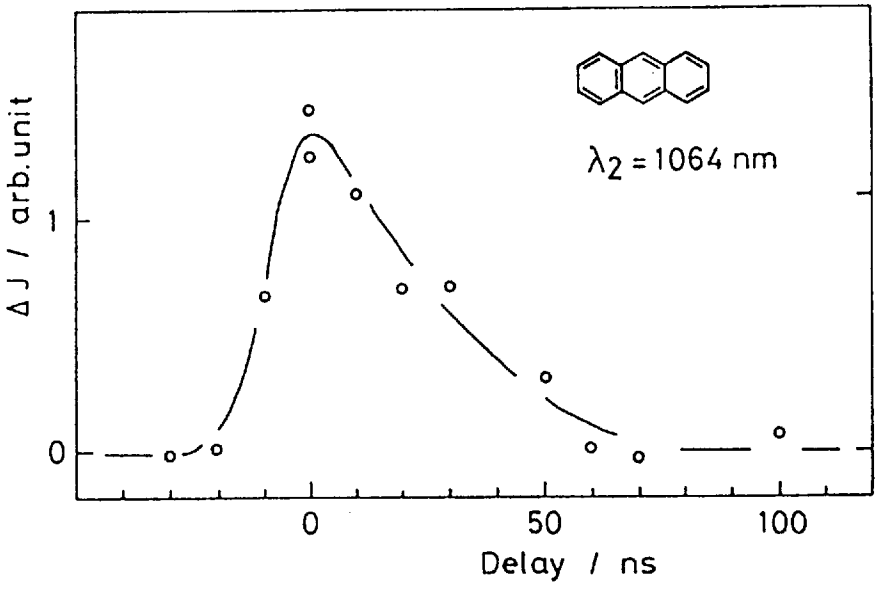

Fig. 5.13 The time dependence of the excess photocurrent on the delay between the two pulses (λ_2 = 1060nm) in anthracene.

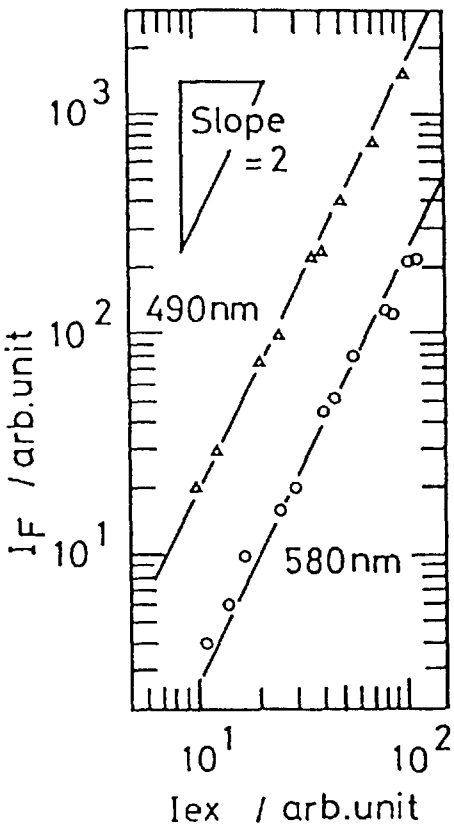

Fig. 5.14 Dependence of the fluorescence intensity I_F on the excitation light intensity (I_{ex}: λ = 490 and 580 nm) in anthracene.

The action spectra of photoionization of the singlet exciton is shown in Fig. 5.15. The electric field vector E of the exciton-generating light (λ_1 = 420 nm) is parallel to the crystal a-axis in both spectra in Fig. 5.15. The E vector of the ionization light (λ_2 = 450 - 620 nm) is parallel to the a-axis in (a,a), and is parallel to the b-axis in (a,b).

[p-Terphenyl]

Excitation is made with λ = 340 nm light in the absorption edge of this material [see Appendix 1]. Excitation occurs in the bulk of a crystal homogeneously. Hence, the volume recombination of charge carriers and the fusion of two singlet excitons can thus be effectively reduced.

When a 570 nm pulse irradiates the sample specimen simultaneously with a 340nm pulse, an enhancement of the photocurrent is observed. This additional photocurrent $\triangle$ N is proportional to the 570 nm light intensity I_2 (Fig.5.16). This indicates that the enhancement of photocurrent is due to photoionization of singlet exciton. When the intensity of the second-step pulse is much higher than normally used in the experiment, charge carriers are generated with a two-photon and a three-photon process (Appendix 1).

The photoionization spectrum of the singlet exciton is shown in Fig. 5.17. The electric field vector E of the exciton-generating light (λ_1 = 340 nm) is parallel to the crystal b-axis. The E vector of the ionization light (λ_2 = 430 - 680 nm) is

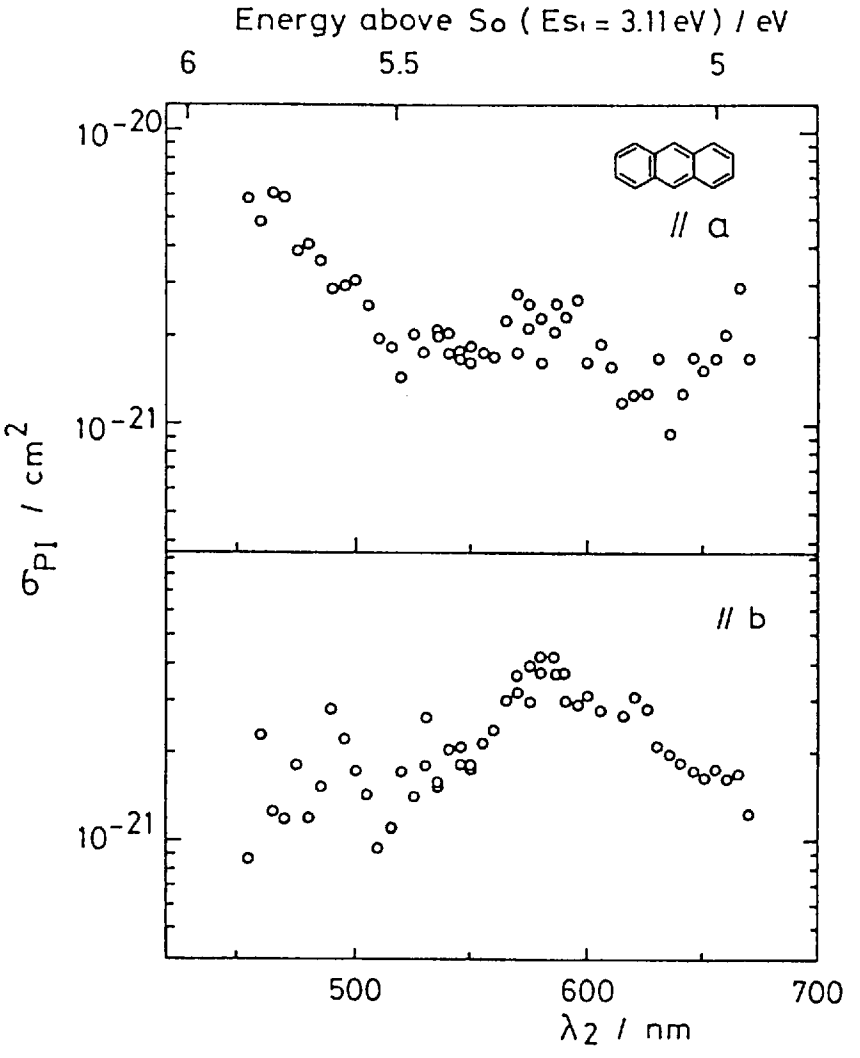

Fig. 5.15 The photoionization spectra of the singlet exciton in anthracene.

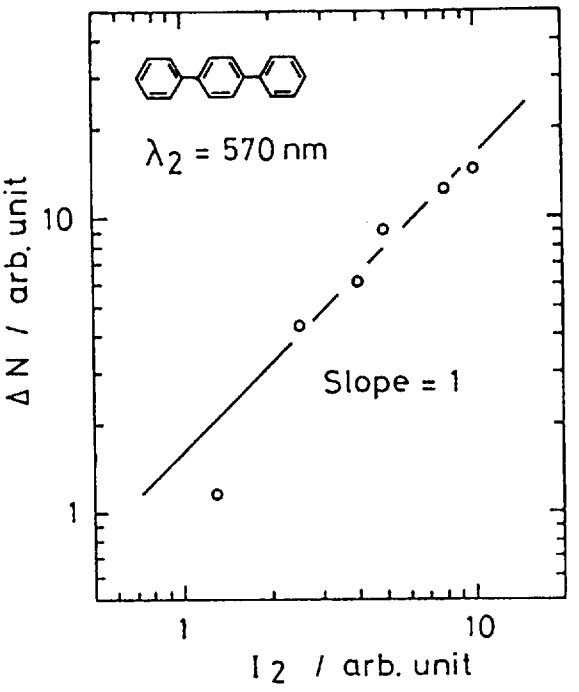

Fig. 5.16 Dependence of the excess photocurrent (Δ j) on the ionizing pulse intensity (I_2) in p-terphenyl.

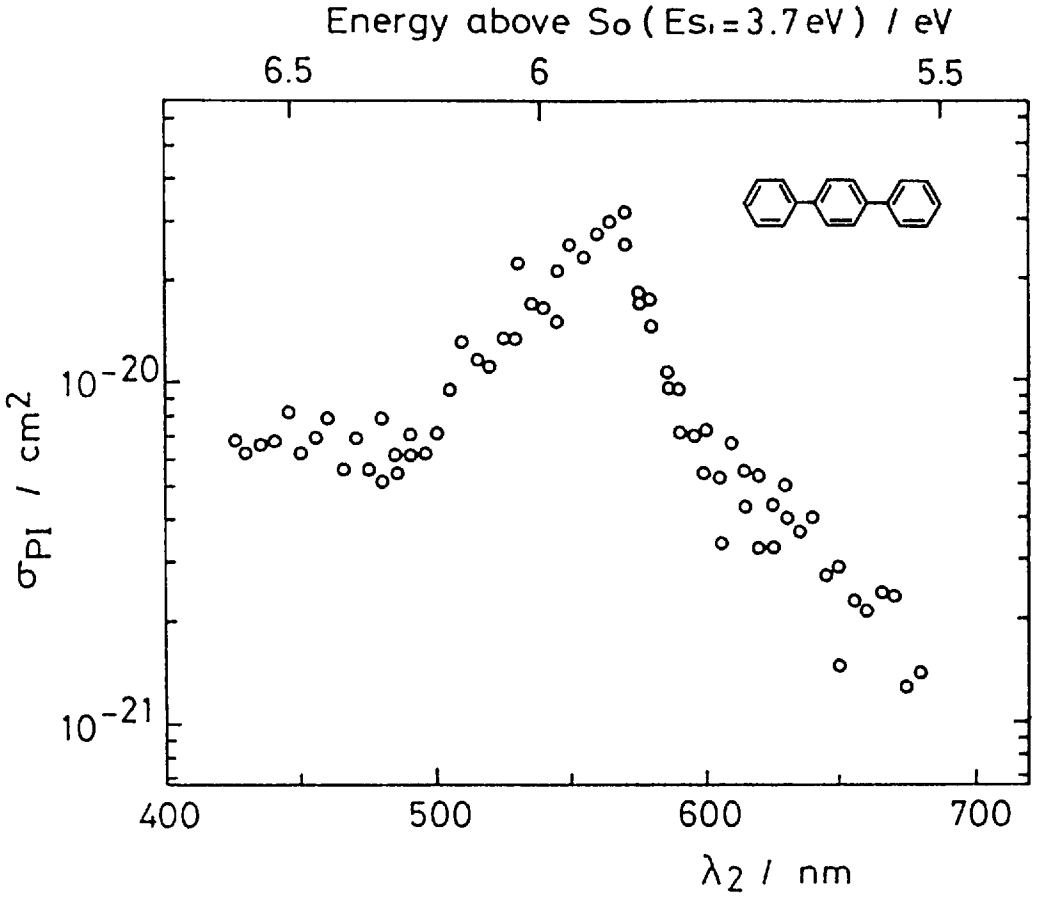

Fig. 5.17 The photoionization spectra of the singlet exciton in p-terphenyl.

parallel to the b-axis. When a-polarized light is used for the exciton-ionizing pulse, the photoionization of singlet exciton is much smaller. Excitation energy from the ground state can be estimated from the energy of the singlet exciton (3.69 eV [5.34]) plus photon energy for the second-step ($E_{S*} + h\nu_2$).

[t-Stilbene]

A photocurrent which is proportional to I_{ex}^2 is observed by excitation of λ = 360 nm light, which corresponds to the absorption edge of this material. Energy of the singlet exciton is 3.6 eV [5.23]. When a 570 nm pulse irradiated the sample specimen simultaneously with a 360 nm pulse, an enhancement of the photocurrent is observed. This additional photocurrent $\triangle$ N is proportional to λ = 570 nm light intensity I_2 (Fig. 5.18). This indicates that it is due to the photoionization of singlet excitons generated by irradiation of 570 nm light.

The photoionization spectrum of the singlet exciton is shown in Fig. 5.19. Unpolarized light (λ_1 = 360 nm) is used for the generating excitons. The E vector of the ionizing light (λ_2 = 435 - 685 nm) is parallel to the b-axis. When c-polarized light is used as exciton-ionizing light, the photoionization of singlet exciton is much smaller.

5.5.3 Cross section of photoionization of singlet exciton through two-color, two-step excitation

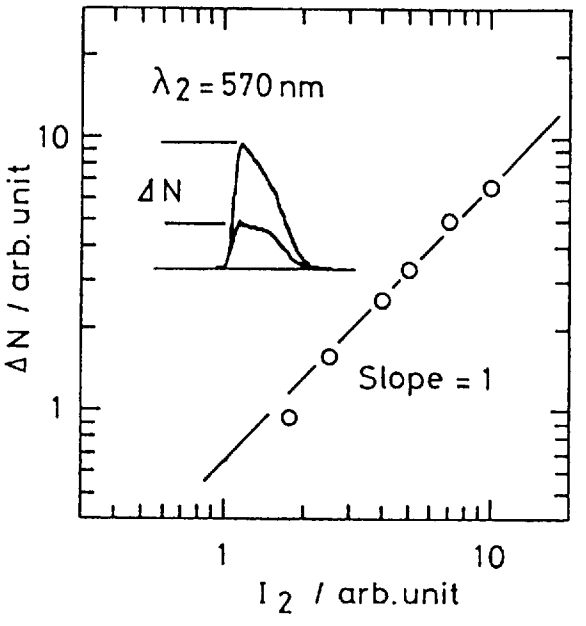

Fig. 5.18 Dependence of the excess photocurrent (Δ j) on the ionizing pulse intensity (I_2) in trans-stilbene.

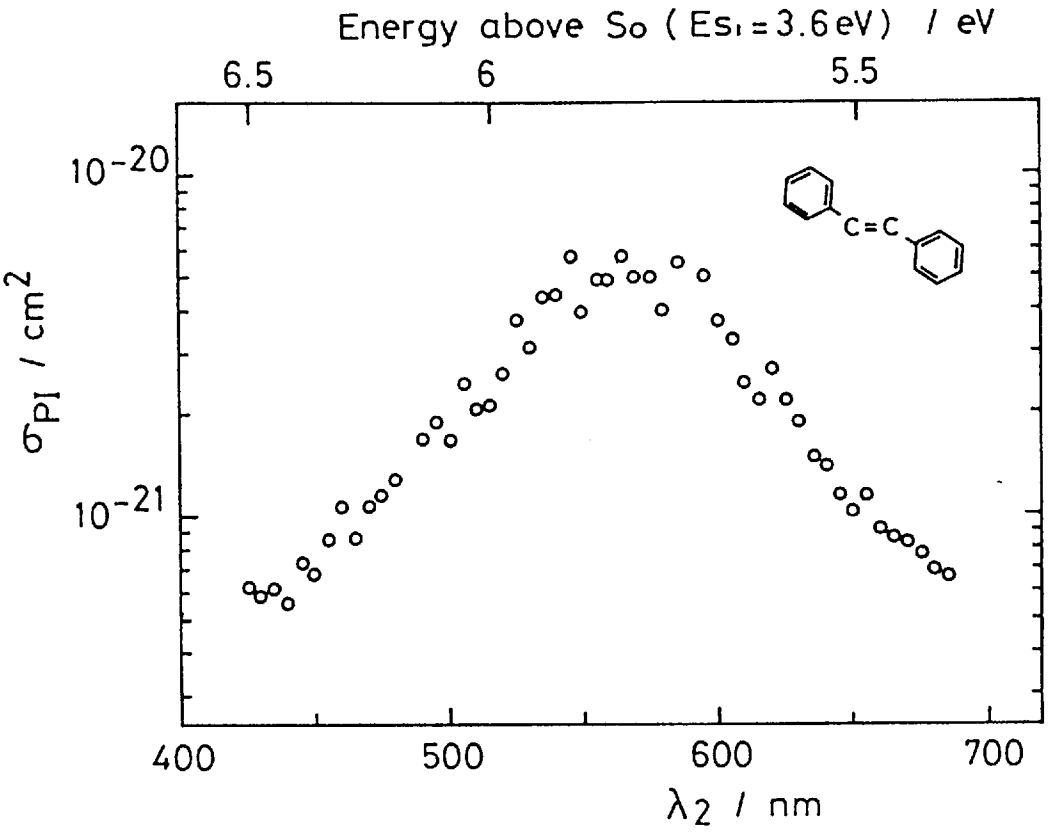

Fig. 5.19 The photoionization spectra of the singlet exciton in trans-stilbene.

In the case of p-terphenyl, where the light intensity was kept low and the excitation pulse (8 ns) was longer than the lifetime of singlet exciton (2.1 ns [5.30]). In this case [S*] can be described using Eq. (3.1) as (cf. Eq. (3.2))

$$[S^*] = \alpha \tau_s I_1 . \qquad (5.11)$$

On the other hand, in the case of anthracene and trans-stilbene the steady-state approximation is not strictly valid, as the exciton lifetime (20 ns in anthracene [3.35], 14 ns in trans-stilbene [5.31]) is longer than the pulse duration of exciting light (8 ns). Accordingly, the singlet exciton concentration is computed numerically with Eq. (3.1). The density of charge carriers generated by singlet exciton photoionization, $[\triangle N]$, is given by (cf. Eq. (5.4) and (5.9))

$$[\triangle N] = \sigma_{PI} [S^*] I_2 \tau_P , \qquad (5.12)$$

where σ_{PI} is the cross section of photoionization of singlet exciton, I_2 is the intensity of the second-step light (ionizing light) pulse and τ_P is the duration of the exciting light pulse. The photoionization cross section of the singlet exciton can be evaluated using these values. Results are summarized in Table 5.3. It is interesting to note that these cross section are smaller than that of the values with absorption edge excitation (§ 5.4 Table 5.2).

Table 5.3 Cross section for photoionization of singlet exciton with two-color, two-step excitation.

	λ_2	Polarization of $h\nu_2$	E_{S_1}	Excitation energy	Cross section σ_{ES}
	nm		eV	eV	cm^2
Anthracene	580	//b	3.11	5.25	4×10^{-21}
p-Terphenyl	570	//b	3.69	5.88	2.8×10^{-20}
trans-Stilbene	570	//b	3.60	5.78	4.9×10^{-21}

Excitation energy = $E_{S_1} + h\nu_2$

5.6 Initial separation in geminate electron-hole pair

5.6.1 Introduction

The efficiency of photocarrier generation is not only a function of excitation energy, but also a function of temperature and electric field. The dependence on temperature and on electric field has been explained by the Onsager theory. In this section I will present outline of the Onsager model and results of photoconductivity measurements of an anthracene crystal as a function of temperature and electric field. I discuss reliability of the results and give an estimation of the initial separation in a geminate electron-hole pair based on the Onsager model.

5.6.2 Onsager model

When photoionization of a molecule occurs in a condensed phase, the electron emitted from a molecule is scattered by the surrounding molecules. Thermalized electron and parent cation (hole) form a so-called geminate electron-hole pair. The dielectric constant in organic crystals is relatively small and the Coulombic attraction between an electron and a hole is strong. Hence, only small fraction of the geminate electron-hole pairs can dissociate and contribute to the photocurrent. The apparent ionization efficiency, i.e., the number of separated charges divided by the number of photons absorbed, is dominated by the geminate recombination of electrons and holes and is accordingly small. The apparent ionization efficiency Φ can be written by

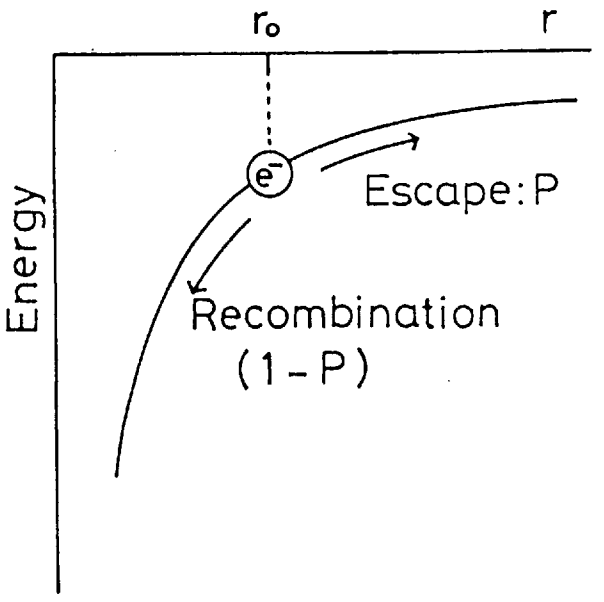

Fig. 5.20 Onsager model, geminate recombination of an electron and a hole in the Coulomb potential.

$$\Phi = \Phi_{GP} P(r_0, E, T) \quad (5.13)$$

where Φ_{GP} is the generation efficiency of geminate electron-hole pairs, $P(r_0, E, T)$ is the escape probability of an electron from the Coulomb potential, r_0 is the initial separation between an electron and a hole and E is the electric field (Fig. 5.20).

Onsager has calculated the escape probability P of an electron from the Coulomb potential made by its counter charge under presence of external electric field [5.36]. For low electric fields the escape probability P is approximated as [5.37],

$$P = \exp(-r_c/r_0)\{1 + (e\, r_c/2kT)E\} \quad (5.14)$$

where $r_c = e^2/4\pi\,\varepsilon\,\varepsilon_0 kT$. It is a linear function of E with a slope S and finite intercept I. The slope-to-intercept ratio S/I $= er_c/2kT$ depends on the temperature and the dielectric constant of the medium. Chance and Braun measured photocurrent in an anthracene crystal as a function of electric field strength, and obtained S/I ratio which is in good agreement with the Onsager theory [5.38]. This verified that the small carrier yield is essentially due to the geminate recombination. The original Onsager theory could be applied to isotropic media, such as dense gas and liquid. Tachiya [5.39] and Mozumder [5.40-42] have extended the theory to anisotropic media.

Initial separation r_0 between an electron and a hole can be determined through measurements of ionization efficiency as a function of temperature, or of electric field. According to the Onsager model a photocurrent increases with temperature T and with external electric field E. By comparing experimental results with theory the initial separation r_0 can be obtained.

5.6.3 Temperature dependence of photoconductivity in an anthracene crystal

The temperature dependence of the number of charge carriers N generated by a light pulse can be obtained from the initial photocurrent after corrected for the temperature dependence of the mobility of charge carriers (Fig. 5.6). Figure 5.21 shows photocurrent as a function of temperature when an anthracene crystal is excited in the absorption edge (λ = 420nm). Polarization of the electric field vector E of the exciting light is parallel to the crystal a-axis. The intensity is kept low to avoid the volume recombination of electrons and holes. The number of charge carriers generated increases with temperature with an activation energy of E_a = 0.11eV when the excitation is made at λ = 420nm.

Figure 5.21 also shows the absorption coefficient α of the ground state crystal as a function of temperature. Under the present experimental condition the penetration depth of the exciting light is much smaller than the crystal thickness and the light is absorbed completely by the specimen. In a PI case (see Sec. 5.4) the photocurrent is proportional to the total number of the singlet excitons generated in the specimen. The number of singlet excitons is independent of the absorption coefficient when the absorption is complete, and hence N is expected to be insensitive to a small change of α (a change in the reflectance may influence N). In a CI case the density, not the total number, of the singlet excitons is essential and the photocurrent

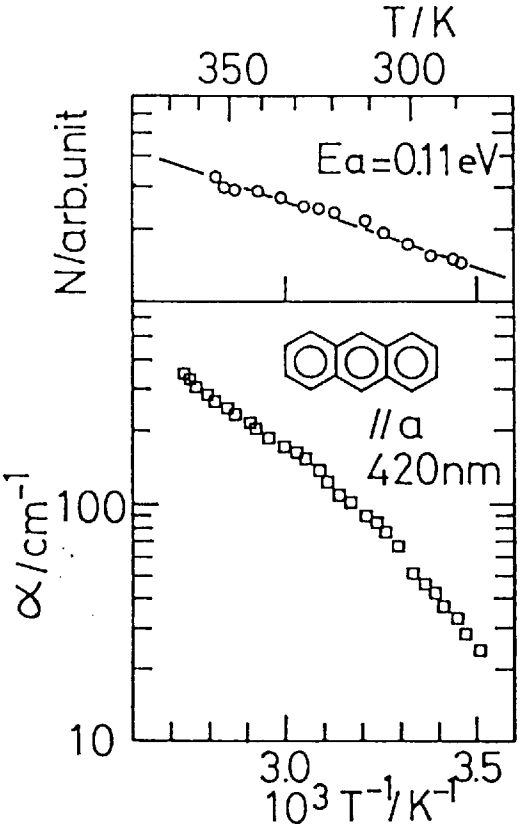

Fig. 5.21 Number of charge carriers (N) and absorption coefficient (α) versus reciprocal temperture for λ = 420 nm excitaiton in anthracene.

is linearly proportional to α when integrated over the crystal thickness. As may be seen from Fig. 5.21 the absorption coefficient changes by about one order of magnitude in the temperture range of the experiment, whereas the number of the charge carriers changes only by a factor of two. This also supports the photoionization of the singlet excitons (see § 5.4).

Figure 5.22 shows photocurrent in an anthracene crystal due to photoionization of singlet exciton through two-color, two-step excitation as a function of temperture with 490 nm or 580 nm excitations above the singlet exciton level. With 580 nm excitation photocurrent increases with temperture but it decreases with 480 nm excitation. The activation energy for charge carriers generated with 580 nm light is found to be E_a = 0.13eV (Fig. 5.23).

Excitation energies ($S^* + h\nu$) and activation energies E_a are summarized in Table 5.4. If Φ_{GP} is insensitive to temperature change, the initial separation r_0, which is defined in the Onsager model, can be estimated through the temperature dependence of the number of charge carriers generated. Using Eq. (5.14) the initial separation r_0 can be estimated. They are 36 Å for 420 nm excitation and 25 ± 5 Å with 580 nm excitation. In the case of 490 nm excitation the temperture dependence, which is not of thermal activation type, cannot be interpreted by the Onsager theory. Details of the temperature effects will be discussed in § 5.6.5.

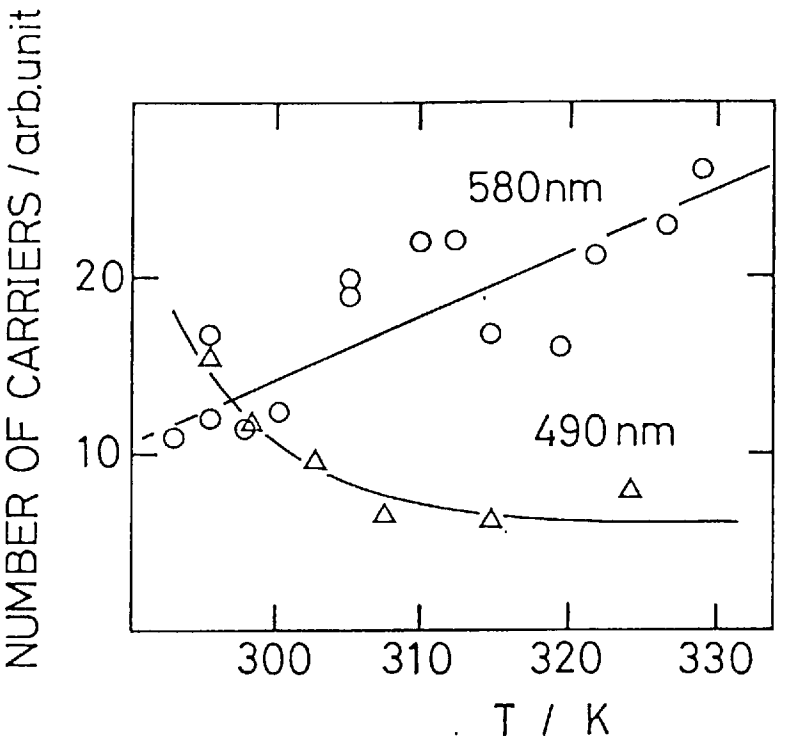

Fig. 5.22 Temperature dependence of excess photocurrent with λ = 480 nm and 580 nm excitation in anthracene.

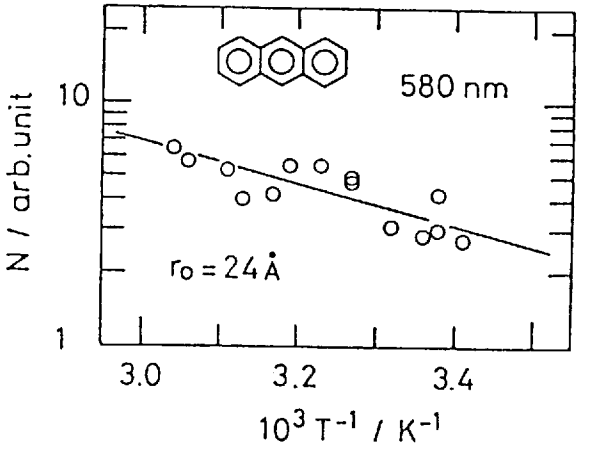

Fig. 5.23 Number of excess charge carriers (Δ N) versus reciprocal temperture for λ = 580 nm excitaiton in anthracene.

5.6.4 Electric field dependence of photoconductivity in an anthracene crystal

Initial separation r_0 between an electron and a hole can be also estimated through the analysis of photocarrier yield at high fields. Mozumder has given an expression of the escape probability in a series expansion for high fields [5.43]. For low electric fields photocurrent increases linearly with finite intercept I (see Eq. (5.14)). Relatively high electric fields ($\sim 10^7$ V/m) seem to be necessary to observe the expected deviation from the linearity of photocurrent. I succeeded to measure the photocurrent in an anthracene crystal as a function of external electric field E up to 1.8×10^7 V/m. Figure 5.24 shows the energy scheme for the excitation mode. With excitation at 420 nm charge carriers are generated by a two-photon process. A three-photon process is observed with excitation at 640 nm. It has been established that the charge carrier generation is due to photoionization of singlet exciton in both cases [5.13,5.21]. Total excitation energies are 6.1eV with 420 nm excitation and 5.1 eV with 640 nm excitation. The energy of the singlet exciton is 3.1117eV [5.23].

In Fig. 5.25 the reciprocal transit time $1/\tau$ for electrons is plotted against the applied electric field E with 308 nm light excitation. A current transient with an electric field of 1.8×10^7 V/m is also shown. It may be seen that the reciprocal transit time is proportional to the applied field (the mobility is not field-dependent) and that the charge carriers are free from trapping during the experimental observation time of several microseconds.

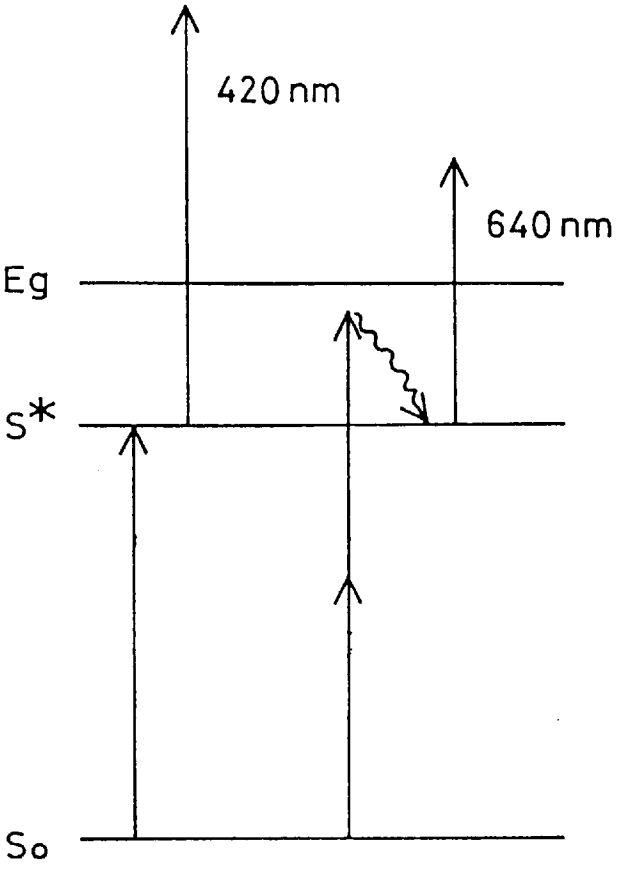

Fig. 5.24 Excitation modes with λ = 420 nm and 640 nm light in anthracene. Charge carrier are generated by photoionization of singlet exciton in both cases.

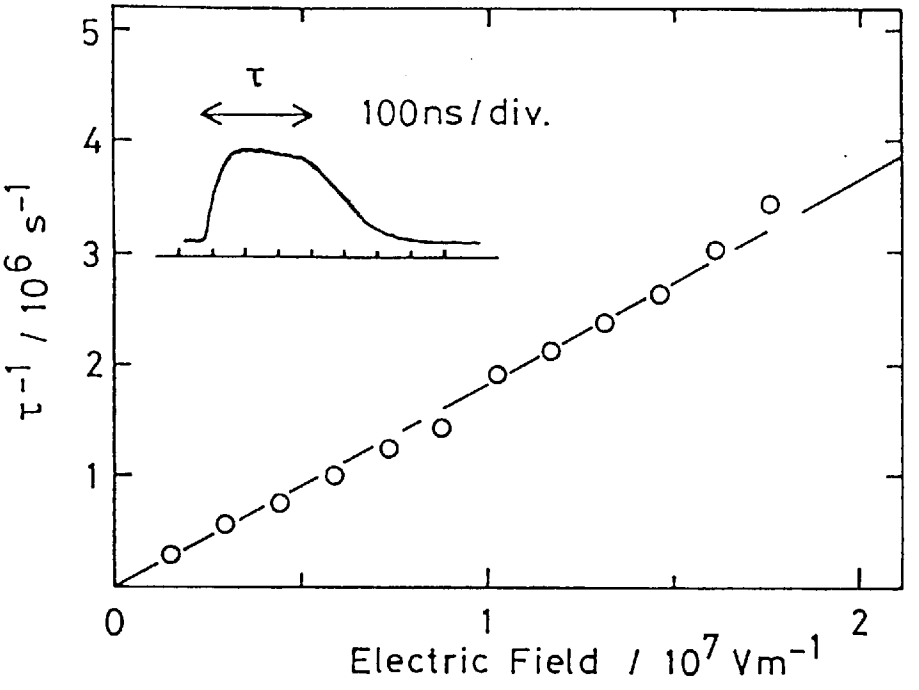

Fig. 5.25 Reciprocal transit time plotted aginst electric field E in anthracene. The shape of the current pulse with E = 1.8× 10^7 V/m is also shown.

The number of charge carriers generated N, normalized to that at zero electric field N_0, is measured as a function of electric field E for excitation wavelengths of 420 nm and 640 nm. The results are shown for relatively low fields in Fig. 5.26. The exciting light intensity is kept low to avoid volume recombination of electrons and holes. It may be seen that N is linearly dependent on the electric field with an intercept for both excitation wavelengths. The slope-to-intercept ratios S/I are given in Table 5.4. The Onsager theory predicts a value of 3.34×10^{-7} m/V for ε = 3.23 [5.45] and T = 300K. The rather good agreement between the experimental S/I and the expectation based on the Onsager theory indicates that the sample is well-behaved and that the Onsager theory can be applied.

The number of charge carriers generated N at relatively high electric fields, normalized to the number of charge carriers at zero electric field N_0, is shown in Fig. 5.27 for excitation wavelengths of 420 and 640 nm. It may be seen that the carrier yield saturates gradually at high fields. The results can be fitted with the series expansion given in Ref.5.43, using the initial separation r_0 as a parameter. I assume that the distribution of the initial separation is a delta function and the dielectric constant is isotropic (ε = 3.23). The calculated functional form of N(E) for various r_0 are shown with solid lines in the Figure. The best fit is obtained with r_0 = 95Å (with 420 nm excitation) and r_0 = 85Å (with 640 nm excitation).

A small deviation of the measured points from the calculated curves is present in Fig. 5.27. This could be due to the

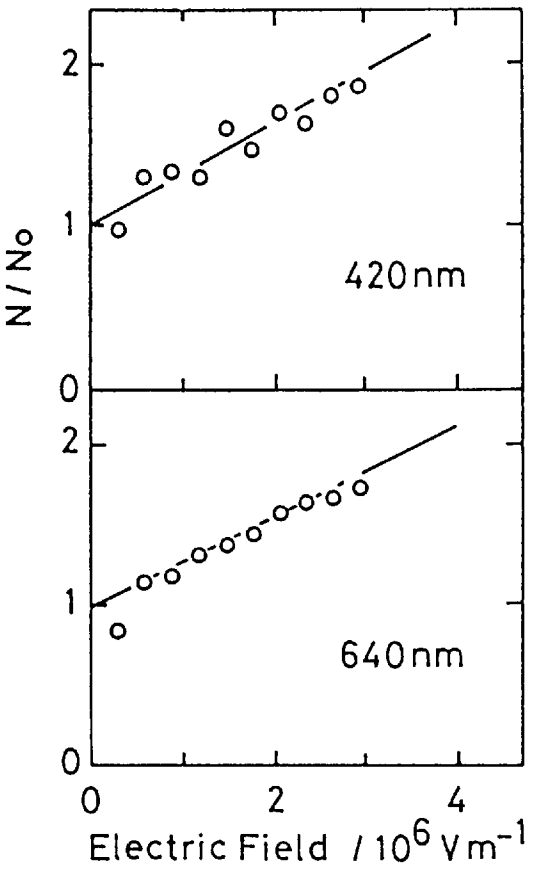

Fig. 5.26 The number of generated charge carriers N, normalized to the number of charge carriers at zero electric field N_0, is plotted as a function of relatively low electric field E in anthracene.

Table 5.4 Slope-to-intercept ratio for photocurrent as a function of electric field.

	S/I / mV^{-1}
420 nm	3.2×10^{-7}
640 nm	2.8×10^{-7}
Onsager	3.34×10^{-7}

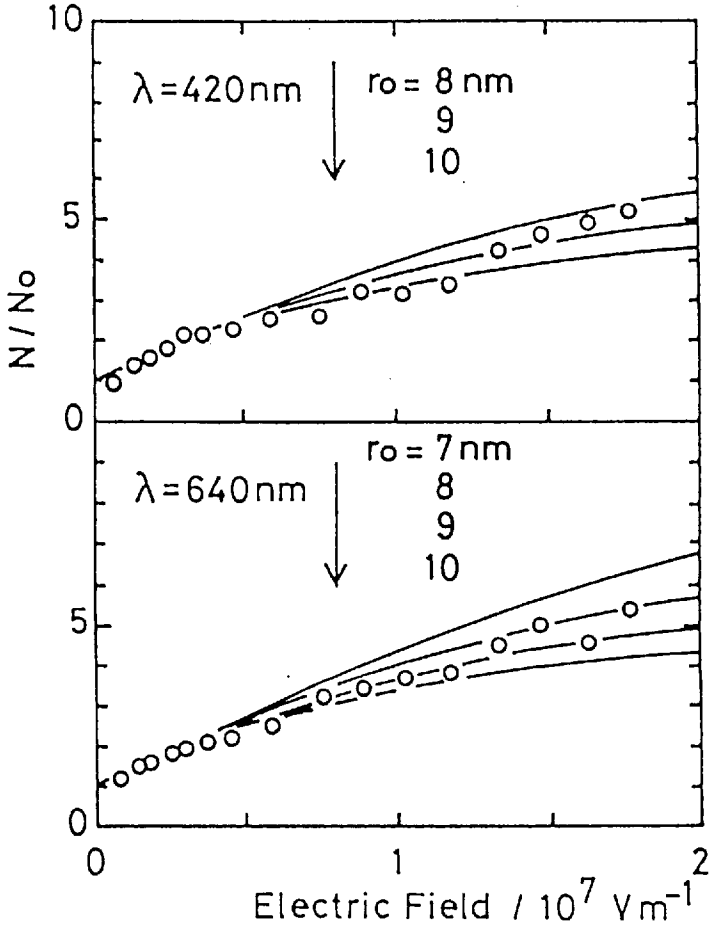

Fig. 5.27 The number of generated charge carriers N, normalized to the number of charge carriers at zero electric field N_0, is plotted as a function of electric field E up to E = 1.8× 10^7 V/m in anthracene. Solid lines are predicted by the Onsager theory for various r_0.

anisotropy, or the angular distribution, of the initial separation, or both, which are not considered in the present calculation. Tachiya has extended the Onsager theory to anisotropic media [5.39]. Pimblott and Mozumder have calculated S/I ratio [5.40-42] for anthracene taking the anisotropy and distribution of the size of a geminate electron-hole pair into consideration. However, their calculations are limited to low electric fields ($<10^6$ V/m) and cannot be applied to the present results.

5.6.5 Initial separation in geminate electron-hole pair

Photocurrent was measured as a function of temperature (§ 5.6.3) and external electric field (§ 5.6.4). From the results the initial separation r_0 can be estimated. There have been some estimations of r_0 from the temperature dependence of photocurrent in anthracene crystals. Chance and Braun have determined r_0 as a function of excitation energy. Initial separation was found to be 50 Å (for excitation energies of 4.4-5.2 eV) and 67 Å (5.4-6.2 eV) [5.45]. Ryan et al. have measured photoconductivity as a function of temperature with two-photon excitation [5.46]. They also estimated the initial separation as a function of excitation energy. These values are summarized in Table 5.5. It seems that there is a large scatter in the values of r_0 differ obtained by different researchers and under differnt experimental conditions.

To obtain initial separation from photocurrent measurements temperature dependence of many other processes should be considered. It is well known that dielectric properties, such as

absorption coefficient and refractive index, depend on temperature. Generation efficiency Φ_{GP} of geminate electron-hole pair may be also sensitive to temperature. This has been studied in poly(N-vinylcarbazole) [5.47]. In the present study photocurrent decreases with increasing temperature with 490 nm excitation (5.6 eV above the ground state). This indicates that photocurrent observed does not reflect temperature dependence of escape process only. It is difficult to estimate the initial separation r_0 only from temperature dependence of photocurrent.

Elecrtric field dependence of other processes, such as absorption, may be neglected in the measurement of photocurrent. The validity of the Onsger model at high fields has been verified in triphenylamine doped-polycarbonate [5.48] and in photoionization of molecules in nonpolar solvents [5.49]. Hence, an estimation of r_0 based on the electric field dependence of photocurrent is considered to be more reliable compared with that from measurements of temperature dependence. Silinsh et al. have observed an increase of the initial separation with electric field strength in a pentacene crystal [5.50]. In the present results (Fig. 5.27), however, the initial separation r_0 does not seem to increase with external electric field.

From these considerations I prefer the initial separations which are determined through the photocurrent measurements as a function of electric fields.

Table 5.5 Initial separations r_0 between an electron and a hole estimated from the measurements of temperture dependence and electric field dependence of the photocurrent. In this work r_0 which is estimated by electric field dependence is adopted.

Excitation energy	Initial separation r_0			
eV	Å			
	T-dependence			E-dependence
	Chance & Braun	Ryan et al.	This work	This work
6.1	67		36	95
5.7	67			
5.3	60	160	25	
5.1	50	100		85

References

[5.1] Proceeding of the "Oji International Seminar on Organic Semiconductors-40 Years", Eds. H.Inokuchi, M.Sano and N.Sato, Mol. Cryst. Liq. Cryst. 171 (1989).

[5.2] G.Castro and J.F.Hornig, J. Chem. Phys. 45 (1966) 2693.

[5.3] N.Geacintov and M Pope, J. Chem. Phys. 45 (1966) 3884.

[5.4] N.Geacintov and M.Pope, J. Chem. Phys. 47 (1967) 1194.

[5.5] N.Geacintov and M.Pope, J. Chem. Phys. 50 (1969) 814.

[5.6] R.G.Kepler, Phys. Rev. 119 (1960) 1226.

[5.7] O.H.LeBlanc.Jr., J. Chem. Phys. 33 (1960) 626.

[5.8] A.Bergman, M.Levine and J.Jortner, Phys. Pev. Lett 18 (1967) 593.

[5.9] J.Jortner, Phys. Rev. Lett. 20 (1968) 244.

[5.10] C.L.Braun, Phys. Rev. Lett. 21 (1968) 215.

[5.11] C.L.Braun, J. Chem. Phys. 53 (1970) 2718.

[5.12] R.G.Kepler, Phys. Rev. Lett. 18 (1967) 951.

[5.13] A.Bergman and J.Jortner, Phys. Rev. B9 (1974) 4560.

[5.14] M.Schott and J.Berrehar
Phys. Stat. Sol. B59 (1973) 175.
[5.15] E.Morikawa, Y.Isono and M.Kotani,
J. Chem. Phys. 78 (1983) 2691.
[5.16] E.Morikawa and M.Kotani,
J. Chem. Phys. 91 (1989) 180.
[5.17] M.Kotani, E.Morikawa and R.Katoh,
Mol. Cryst. Liq. Cryst. 171 (1989) 305.
[5.18] Y.Isono, E.Morikawa and M.Kotani,
Chem. Phys. Lett. 125 (1986) 344.
[5.19] P.Holzman, R.Morris, R.C.Jarnagin and M.Silver,
Phys. Rev. Lett. 19 (1967) 506.
[5.20] F.C.Strome, Jr.,
Phys. Rev. Lett. 20 (1968) 3.
[5.21] R.G.Kepler,
Phys. Rev. B15 (1974) 4468.
[5.22] L.B.Schein and D.W.Brown,
Mol. Cryst. Liq. Cryst. 87 (1982) 1.
[5.23] N.Karl,
in: Landort-Burnstein numerical data and fundamental relationships in science and technology, New series, Vol.17, eds. O.Madelung, M.Schulz and H.Weiss (Springer, Berlin, 1985).
[5.24] R.Raman and S.P.McGlynn,
J. Chem. Phys. 40 (1964) 515.
[5.25] A.Kostin, V.V.Savel'ev and A.V.Vinnikov,
Soviet Phys. Solid State 20 (1978) 504.
[5.26] A.Kostin, V.V.Savel'ev and A.V.Vinnikov,
Phys. Stat. Sol. (b) 87 (1978) 255.
[5.27] A.Matsui.

J. Phys. Soc. Japan 21 (1966) 2212.

[5.28] N.Karl and G.Sommer,
Phys. Stat. Sol. 6 (1971) 231.

[5.29] E.Morikawa,
Ph.D. thesis, Department of Chemistry, Faculty of Science, Gakushuin University (1985).

[5.30] A.C.Jones, K.J.Styrcz, D.A.Elliott and J.O.Williams,
Chem. Phys. Lett. 80 (1981) 413.

[5.31] R.Katoh, E.Yamazaki and M.Kotani,
to be published.

[5.32] E.A.Silinsh,
"Organic Molecular Crystals. Their electronic properties" (Springer, Berlin, 1980).

[5.33] N.Sato, H.Inokuchi and E.A.Silinsh,
Chem. Phys. 115 (1987) 269.

[5.34] C.Kryschi, W.Klufer and H.Kupka,
Chem. Phys. 146 (1990) 231.

[5.35] H.Nishimura, T.Yamaoka, K.Hattori, A.Maysui and M.Mizuno,
J. Phys. Soc. Japan 54 (1985) 4370.

[5.36] L.Onsager,
Phys. Rev. 54 (1938) 554.

[5.37] R.H.Batt, C.L.Braun and J.F.Hornig,
J. Chem. Phys. 59 (1968) 1967.

[5.38] R.R.Chance and C.L.Braun,
J. Chem. Phys. 49 (1973) 2269.

[5.39] M.Tachiya,
J. Chem. Phys. 69 (1978) 2375.

[5.40] A.Mozumder, S.M.Pimblott, P.Clifford and N.J.B.Green,
Chem. Phys. Lett. 142 (1987) 385.

[5.41] S.M.Pimblott and A.Mozumder,

Chem. Phys. Lett. 168 (1990) 511.

[5.42] S.M.Pimblott, A.Mozumder and N.J.B.Green,
J. Chem. Phys. 90 (1989) 6595.

[5.43] A.Mozumder,
J.Chem.Phys. 60 (1974) 4300.

[5.44] R.W.Munn, J.R.Nicholson, H.P.Schwob and D.F.Williams,
J.Chem.Phys. 58 (1973) 3828.

[5.45] R.R.Chance and C.L.Braun,
J. Chem. Phys. 64 (1976) 3573.

[5.46] C.S.Ryan, J.B.Webb and D.F.Williams,
Mol. Cryst. Liq. Cryst. 56 (1979) 69.

[5.47] P.M.Borsenberger and A.I Ateya,
J.Appl.Phys. 49 (1978) 4035.

[5.48] P.M.Borsenberger, L.E.Contois and D.C.Hoesterey,
J. Chem. Phys. 68 (1978) 637.

[5.49] H.T.Choi, D.S.Sethi and C.L.Braun,
J. Chem. Phys. 77 (1982) 6027.

[5.50] E.A.Silinsh,
"Organic Molecular Crystals. Their electronic properties"
(Springer, Berlin, 1980) p116.

6 Primary processes of charge carrier generation in aromatic hydorocarbon crystals

6.1 Introduction

There are many studies for photoconductivity in aromatic hydrocarbon crystals, which is introduced below. However, interpretation of charge carrier generation does not established. In this chapter primary processes of Charge carrier generation will be discussed based on the experimental results. In § 5 results for photoconductivity by photoionization of singlet excitqn are presented. It is found that the Onsager model is valid. Ionization efficiency Φ of a singlet exciton is obtained as a function of the excitation energy by comparing the action spectra of photoionization of singlet exciton (§ 5.5) with the transient absorption spectra (§ 4.3). Efficiency of generating a geminate electron-hole pair is estimated from ionization efficiency and initial separation between an electron and a hole. From these consideration model for photocarrier generation and comparison with other condensed phasees are presented.

Efficiency for photoconductivity in aromatic hydrocarbon crystals is very low ($\sim 10^{-3}$). This is due to geminate recombination between an electron and hole. Batt et al. have measured photoconductivity in an anthracene crystal as a function of the electric field [6.1] and found that the Onsager model could be applied to photocarrier generation in this material. As a result quantitative discussion can be made for geminate recombination. Hughes also applied the Onsager theory to carrier generation in an anthracene crystal by X-ray excitation [6.2].

Chance and Braun have measured electric field dependence of photoconductivity of anthracene in detail [6.3].

Measurement of ionization efficiency Φ and activation energy as a function of excitation energy is important to understand the ionization mechanism in condensed phase. Batt et al. measured the activation energy for photoconductivity in an anthracene crystal as a function of the excitation energy and estimated the initial separation between an electron and a parent cation by applying the Onsager theory [6.1]. They found that it increases stepwise, rather than gradually, with increasing excitation energy. This indicates that neutral excited state generated by a photon having an energy which exceeds the ionization potential is not ionized promptly, but auto-ionization occurs after a vibrational relaxation. Chance and Braun measured temperature dependence of photoconductivity in detail [6.4] and also estimated the initial separation as a function of excitation energy. They also observed a stepwise change in activation energy. They considered that vibrational energy of higher excited state was not converted to kinetic energy of photoelectron but it became vibrational energy of the cation. Kato and Braun made the same kind of measurements in the energy range close to the threshold for photoconduction [6.5]. They estimated not only the initial separation, but also the efficiency of geminate pair generation as a function of the excitation energy. They proposed that auto-ionization occured from the third excited state of anthracene crystal. Lyons and Milne made the same type of measurements [6.6]. Morikawa and Kotani measured photoconductivity od p-terphenyl due to photoionization of singlet excitons using two-color, two-step

excitation [6.7]. Ionization efficiencies could be estimated by comparing the action spectrum for photoconductivity with transient absorption spectrum. They found that the ionization efficiency changes stepwise with the excitation energy.

A stepwise change with excitation energy has been observed in the initial separation not only in organic crystals, but also in polymers. Borsenberger and Ateya measured photoconductivity in poly(N-vinylcarbazole) as a function of electric field and temperature [6.8]. Their results support auto-ionization after a rapid relaxation. They also found that generation of a geminate pair is a thermally activated process.

As presented above, such a stepwise change in the ionization efficiency or in the initial separation between an electron and its parent cation with excitation energy is frequently observed in this class of material. On the contrary, in the case of photoconduction in hydrocarbon liquids the initial separation increases gradually with excitation energy [6.9]. Accordingly, a stepwise change of ionization efficiency Φ may be characteristic of photoconductivity of this class of material.

In external photoelectron emission the kinetic energy of emitted electrons generally increases with photon energy. This shows that photoelectrons are generated by direct ionization. Experimental evidence demonstrates that electrons involved in photoconductivity, on the other hand, originate through indirect process. This discrepancy obviously indicates that the mechanism of the photoionization changes with increasing excitation energy.

6.2 Ionization efficiency of a singlet exciton

Ionization efficiency Φ of a singlet exciton can be obtained as a function of the excitation energy by comparing the action spectra of photoionization of singlet exciton (§ 5.4) with the transient absorption spectra (§ 4.3). Figure 6.1 illustrates the kinetic scheme for photocarrier generation with two-color, two-step excitation. A singlet exciton S* is generated by the first-step light ($h\nu_1$). When singlet exciton S* absorbs another photon (the second-step light, $h\nu_2$), a higher excited state S** and a geminate electron-hole pair are generated with an efficiency
Φ_{GP}. A free charge carrier is generated by dissociation of the geminate electron-hole pair with probability P. The overall ionization efficiency Φ of a singlet exciton is defined as

$$\Phi = \sigma_{PI}/\sigma_A, \qquad (6.1)$$

where σ_{PI} is the cross section for photoionization of singlet exciton and σ_A is the cross section for its optical absorption. The absoption spectra (Abs), action spectra of photoconductivity (PI) and ionization efficiency (Φ) for materials studied are shown in Fig. 6.2-6.5 as a function of excitation energy above the ground state. The excitation energy is defined as the energy of the lowest singlet exciton plus the photon energy of the second-step light. The 0-0 band energies for the absorption (3.1117 eV in anthracene [6.10], 3.69 eV in p-terphenyl [6.11] and 3.6000 eV in trans-stilbene [6.10]) are used as the energy of the lowest singlet exciton. Figures 6.2 and 6.3 show the results for anthracene for the ionizing light (second-step) of different polarizations. Figure 6.2 shows the results for a-polarization

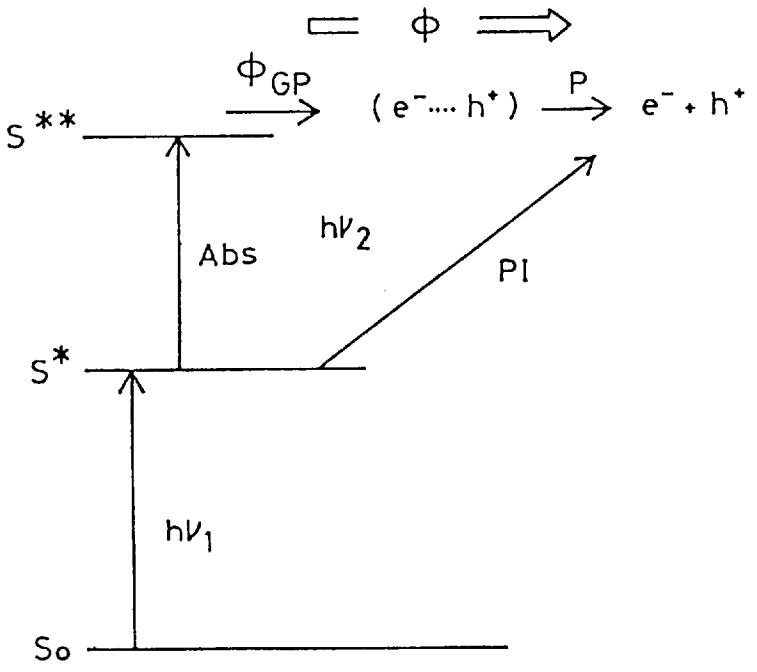

Fig. 6.1 Ionization efficiency Φ and generation efficiency of the geminate pair Φ_{GP}.

(with electric vector E of the second-step light parallel to the a-axis), and the Fig. 6.3 shows the data for b-polarized excitation. In calculating the ionization efficiency of the singlet exciton in p-terphenyl the absorption spectrum is used from which the absorption due to triplet exciton has been subtracted (the solid line in Fig. 6.4). From these spectra it may be clear that Φ is insensitive to the exciting energy in the lower energy range and increases sharply above 5.5 eV in anthracene and above 6.2 eV in p-terphenyl. In trans-stilbene this sharp increase is not observed. It is notable that ionization efficiencies as a function of excitation energy for different polarizations are similar with each other (Fig. 6.2 and 6.3). This insensitivity implies that the ionization efficiency of the singlet exciton does not depend on the polarization of the ionizing light, although both σ_{PI} and σ_{A} do depend on polarization.

Absolute values of ionization efficiency Φ can be estimated using the values of σ_{A} and σ_{PI} (see Table 4.1 and 5.3). Table 6.1 summarizes the values in the energy range in which Φ is independent of the excitation energy. These values are accurate within the factor of three. Ionization efficiencies are almost the same for the meterials studied in this energy range.

The ionization efficiency Φ increases steeply above 5.5 eV in anthracene and 6.2 eV in p-terphenyl. These onset energies E_c are close to the threshold energy E_{th} for external photoemission via singlet excited state (table 3.1). These values are summarized in Table 6.2.

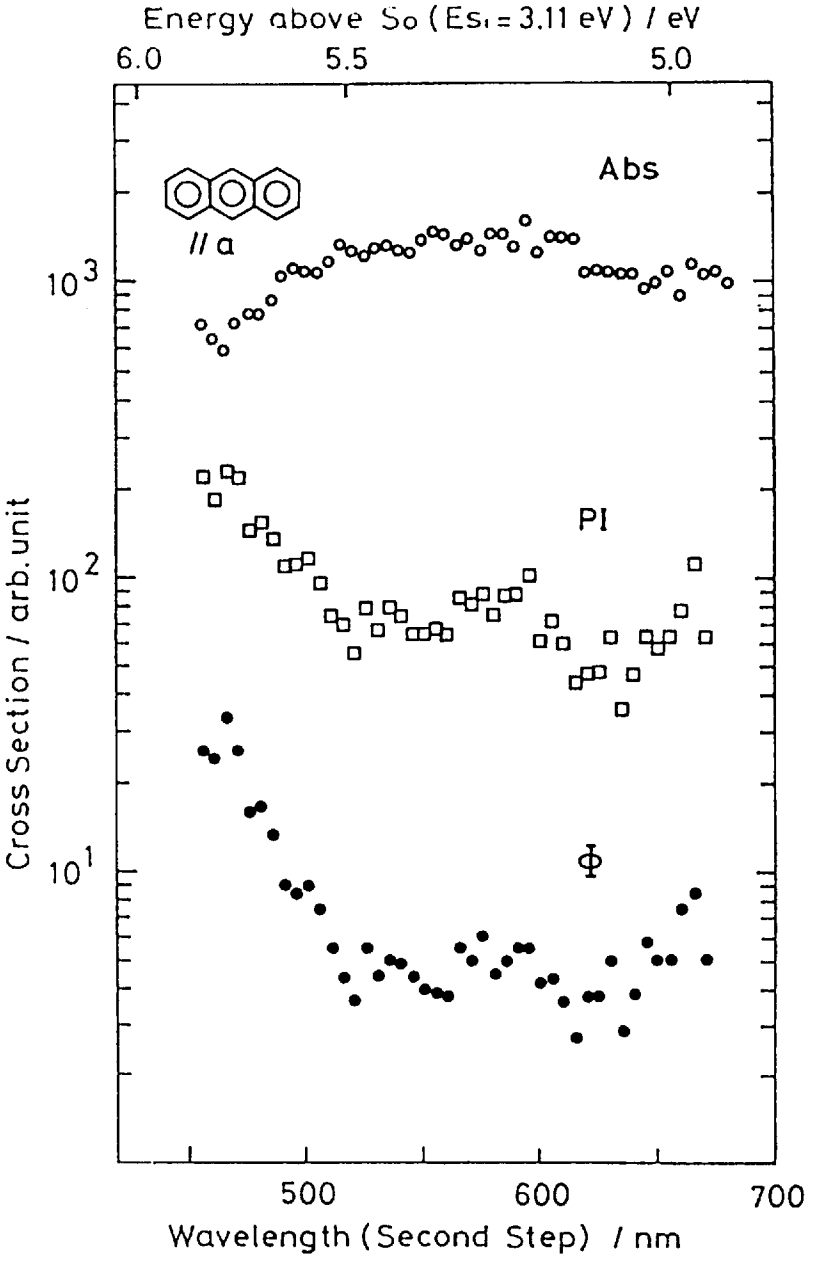

Fig. 6.2 Absorption (Abs), photoionization (PI) and ionization efficiency (Φ) in anthracene (E//a).

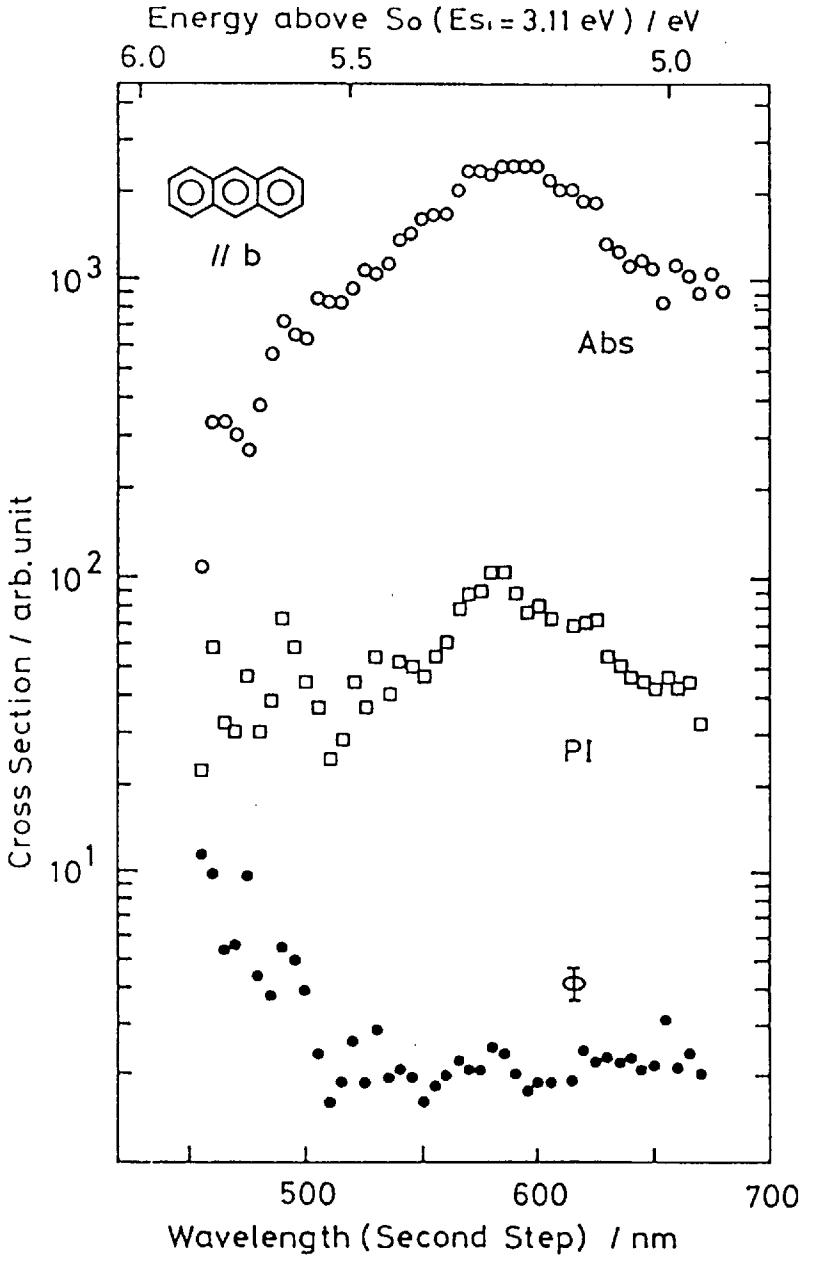

Fig. 6.3 Absorption (Abs), photoionization (PI) and ionization efficiency (Φ) in anthracene (E//b).

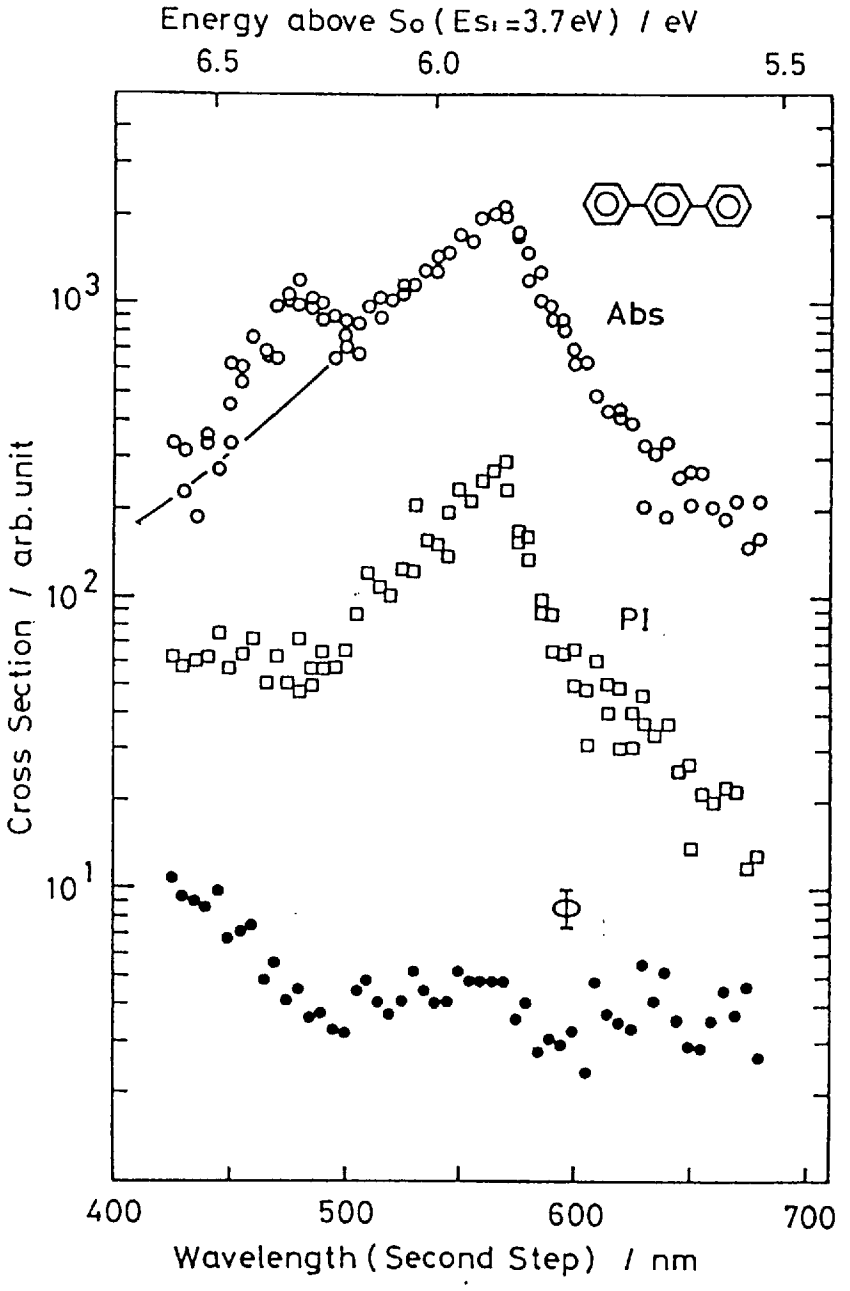

Fig. 6.4 Absorption (Abs), photoionization (PI) and ionization efficiency (Φ) in p-terphenyl.

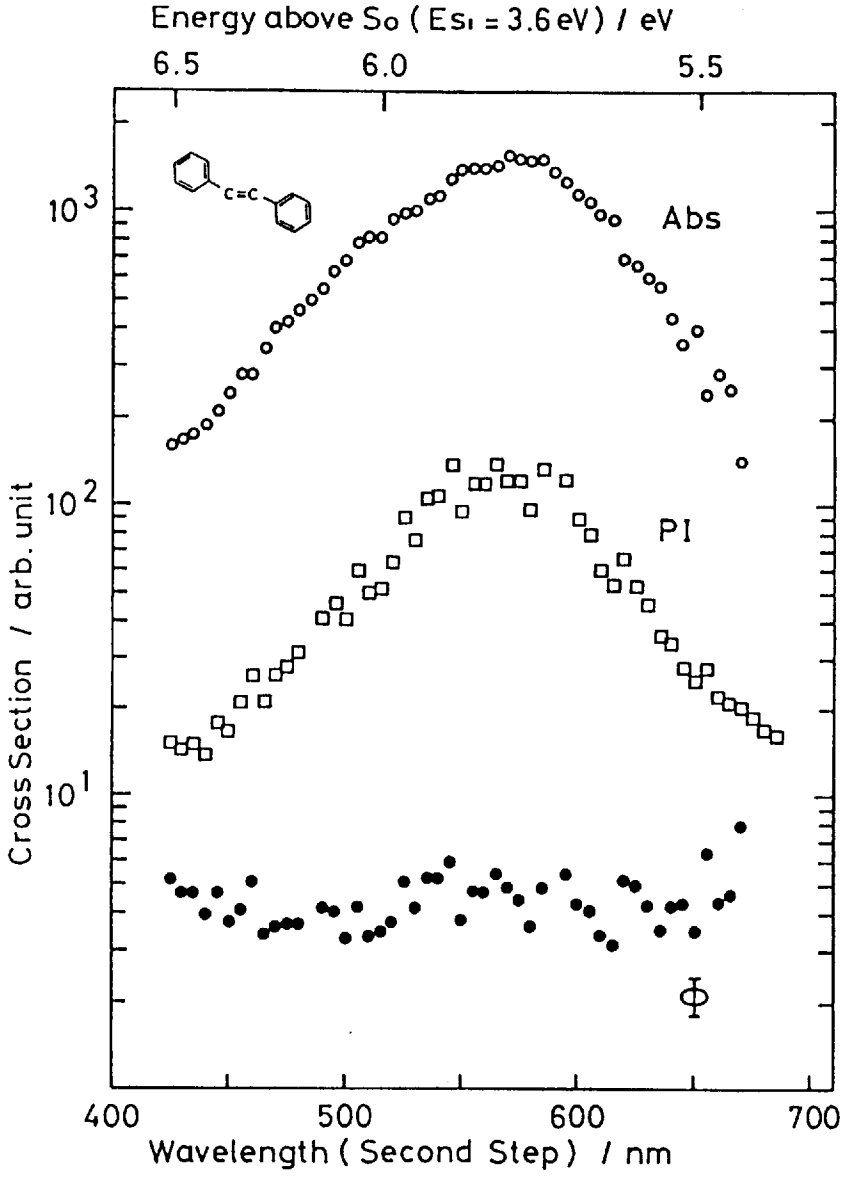

Fig. 6.5 Absorption (Abs), photoionization (PI) and ionization efficiency (Φ) in trans-stilbene.

Table 6.1 Ionization efficiency Φ of materials studied.

	Excitation energy /eV ($E_{s.} + h\nu$)	Ionization efficiency (Φ)
Anthracene	5.25	2.3×10^{-4}
p-Terphenyl	5.88	1.6×10^{-3}
t-Stilbene	5.70	7.0×10^{-4}

Table 6.2 Threshold energies for external photoemission via singlet excitons and changing energies for efficiency of photocarrier generation.

	Photoemission threshold		Changing energy for ϕ
	E_{th} /eV (one photon)	E_{th} /eV (via S^*)	E_c /eV
Anthracene	5.67	5.47	5.5
p-Terphenyl	6.1	6.27	6.2

The threshold energy for the external photoemission is 6.25 eV with trans-stilbene crystal for one-photon excitation [6.12]. Accordingly, it may be expected that Φ increases above this energy. However, there is no indication, up to 6.5 eV, that the ionization efficiency starts to increase in trans-stilbene. This may be due to the difference in the excitation mode (one-color excitation and two-step excitation via singlet exciton) which may have different threshold energies for external photoemission. When some geometrical change occurs in the singlet excited state, the threshold energy for the external photoemission via singlet exciton may be higher than that with the direct one-photon excitation. Such a difference of the threshold energy between excitation modes has been observed in p-terphenyl and naphthalene (see Table 3.1).

According to the Onsager model (Fig. 6.1) the ionization efficiency Φ can be devided into two factors.

$$\Phi = \Phi_{GP}\, P(E,T,r_0) \qquad (6.2)$$

where Φ_{GP} is the generation efficiency of a geminate electron-hole pair and P is the escape probability, which is a function of the electric field E, temperature T and initial separation r_0 between the electron and the hole. The efficiency of geminate electron-hole pair generation Φ_{GP} can be estimated using Φ and P. Escape probability P can be evaluated from initial separation r_0 using the Onsager theory (Eq. (5.14)). In the case of anthracene it turns out that $\Phi_{GP} = 0.3$ for the energy of 6.1 eV (420 nm excitation) and $\Phi_{GP} = 0.001$ for the energy of 5.1 eV (640 nm excitation). These values are shown in Table 6.3.

Ionization efficiencies Φ from a singlet exciton are

summarized in Fig. 6.6 as a function of exciting energy in the materials studied. The efficiency Φ is insensitive to the excitation energy below the threshold energy E_{th} for external photoemission and above that energy it increases steeply except for trans-stilbene. Efficiency Φ_{GP} of geminate electron-hole pair generation increases drastically with the excitation energy in anthracene (Table 6.3). These experimental results suggest that ionization mechanism changes at the threshold energy E_{th} for external photoemission. Below E_{th} photoionization may occur by an indirect process, such as electron transfer from a neutral excited state to neighboring molecule, since Φ_{GP} is considerably low in this energy range. Above that energy Φ_{GP} is nearly unity. It seems that direct ionization is the dominant process for generating charge carriers.

6.3 Model for photoionization in aromatic hydorocarbon crystals

6.3.1 Polarization model and modes of ionization

As mentioned in § 1, organic molecular crystals have weak intermolecular interaction so that electronic states of a solid have energies not very different from those of isolated molecules. In this case a theory for photoelectric effects in metals and semiconductors, such as those based on jellium model, is not a good approximation because electrons are tightly bound to a molecule. Photoconduction and photoemission in an organic crystal should be treated as the photoionization of molecules in the crystal. When ionization occurs, a large electronic polarization is induced by surronding molecules, so that

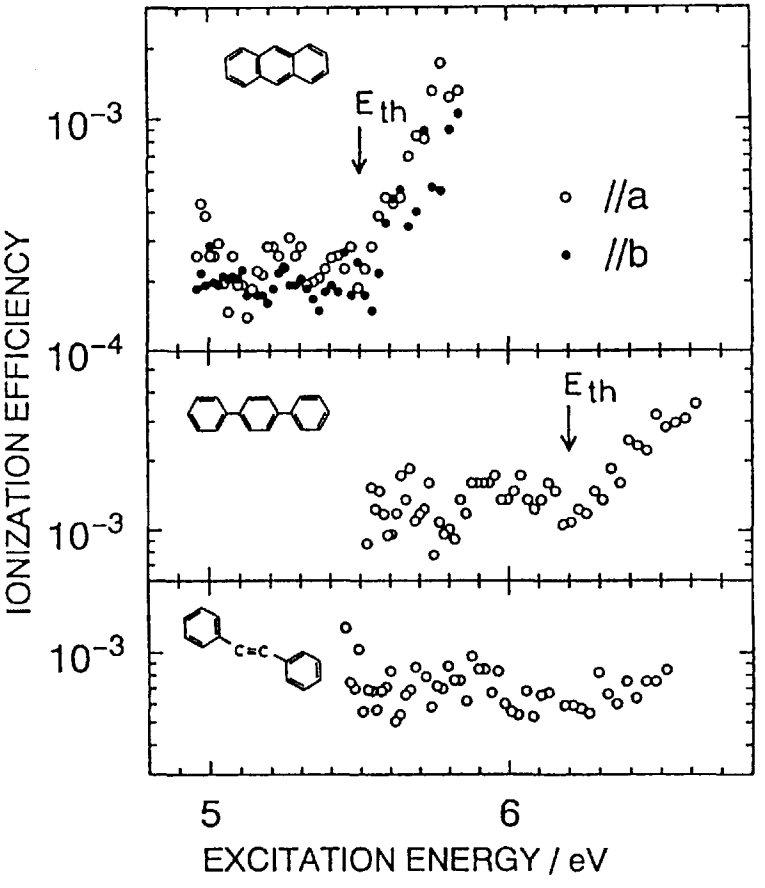

Fig. 6.6 Excitation energy dependence of ionization efficiency (Φ) in materials studied.

Table 6.3 Generation efficincy of the geminate electron-hole pair in anthracene.

	Excitation Wavelength	
	420nm	640nm
Excitation Energy /eV	6.1	5.1
Initial separation r_0 /Å	95	85
Escape Probability P	0.24	0.20
Ionization Efficiency Φ ($\Phi = \Phi_{GP} \cdot P$)	6×10^{-2}	2×10^{-4}
Generation Efficiency Φ_{GP}	0.3	0.001

behaviors of the conduction electron cannot be described by using the band model which is one-electron approximation in nature. In this case the energy level of the ionic species can be predeicted by the polarization model introduced originally by Lyons [6.13] (see § 1.3).

Two types of primary processes of ionization can be considered, one is electron emission from a molecule and the other is electon transfer from a molecule in a higher neutral excited stete to another molecule. The threshold energy for each process can be predicted by the polarization model. Figure 6.7 indicates the energy levels for ionic species, such as molecular cation, anion and free electron.

(I) Electron emission (EE)

In this process a photoelectron is directly generated by optical transition.

$$M + h\nu \Rightarrow [M^+] + [e^-],$$

where [ ] means electronic polarization. The onset energy E_0^{EE} for photoconduction can be written by

$$E_0^{EE} = I_G - P_+ - S_-^{free}, \qquad (6.3)$$

where I_G is the ionization potential for an isolated molecule, P_+ is the polarization energy induced by a positive charge and S_-^{free} is the stabilization energy for a free electron, which is not localized on the molecule. In aromatic hydrocarbon crystals electron affinity of a molecule is positive so that free electron is captured easily by a neutral molecule and a geminate ion pair is formed. A small fraction of the pairs can dissociate to free charge carriers.

(II) Electron transfer from an excited molecule (ET)

When a higher neutral excited state is promptly generated by optical transition, a small fraction of the state can relax to an ion pair state.

$$M + M + h\nu \Rightarrow M^* + M \Rightarrow [M^+] + [M^-].$$

The onset energy E_0^{ET} for this electron transfer can be written by

$$E_0^{ET} = I_G - P_+ - S_{-}^{ion}, \tag{6.4}$$

where S_{-}^{ion} is the stabilization energy for a molecular anion. Stabilization energy S_{-}^{ion} is given by

$$S_{-}^{ion} = P_- + E_A(g), \tag{6.5}$$

where P_- is the polarization energy induced by a molecular anion and $E_A(g)$ is the electron affinity of a molecule (see § 1). After the electron transfer the negative charge may be located in the Coulomb potential originating from the positive charge. This can be regarded as the geminate ion pair. A free charge carrier is generated on escape from the Coulomb potential well. This electron transfer process can be also regarded as an internal conversion (IC) from a higher excited state into the ion pair state (charge transfer state).

In a first apporoximation the threshold energies for both the ionization modes are identical, since S_{-}^{free} equals S_{-}^{ion}. However, it is neccesary to take the time response of electronic polarization into consideration because the emitted electron has a finite velocity whereas molecular anion state is localized. If the emitted electron moves faster than the response time of the polarization, S_{-}^{free} is nearly zero, while S_{-}^{free} has the same magnitude as S_{-}^{ion} if it moves relatively slow.

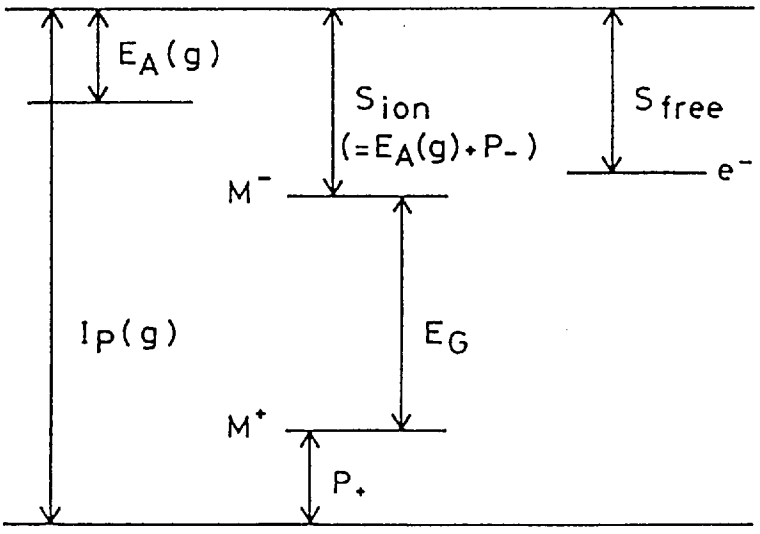

Fig. 6.7 Energy levels of charged species in organic crystals.

6.3.2 Comparison of the model with the experimental results

Experimental results indicates that, below the threshold energy for external photoemission E_{th}, the ionization efficiency of an excited state is insensitive to the excitation energy. A possible interpretation is that photoionization occurs by electron transfer (mechanism (II); ET) from a certain electronic state after a rapid relaxation. When excitation energy exceeds the threshold energy for external photoemission E_{th}, photoionization by electron emission (mechanism (I); EE) is expected to occur. This is supported by the experimental finding that the efficiency for generating a geminate electron-hole pair is close to unity and that ionization efficiency increases steeply above E_{th}. These observations clearly indicate that the ionization process changes from indirect process to direct one with increasing excitation energy.

In the case of direct ionization the threshold energy E_o^{EE} is the same as that for external photoemission E_{th}. Hence, the stabilization energy for a free electron should be zero ($E_{th} = I_G - P_+$ and $E_o^{EE} = I_G - P_+ - S_{-free}$). Figure 6.8 illustrates the model for photoionization in aromatic hydrocarbon crystals. Details will be discussed below.

[Electron transfer mechanism ($h\nu < E_{th}$)]

For excitation energy below the E_{th}, transient absorption spectra are similar to those of solution. This indicates that it is neutral excited states which are generated by light

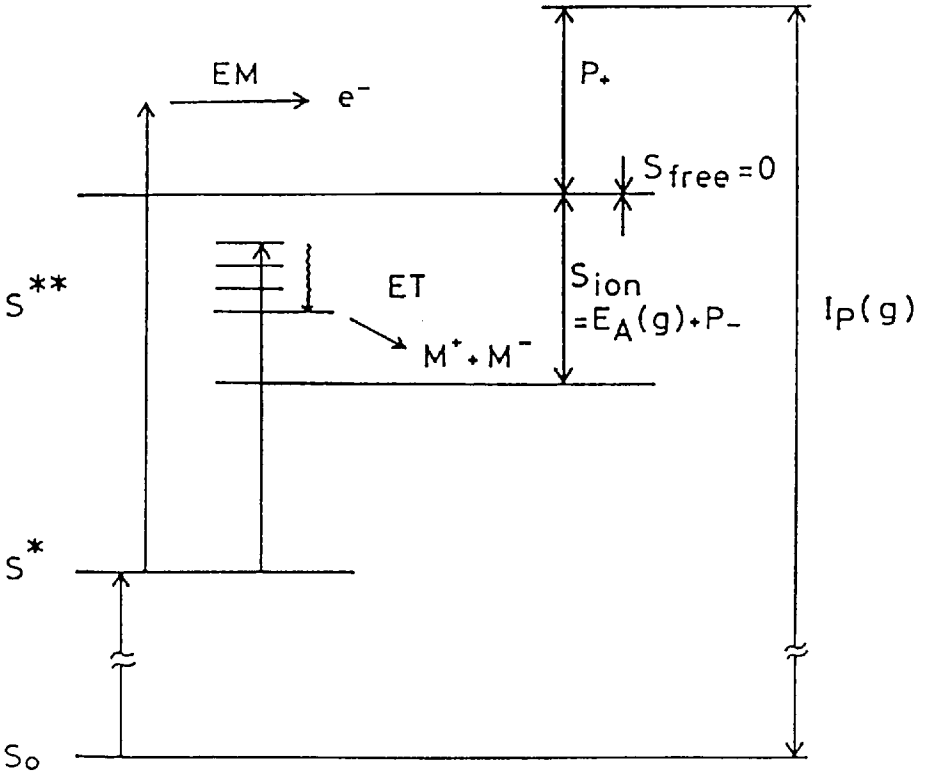

Fig. 6.8 Energy levels for photocarrier generation in aromatic hydrocarbon crystals.

excitation. Ionization (charge separation) may occur succeedingly by electron transfer from the higher excited state to a neighboring molecule. This process can be also considered as internal conversion of the higher neutral excited state to the charge transfer state (CT state).

When exciting light irradiates the crystal, a higher neutral excited state with some vibrational excitation is generated. The vibrational energy of this state is redistributed rapidly to other vibrational modes (intramolecular vibrational redistribution, IVR), to form a relaxed higher excited state. The IVR may be faster than internal conversion (IC). Hence, electron transfer, namely the internal conversion to a charge transfer state, occurs after IVR. This explains that the ionization efficiency is insensitive to excitation energy. Relaxed higher excited states have some vibrational energy because relaxation of vibrational excitation is relatively slow, i.e. relaxation time for vibrational energy in a condensed phase is on the order of 10^{-11} sec [6.32-34]. Vibrational energy of the higher excited state after IVR may be converted to vibrational energy of the molecular ion.

As discussed § 6.2, the efficiency of the geminate electron-hole pair generation Φ_{GP} is small ($\sim 10^{-3}$) below the threshold energy E_{th} for external photoemission. In the case of electron transfer Φ_{GP} can be considered as efficiency of CT state generation. It is limited by the competition between internal conversion to the ground state and that to a CT state. According to the Fermi golden rule a rate is determined by the Franck-Condon factor between two states. The orbital of a CT state is

spread among other molecules, therefore, the orbital shape of the CT state may be much different from that of a higher excited state. Hence, the Franck-Condon factor between the higher neutral excited state and the CT state may be small. As a result internal conversion to a CT state may be inefficient.

Being purely electrostatic, the Onsager model cannot give a quantitative account of the ionization efficiency. The size of a geminate ion pair generated by electron transfer process is the same as the nearest intermolecular distance (~ 6Å), so that the model gives as escape probability from the Coulomb potential of $\sim 10^{-14}$. This is smaller by many orders of magnitude than 10^{-1} which is experimentally estimated (Table 6.3).

It is possible that a charge transfer state is an intermediate state in photocarrier generation. Such a treatment was reported by Braun [6.17]. The model shows that a CT state can dissociate thermally with relatively high probability. It is remarkable that the model predicts a slope-to-intercept ratio in electric field dependence which is identical to the value expected from the Onsager model. For further understanding of the photocarrier generation in aromatic hydrocarbon crystals the role of CT states should be clarified.

[Electron emission mechanism ($h\nu > E_{th}$)]

When a photon energy exceeds the threshold energy for the external photoemission, Φ increases steeply and Φ_{GP} becomes close to unity. This clearly indicates that ionization through

electron emission (I) occurs. "Hot electrons" generated are thermalized to conduction electrons by inelastic scattering in the medium and contribute to the photocurrent. Polarization energy for the hot electrons depends on the its velocity because electronic polarization has a finite response time with respect to the mobile electron. Experimental results indicate that S_{free} is zero. Namely, the electronic polarization cannot respond to the hot electron generated by photoionization.

The velocity v_e of the hot electron can be given by

$$v_e = (2E_{kin}/m^*)^{1/2}, \tag{6.6}$$

where E_{kin} is the kinetic energy of the hot electron and m^* is the effective mass of the electron in the crystal. In the first apporoximation, m^* is the rest mass of an electron. The transfer time τ_t for an electron between two neighboring lattice sites may be given by

$$\tau_t = a_0/v_e, \tag{6.7}$$

where a_0 is the lattice constant. When ionization occurs, electron emitted has a kinetic energy which has the same magnitude as ionization potential. The transfer time τ_t can be estimated to be $\tau_t = 10^{-16}$ sec using the values of $E_{kin} = 5$ eV and $a_0 = 6.2$ Å .

The response time of electronic polarization can be estimated from resonance frequency of the electronic state. In aromatic hydrocarbon crystals electronic polarization is limited by deformation of π electrons. Response time τ_{res} can, therefore, be written by

$$\tau_{res} = 1/\nu_{res}, \tag{6.8}$$

where ν_{res} is the resonance frequency of π electron. In a

first approximation ν_{res} is the frequency for HOMO-LUMO transition. In the case of anthracene, which has the energy of 3.1117 eV [6.26] for HOMO-LUMO transition, the response time is $\tau_{res} = 1.3 \times 10^{-15}$ sec. This is longer than the transfer time of an electron ($\tau_t = 10^{-16}$ sec). Hence, in the case of photoionization by electron emission electronic polarization can not respond to motion of photo-emitted electrons in this class of material.

6.4 Comparison with photoionization processes in other types of condensed phases

Photoionization of a molecule in a condensed phase has been studied in various media, such as alkanes, alcohols and molecular crystals. However, ionization process is different from different media. Photoionization of a molecule in condensed phase can be considered from following points of view.

(1) Threshold energy of photoionization
(2) Geminate recombination kinetics
(3) Excitation energy dependence of ionization efficiency
(4) Photoionization mechanism

They will be discussed by comparing with various types of condensed phases.

Photocarrier generation in an aromatic hydrocarbon crystal can be viewed as photoionization of a molecule in the crystal. The characteristic features can be considered based on the experimental results presented previous chapters and reported studies. These are:

(1) The threshold energies for photoconduction and for photoelectron emission can be interpreted by the polarization model [6.18].
(2) Geminate recombination kinetics can be explained by the Onsager model. This is confirmed by the study of photoconductivity as a function of a electric field [§ 5.6, 6.1-3].
(3) Ionization efficiency is low ($\sim 10^{-3}$), limited by geminate recombination. Ionization efficiency and initial separation between an electron and its parent cation changes stepwise with increasing excitation energy [§ 6.3].
(4) The mechanism of ionization change with exciting energy, from a indirect process, such as electron transfer, to a direct process. Charge transfer state may play an important role as an intermediate state in photoconduction.

In alkane solutions photoionization of a molecule have several features not found in aromatic hydrocarbon crystals. They are [6.19]:

(1) Threshold energy of the photoconductivity can be estimated by the polarization model using conduction band energy V_0 and polarization energy for a positive charge estimated by the Born formula [6.20].
(2) Geminate recombination kinetics can be accounted for by the Onsager model. This is verified through the study of photoconductivity as a function of an electric field [6.21] and time resolved spectroscopy [6.22-24].
(3) Initial separation between an electron and its parent cation

increases gradually with excitation energy [6.9, 6.21 6.25].
(4) Action spectrum for photoconductivity indicates direct ionization [6.26-27].

In polar solvents, such as methanol and acetonitrile, photoionization of a diamine molecule occurs from its lowest singlet excited state [6.28-29]. In this case the photoionization is characterized by the following features.

(1) Threshold energy decreases by a large amount due to polarization of the molecules which have permanent dipole moment. However, quantitative interpretation is not established yet.
(2) Positive and negative charges form a stable ion pair by large polarization, so that recombination kinetics does not follow the Onsager model [6.30].
(3) No reliable studies of energy dependence of photoconductivity exist.
(4) In an alcohol solution photoionization occurs by electron transfer from singlet excited state to the solvent cluster so that solvated electron is formed [6.30]. In acetonitrile solution electron transfer occurs from singlet excited state to a solvent molecule. Successively a dimer anion of solvent molecules is formed [6.31-32].

Photoionization of a molecule in different condensed phases have different features. These differences can be qualitatively understood by considering the polarization process and electron affinity of the molecule in a medium.

An alkane molecule has negative electron affinity and no

parmanent dipole moment. When photoionization occurs in alkane solution, a parent cation and an electron emitted are stabilized by electronic polarization. The electron does not localize on a molecule but forms a solvated electron. In such a case recombination kinetics can be treated as scattering process of an electron by the surrounding molecules. Hence, ionization in an alkane liquid can be explained as following picture. When molecules in an alkane are irradiated with light, electrons with some kinetic energy are emitted. After thermalization the electrons moves diffusively and most electrons recombine with a parent cation (geminate recombination). Quantitative interpretation of this process can be made by the Onsager theory. Ionization efficiency increases with the energy of exciting light because initial separation between a thermalized electron and a parent cation increases.

In the case of polar solvent which have parmanent dipole moment, such as alcohol and acetnitrile, polarization due to molecular reorientation is important for stabilization of charged species. In this case ion pair is stabilized efficiently by orientation of surrounding molecules. As a result recombination kinetics cannot be explained by the Onsager theory. For recombination of the charges reorientation of solvent molecules is needed, so that the ion pair has a long lifetime. In such a case two modes for the indirect process have been found, i.e., an electron transfer from neutral excited state to a favorable site of the medium and to a neighbering molecule.

Most aromatic hydrocarbon molecules have no parmanent dipole moment. Hence, ionic species are stabilized only by the

electronic polarization, which is larger than that of alkane molecule by deformation of π orbital. Ion pair is stabilized by the electronic polarization and it has a long lifetime. This state can be recoginized as a charge transfer state. As a result indirect charge separation process, which is electron transfer from neutral excited state to a neighboring molecule, is expected as well as in the case of a polar solution. Electron affinity of the aromatic hydrocarbon molecule in a crystal is positive, so that electron transfer occurs from neutral excited state to a neighboring molecule. As discussed in § 6.3, direct ionization occurs when exciting energy exceeds to threshold energy of external photoelectron emission. The difference in the threshold energies between electron transfer and direct ionization is due to response time of electronic polarization (§ 6.3).

References

[6.1] R.H.Batt, C.L.Braun and J.F.Hornig,
J. Chem. Phys. 49 (1968) 1967.

[6.2] R.C.Hughes,
J. Chem. Phys. 55 (1971) 5442.

[6.3] R.R.Chance and C.L.Braun,
J. Chem. Phys. 59 (1973) 2269.

[6.4] R.R.Chance and C.L.Braun,
J. Chem. Phys. 64 (1976) 3573.

[6.5] K.Kato and C.L.Braun,
J. Chem. Phys. 72 (1980) 172.

[6.6] L.E.Lyons and K.A.Milne,
J. Chem. Phys. 65 (1976) 1474.

[6.7] E.Morikawa and M.Kotani,
J. Chem. Phys. 91 (1989) 180.

[6.8] P.M.Borsenberger and A.I Ateya,
J. Appl. Phys. 49 (1978) 4035.

[6.9] Y.Hirata, N.Mataga,
J. Chem. Phys. 95 (1991) 1640.

[6.10] N.Karl,
in: Landort-Burnstein numerical data and fundamental relationships in science and technology, New series, Vol.17, Eds. O.Madelung, M.Schulz and H.Weiss (Springer, Berlin, 1985).

[6.11] C.Kryschi, W.Klufer and H.Kupka,
Chem. Phys. 146 (1990) 231.

[6.12] N.Sato private communication.

[6.13] L.E.Lyons,
J. Chem. Soc. (1957) 5001.

[6.14] R.W.Anderson,
in "picosecond Phenomena II ", Eds., R.M.Hochstrasser,
W.Kaiser and C.V.Shank (Springer, Berlin, 1980), p163.
[6.15] F.Laermer, T.Elsaesser and W.Kaiser,
Chem. Phys. Lett. 156 (1989) 381.
[6.16] Y.Hirata and T.Okada,
Chem. Phys. Lett. 187 (1991) 203.
[6.17] C.L.Braun,
J. Chem. Phys. 80 (1984) 4162.
[6.18] N.Sato, H.Inokuchi,
Chem. Phys. 115 (1987) 269.
[6.19] B.S.Yakovlev and L.V.Lukin,
Adv. Chem. Phys. 60 (1985) 99.
[6.20] R.A.Holroyd, J.M.Preses and N.Zevos,
J. Chem. Phys. 79 (1983) 483.
[6.21] H.T.Choi, D.S.Sethi and C.L.Braun,
J. Chem. Phys. 79 (1983) 483.
[6.22] C.L.Braun and T.W.Scott.,
J. Chem. Phys. 87 (1983) 4776.
[6.23] C.L.Braun, S.N.Smirnov, S.S.Brown and T.W.Scott.,
J. Chem. Phys. 95 (1991) 5529.
[6.24] Y.Yoshida, S.Tagawa and Y.Tabata,
Radiat. Phys. Chem. 28 (1986) 201.
[6.25] D.W.Tweeten and S.Lipsky,
J. Phys. Chem. 93 (1989) 2683.
[6.26] U.Sowada and R.A.Holroyd,
J. Chem. Phys. 70 (1979) 3586.
[6.27] G.F.Hoffman and A.C.Albrecht,
J. Phys. Chem. 94 (1990) 4455.
[6.28] Y.Hirata, N.Mataga, Y.Sakata and Y.Misumi,

J. Phys. Chem. 86 (1982) 1508.

[6.29] Y.Hirata and N.Mataga,

J. Phys. Chem. 89 (1985) 4031.

[6.30] Y.Hirata and N.Mataga

J. Phys. Chem. 87 (1983) 3190.

[6.31] Y.Hirata, N.Mataga, Y.Sakata and S.Misuni,

J. Phys. Chem. 87 (1983) 1493.

[6.32] Y.Hirata, Y.Tanaka and N.Mataga

Chem. Phys. Lett. 193 (1992) 36.

7. Relaxation of higher excited states generated by singlet exciton fusion in an anthracene crystal

7.1 Introduction

Higher excited states in organic crystals can be important as intermediates in charge carrier generation. This problem was already discussed in § 6. Silinsh and Inokuchi have also discussed the charge carrier generation after vibrational relaxation of a higher excited states [7.1]. There are not many studies of relaxation channels of higher excitons in organic crystals.

When fusion of two singlet excitons S^* occurs, a higher excited states S^{**} can be populated.

$$S^* + S^* \xrightarrow{\gamma_{ss}} S^{**}$$

When the S^* are generated in a high density, the majority of the S^* state undergoes fusion and populates S^{**} states. At low excitation intensities the singlet excitons decay predominantly by a unimolecular process, hence, the relaxation from the higher excited states cannot be studied.

This singlet exciton fusion can be studied by observing the quantum yield of fluorescence which starts to decrease above a certain exciting light intensity [7.2] and fluorescence decay which becomes nonexponential at high excitation intensities [7.3]. The second order rate constant for singlet exciton fusion γ_{ss} in an anthracene crystal is known [7.3]. The energy of a singlet exciton is 3.1117 eV in anthracene crystal [7.4]. The

higher excited state S^{**} generated by the fusion of two relaxed singlet excitons, has accordingly an energy of 6.22 eV. This energy exceeds both the band gap (4.1 eV [7.5]) and the threshold energy for external photoemission (5.67 eV [7.6]) in anthracene crystal. As expected, photoconductivity [7.7] and external photoemission (see § 3.4) have been observed on singlet exciton fusion.

Here other types of decay channels of higher excited state populated by the fusion, i.e. fluorescence from higher excited states and fission into two triplet excitons, will be discussed. Figure 7.1 summarizes generation and decay channels of higher excited states populated by the fusion of two singlet excitons.

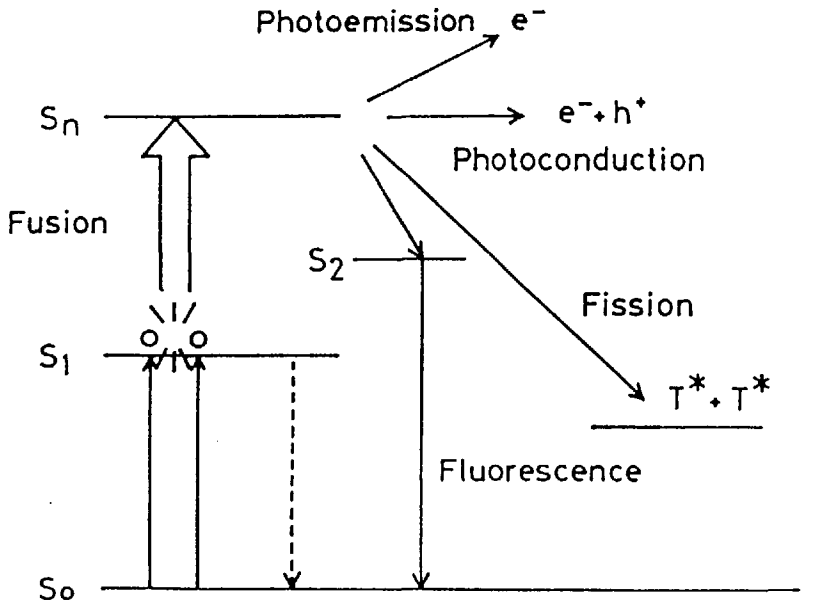

Fig. 7.1 Decay channels for higher excited states populated by fusion of two singlet excitons.

7.2 Fluorescence from higher excited states (S_2 and S_3)

7.2.1 Introduction

Fluorescence from higher excited states of a molecule in solution has been studied [7.8-7.11]. Experimentally, its observation is difficult because its quantum efficiency is very low and emission from optics and impurities often disturbs detection of a very weak emission. Hirayama et al. have reported spectra and quantum yields of fluorescence from higher excited states of naphthalene and pyrene in 2,2,4-trimethylpentane solution [7.8]. It has been shown that multiphoton [7.9] and two-color, two-step [7.10] excitation are advantageous in reducing experimental difficulties. Nickel and Karbach used annihilation of two triplet solutes to populate higher excited states [7.11]. In a crystalline phase observation of fluorescence from higher excited state is supposed to be even harder because scattering of exciting light at a crystal surface is often very strong. I succeeded to observe a fluorescence from higher excited states populated by the fusion of two singlet excitons.

7.2.2 Experimental

A dye laser (Lambda Physik, FL-3002; laser dye: PBBO), pumped by a XeCl excimer laser (Lambda Physik, EMG-101 MSC), was used as an exciting light source (λ = 397 nm). Duration of the exciting light was 10 ns. The exciting light was incident at 30 ° on ab-plane (cleaved plane) of a single crystal. Fluorescence

from a surface of the sample specimen was observed with a small double-monochromator (Jobin-Yvon, H10D) and two different types of photomultipliers. For λ = 250 - 350 nm light a bialkali photomultiplier (Hamamatsu, R269) was used with a band pass filter (HOYA, U340). The other photomultiplier which was solar blind (Hamamatsu, R431S) was used without filters. In order to know the relative intensity of fluorescence from S_1, S_2 and S_3, the gain of the photomultiplier and the slit width of the monochromator were kept constant and neutral density filters were inserted between the sample and the monochromator. Signal from the photomultiplier was digitized by a 12bit transient digitizer (Autonics, S-210) and was integrated by a microcomputer (EPSON, PC-286VS). All measurements were made at room temperature. Calibration of the spectral sensitivity of the detection system over the range 210 - 530 nm was made using a Rhodamine B quantum counter [7.12].

7.2.3 Results and discussion

The fluorescence spectrum, corrected for spectral sensitivity of the detection system, is shown in Fig. 7.2. In addition to the well-known, strong fluorescence in the visible light range, very weak emission is observed in the UV range. The intensity of the fluorescence in the UV is less than 10^{-6} of that in the visible. It may be seen that the spectrum in the UV has two peaks, one at 5.4 eV (230 nm) and the other at 4.4 eV (280 nm). Below 3.8 eV (330 nm) the fluorescence intensity increases steeply with decreasing photon energy. Photon energy of this fluorescence is larger than that of 0-0 transition of this

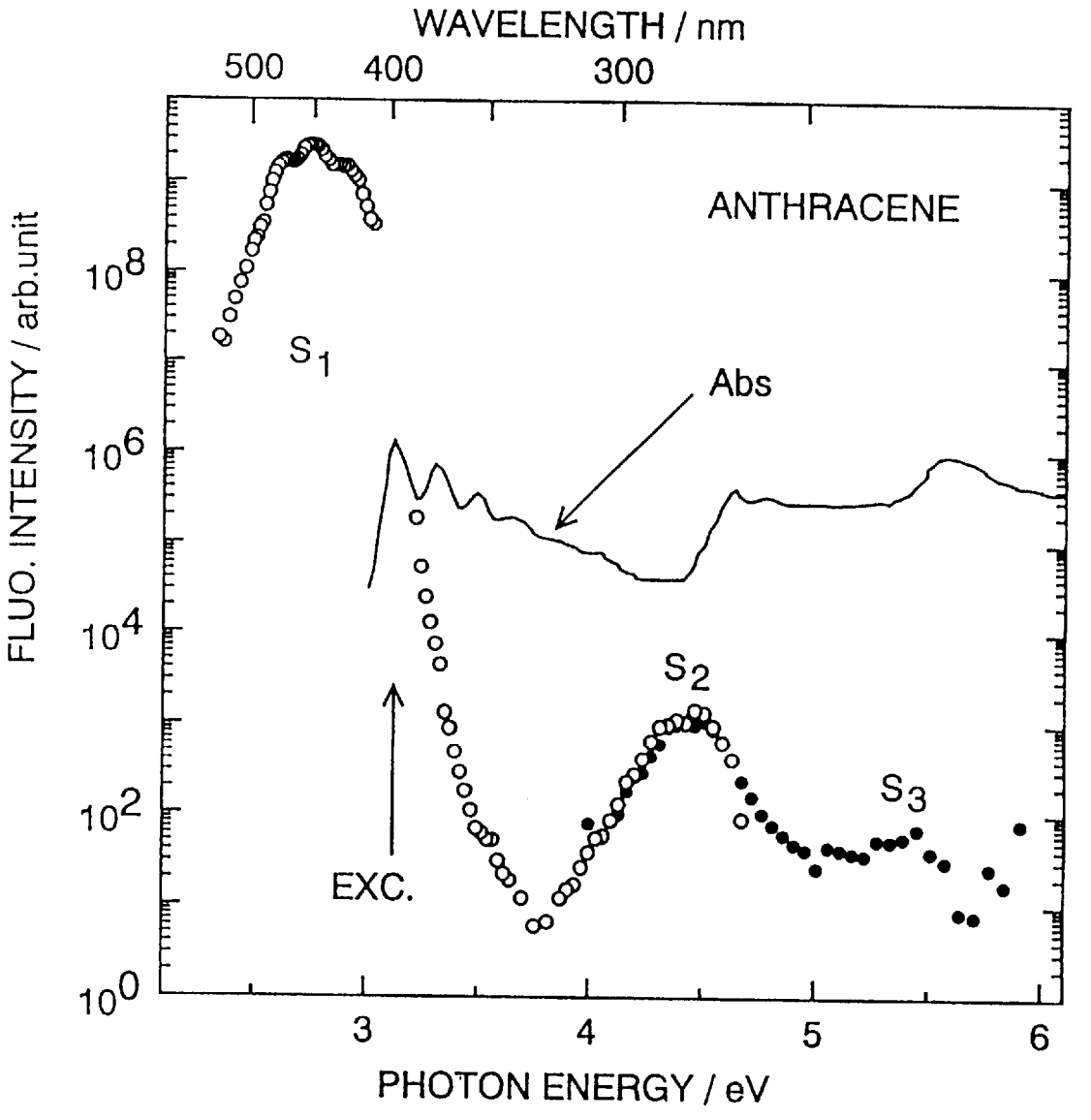

Fig. 7.2 Fluorescence spectrum of an anthracene crystal. Photomultipliers used: ○ R269; ● R431S. Excitation photon energy (3.12 eV, 397 nm) is indicated by an arrow. The drawn-out line indicates the absorption spectrum. A good correspondence to S_1, S_2 and S_3 in the absorption spectrum is obvious.

material (3.1117 eV [7.4]). Hence, this may be due to fluorescence from unrelaxed vibrational levels of S_1.

In Fig. 7.2 is also shown the absorption spectrum of an anthracene crystal (polarized parallel to the crystal b-axis) [7.13]. The absorption spectrum has peaks at 220 nm (5.6 eV), 270 nm (4.6 eV) and 400 nm (3.1 eV) which correspond to the electronic excited states S_3, S_2 and S_1, respectively. A rather clear mirror image relationship is examined between the absorption peaks and the peaks in the fluorescence spectrum. This indicates that the observed fluorescence at 5.4 eV (230 nm) can be assigned to $S_3 \rightarrow S_0$ transition and the peak at 4.4 eV (280 nm) to $S_2 \rightarrow S_0$ transition.

Kinetics of higher exciton states can be written as

$$d[S_1]/dt = \alpha I_{ex} - k_1[S_1] - (1/2)\gamma_{ss}[S_1]^2 \quad (7.1)$$

$$d[S_2]/dt = G_2(1/2)\gamma_{ss}[S_1]^2 - k_2[S_2] \quad (7.2)$$

$$d[S_3]/dt = G_3(1/2)\gamma_{ss}[S_1]^2 - k_3[S_3] \quad (7.3)$$

where α is the absorption coefficient of the ground state, I_{ex} is the intensity of the exciting light, γ_{ss} is the rate constant for singlet exciton fusion, G_2 and G_3 are the population efficiencies of the higher excitons by the fusion of two S_1's and k_2 and k_3 are the decay constants of the higher excitons. In the present study the intensity of the exciting light is high and the third term on the right-hand side of Eq. (7.1) is more important than the $k_1[S_1]$ term. In that case, the density of excitons can be written, in a steady state, as

$$[S_1] = (2\alpha/\gamma_{ss})^{1/2} I_{ex}^{0.5}, \quad (7.4)$$

$$[S_2] = (G_2/2k_2)\gamma_{ss}[S_1]^2 = (G_2/k_2)\alpha I_{ex}^{1.0}, \quad (7.5)$$

$$[S_3] = (G_3/2k_3)\gamma_{ss}[S_1]^2 = (G_3/k_3)\alpha I_{ex}^{1.0}. \quad (7.6)$$

Eqs.(7.4)-(7.6) show that, with increasing intensity of the excitation light, emission from S_2 and S_3 becomes stronger relative to the fluorescence from S_1 with increasing intensity of the excitation light. This is the reason why the fluorescence from the higher excitons can be observed by making use of the singlet exciton fusion.

According to Eq.(7.4) the intensity of fluorescence from S_1 should be proportional to $I_{ex}^{0.5}$ when S_1 is populated directly by photon absorption. S_2 and S_3 cannot be generated directly by one-photon absorption and are populated through the fusion of S_1. In this case intensity of fluorescence from S_2 and S_3 should be proportional to I_{ex}.

Figure 7.3 shows fluorescence intensity, observed at λ = 290, 360, 380 and 450 nm, as a function of intensity of the exciting light I_{ex}. At λ = 380 and 450 nm the fluorescence intensity is proportional to $I_{ex}^{0.5}$. This indicates that fluorescence from S_1 generated by single photon absorption is observed. At λ = 380 nm for high exciting light intensities the fluorescence intensity is proportional to the intensity of the exciting light. This may be the fluorescence from S_1 populated via higher exciton generated by the singlet exciton fusion. At λ = 290 and 360 nm the fluorescence intensity is proportional to I_{ex}. This indicates that the fluorescence is emitted via higher excited states generated by the singlet exciton fusion. This is consistent with the discussion made with Fig. 7.2 and fluorescence at 290 nm can be assigned as $S_2 \rightarrow S_0$ transition. Fluorescence at 360 nm may be from vibrationally unrelaxed S_1 state, populated by relaxation from higher exciton state. (This

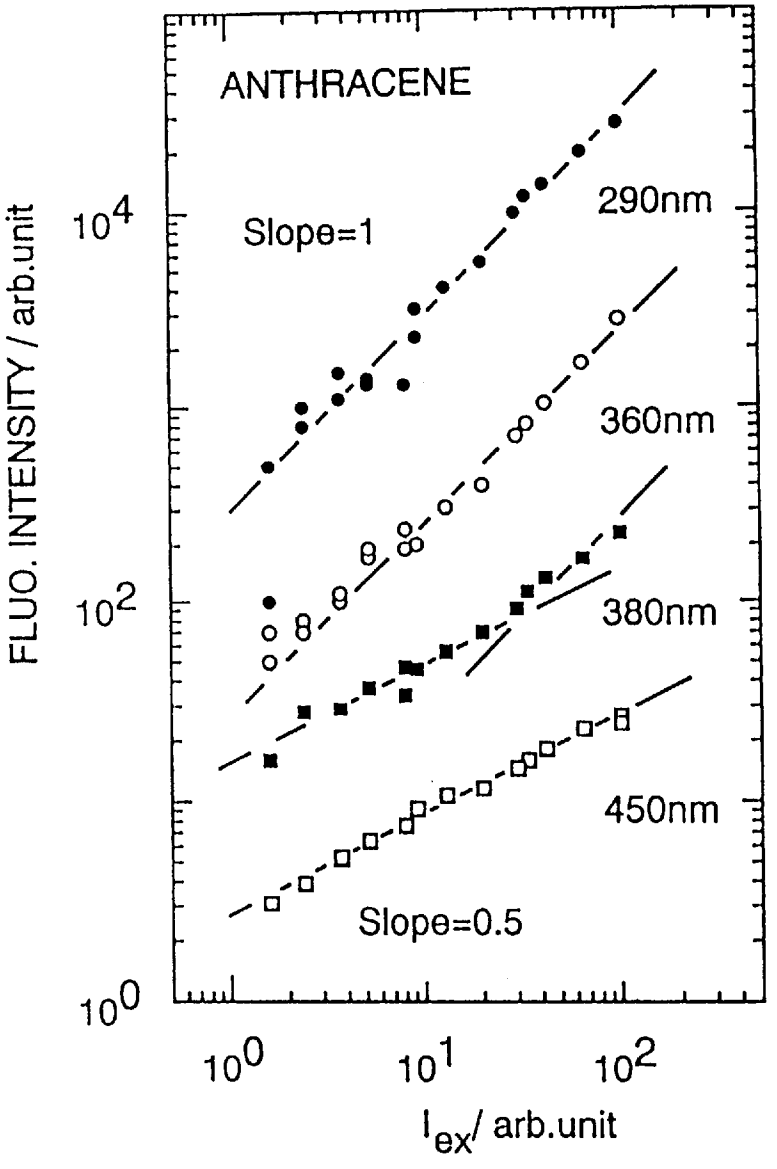

Fig. 7.3 Fluorescence intensities at various wavelengths as a function of the exciting light intensity (λ_{ex} = 397 nm).

path is not considered in Eq. (7.4). In this case S_1 is not populated directly by one-photon absorption, but indirectly through fusion. This type of fluorescence should follow the same kinetics as S_2 and S_3.) Figure 7.4 shows a scheme for fluorescence via higher excited states generated by fusion of two lowest singlet excitons.

Under the present experimental condition higher excitons S_2 and S_3 are populated indirectly. Probabilities and rate constants are not available to allow a quantitative discussion for the generation and decay processes to be made. Here only a rough estimation can be made for the product of the lifetime $\tau_n = 1/k_n$ (n = 2,3) and the population efficiency G_n (n = 2,3) for higher excitons. From eq.(7.4) the density of the lowest singlet exciton is $[S_1] = 6\times 10^{18}$ cm^{-3} using the values of $\alpha = 10^5$ cm^{-1} [7.13], $\gamma_{SS} = 10^8 cm^{-3}s^{-1}$ [7.3] and $I_{ex} = 1.6\times 10^{24}$ photons cm^{-2} s^{-1}. The intensity of the fluorescence reflects the density of the excited states, if the radiative rate constants of S_1, S_2 and S_3 can be assumed to be roughly equal. The density of higher excitons are then estimated to be $[S_2] = 3\times 10^{12}$ cm^{-3} and $[S_3] = 2\times 10^{11}$ cm^{-3}. From Eqs.(7.5) and (7.6) the products are $G_2 \times \tau_{S2} = 2\times 10^{-17}$ s and $G_3 \times \tau_{S3} = 1\times 10^{-18}$ s.

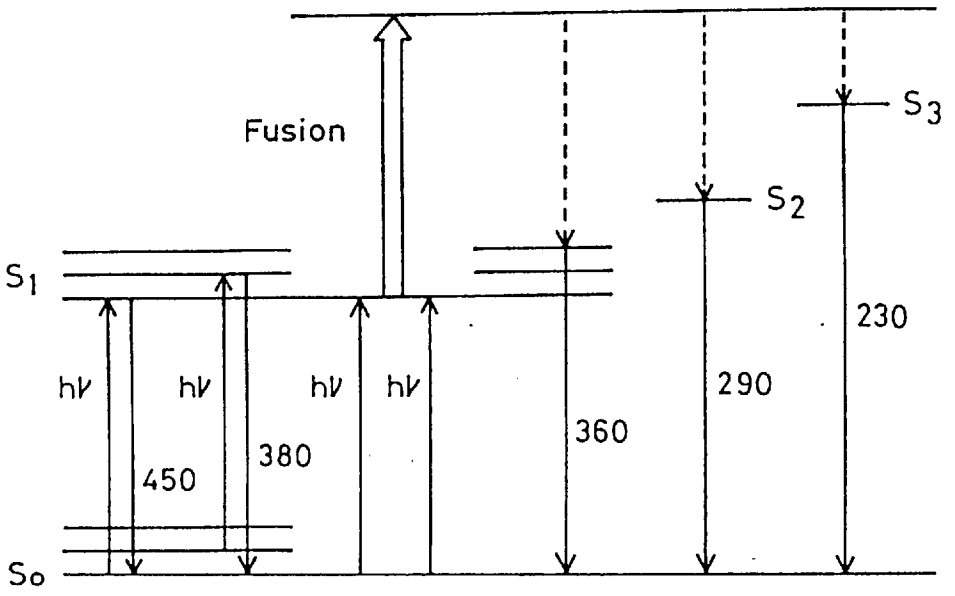

Fig. 7.4 Scheme explaining the fluorescence from S_1, S_2 and S_3 populated by one-photon absorption and fusion of two singlet excitons. Numbers indicate wavelengths of respective transitions (all in nm).

7.3 Fission of higher excited states into triplet excitons

7.3.1 Reaction of excitons in organic crystals

There can be many reaction channels of a excitons in an organic crystal, such as fusion of two excitons and fission from higher excited state into two excitons. Fission into two triplet excitons

$$S^{**} \rightarrow T + T.$$

is possible when the higher excited state S^{**} has an energy more than twice the energy of a triplet exciton T. The overall spin multiplicity has to be conserved in the process, and hence the reaction is sensitive to an external magnetic field. Klein et al. have studied this process in an anthracene crystal with VUV excitation [7.14-15].

Triplet exciton fusion (annihilation), the inverse process of the fission,

$$T + T \rightarrow S^{**} \rightarrow S^{*} \rightarrow S_0$$

$$\gamma_{TT} \qquad\qquad DF$$

has been investigated through magnetic field modulation of delayed fluorescence (DF) with a number of compounds. In the representative case of anthracene the intensity of the delayed fluorescence decreases with increasing magnetic field strength and this decrease saturates at high fields [7.16]. The magnetic field effect has an orientational dependence which is characteristic of a spin-spin dipolar interaction of a triplet exciton. The fission into two triplet excitons exhibits an inverse behaviour: The intensity of the prompt fluorescence increases when a magnetic field is applied [7.14-15].

Fission into two triplet excitons is also energetically possible as the energy of the S** state (6.22 eV) is higher than twice the energy of a triplet exciton (2× 1.83 = 3.66eV) [7.4].

$$S^* + S^* \rightarrow S^{**} \rightarrow T + T$$

fusion fission

It can be detected through modulation of fluorescence intensity by an external magnetic field. When the exciting light intensity is strong, fluorescence observed is emitted from S* state which is populated indirectly through relaxation of S** state and is not fluorescence emitted by S* populated directly by the exciting light. Hence, it may be expected that a magnetic field affects fluorescence intensity only when the excitation is strong.

7.3.2 Experimental

A XeCl excimer laser (Lambda Physik, EMG-101 MSC) was used as the exciting light source (λ = 308 nm). Duration of the exciting light is $\sim$ 50 ns. Experimental arrangement is shown in Fig. 7.5. Sample specimen could be rotated around the c'-axis and magnetic field was in the ab-plane of the crystal. The exciting light was incident at 45° on a sample specimen. Fluorescence was observed at 450 nm with a small double-monochromator (Jobin-Yvon, H10D) and a photomultiplier (Hamamatsu, R268) equipped with a magnetic shield. Signal from the photomultiplier was digitized by a 12bit transient digitizer (Autonics, APC-204) and was integrated by a microcomputer (EPSON, PC-286VS). Magnetic field strength was measured with a gaussmeter (Yokogawa, Type-3251). The measurement system was

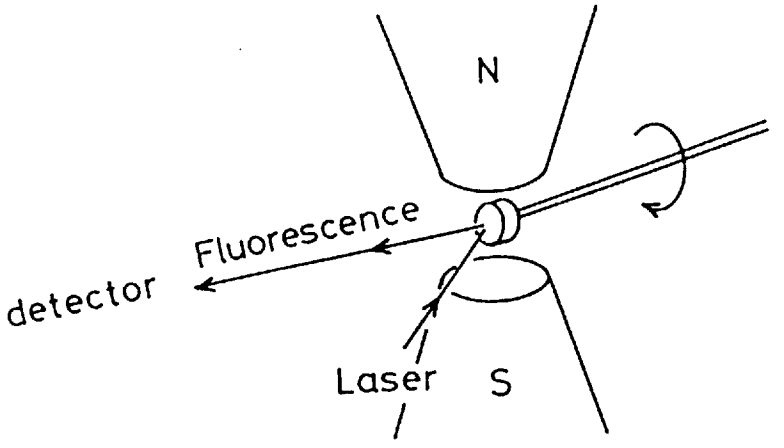

Fig. 7.5 Experimental arragement for observing a magnetic field modulation of fluorescence.

immune to the magnetic field within ± 0.2%. All measurements were made at room temperature.

7.3.4 Results and discussion

The modulation of fluorescence by a magnetic field $\triangle F/F$ is defined as

$$\triangle F/F = \{F(H)-F(0)\}/F(0), \qquad (7.7)$$

where F(H) and F(0) is the fluorescence intensity with and without magnetic field H, respectively. The orientation angle θ is defined as the angle between the magnetic field vector and the crystal b-axis in the ab-plane.

Generation and decay processes of singlet excitons S* can be expressed by

$$d[S^*]/dt = \alpha I_{ex} - [S^*]/\tau_s - \gamma_{ss}[S^*]^2, \qquad (7.8)$$

where α is the absorption coefficient, τ_s is the lifetime of the singlet exciton and γ_{ss} is the rate constant of the singlet exciton fusion. In this experiment the duration of the exciting pulse (τ_p = 50 ns) is longer than the lifetime of the singlet exciton (τ_s = 20 ns [7.17]), and hence, stationary state is a good approximation. In the case of a weak excitation the third term of the right hand side in Eq. (7.8) can be neglected and, accordingly, the concentration of the singlet exciton is proportional to I_{ex}. When an intense excitation is made, the second term of Eq.(7.8) becomes unimportant. Then, [S*] is proportional to $I_{ex}^{0.5}$. Experimental observation verifies this expectation (Fig. 7.6 (a)).

Figure 7.6 (a) shows F(0) and $\triangle$ F/F as a function of the exciting light intensity I_{ex} (λ = 308 nm). The magnetic field strength is 6.8kG and θ =-30° (high field resonance condition. cf. Fig. 7.8). The fluorescence intensity is proportional to I_{ex}^{n}, where n is unity for low exciting intensities and decreases toward 0.5 for higher I_{ex}. It has been observed that the modulation $\triangle$ F/F sets in at the excitation intensity at which the fusion becomes dominant (Fig. 7.6 (b)). This indicates that fission into two triplet excitons occurs from a higher excited state generated by singlet exciton fusion. In Fig. 7.7 $\triangle$ F/F is plotted against the strength of the magnetic field (θ =-30°). Intensity of the exciting light is high enough to ensure that fusion of two singlet excitons is the dominant decay process. It may be seen that $\triangle$ F/F increases with the field strength and gradually saturates. Figure 7.8 shows $\triangle$ F/F as a function of the angle θ between the magnetic field vector and the crystal b-axis in the ab-plane. The magnetic field strength is 6.8kG. The orientation dependence is symmetric with respect to the b-axis and high field resonances can be seen at $\theta \sim \pm 25°$. For comparison the positions of high field resonances on the delayed fluorescence ($\pm$ 23.5° [7.16]) are also shown by arrows in the Figure.

The magnetic field effects observed (Figs.7.7 and 7.8) are the inverse of those for the fusion (delayed fluorescence), apart from its magnitude, and clearly indicate that fission of a higher excited singlet state into two triplet excitons is occurring.

The total energy reached by the fusion of two singlet exciton may be twice the energy of a vibrationally relaxed

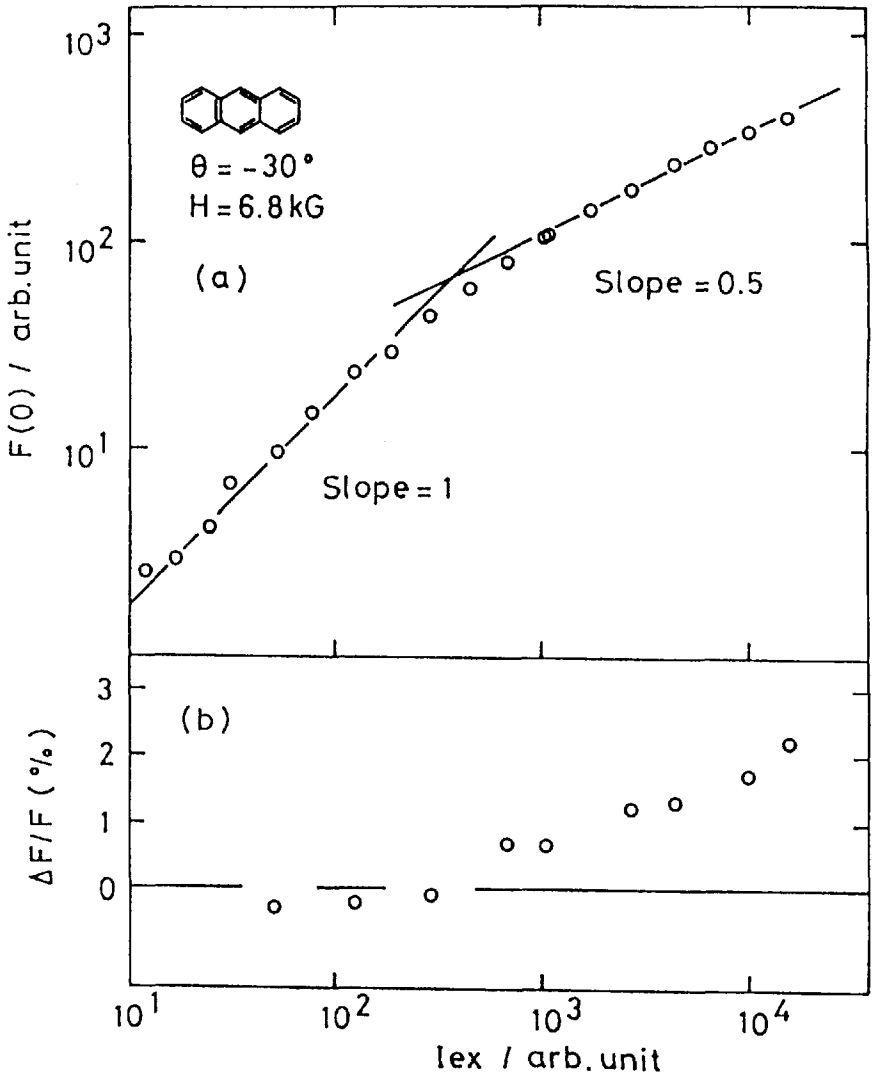

Fig. 7.6 Fluorescence intensity without magnetic field F(0) and the magnetic field modulation Δ F/F poltted against exciting light intensity I_{ex}. H = 6.8 kG, θ = -30° .

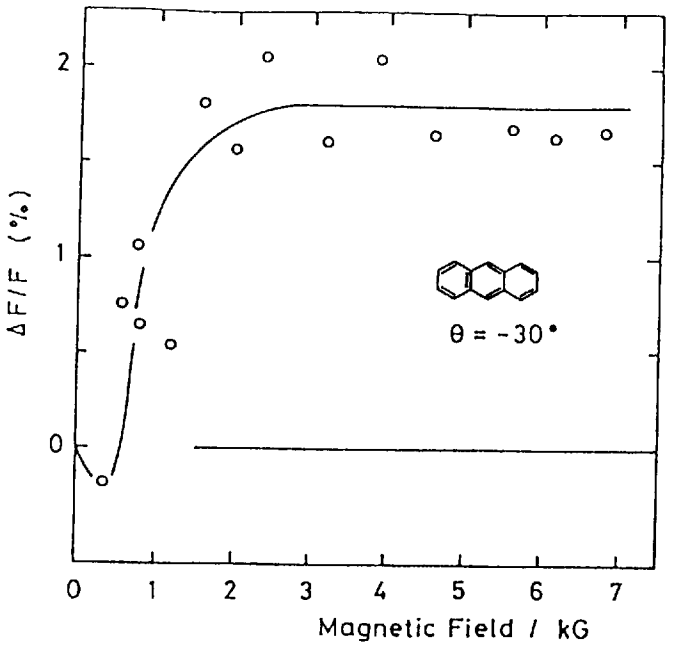

Fig. 7.7 Magnetic field modulation $\Delta F/F$ versus the strength of magnetic field. $\theta = -30°$.

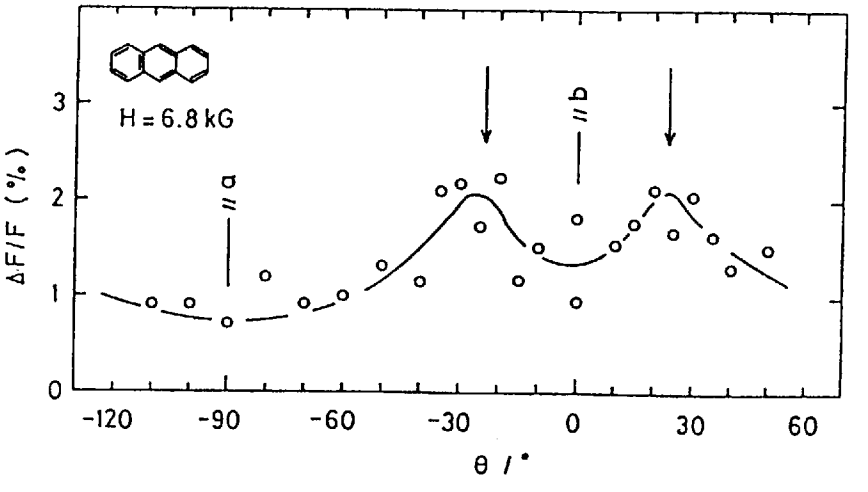

Fig. 7.8 Magnetic field modulation $\Delta F/F$ plotted against the angle θ between the magnetic field vector and the crystal b-axis in the ab-plane. H = 6.8 kG. The arrows ($\theta = \pm 23.5°$) indicate the position of high field resonance for delayed fluorescence.

singlet exciton (3.11 + 3.11 = 6.22eV). The time constant of the fusion may be expressed as $1/\{\gamma_{ss}[S^*]\} = 1/\{\gamma_{ss}\alpha\tau_s I_{ex}\}$. Under the present excitation condition, this characteristic time is 1 ns, using the values $I_{ex} = 10^{21}$ photons cm^{-2} s^{-1}, $\alpha = 5\times 10^3$ cm^{-1} [7.13] and $\gamma_{ss} = 10^{-8}$ cm^3 s^{-1} [7.3] and τ_s=20ns [7.17]. The vibrational relaxation is a very fast process and occurs with time constant of $\sim$ 10ps [7.18-20]. The fusion of two singlet excitons which have some vibrational energy is accordingly not important in the present study.

A small fraction of the fluorescence may originate from recombination of electrons and holes. This fraction must be small, however. The quantum yield of charge carrier generation is quite low, 10^{-4} [7.7]. It has been known that this small quantum yield is determined by geminate recombination of electrons and holes (see § 6). Of the charge carriers generated the majority recombines with the geminate counterpart by the strong Coulomb attraction. Those which have escaped this geminate recombination become charge carriers. The geminate recombination may regenerate only singlet excited states, most probably the lowest singlet state, since it proceeds in a short time, much shorter for the spins of electrons and holes to dephase. Accordingly, this type of recombination is insensitive to a magnetic field. One could argue that cross recombination (recombination of an electron and a hole, which belong to different geminate pairs) can generate triplets as well as singlets, and so can be sensitive to a magnetic field. However, as will be shown below, the cross recombination is unimportant under the present excitaton condition.

When geminate pairs are generated by fusion of two singlet excitons, generation and decay of geminate electron-hole pairs can be expressed by

$$d[G]/dt = (1/2)\Phi_{GP}\,\gamma_{SS}\,[S^*]^2 - [G]/\tau_G, \qquad (7.9)$$

where [G] is the density of the geminate electron-hole pair, τ_G is the characteristic lifetime for the geminate pair. Escape of an electron from the Coulomb potential is neglected, because it is relatively small in this class of materials. The characteristic lifetime τ_G for the geminate electron-hole pair may be given by [7.21]

$$\tau_G = (r_C \times P)^2/D, \qquad (7.10)$$

where r_C is the Onsager length, P is the escape probability and D is the sum of the diffusion constant of an electron and of a hole. Diffusion constant D can be known from the mobility and the escape probability P can be evaluated from the initial separation between an electron and a hole by using the Onsager theory (see § 5). Mobilities (μ_h = 0.73 cm^2/Vs, μ_e = 0.39 cm^2/Vs [7.4]) and the initial separation (r_0 = 9 nm (see § 5.6), which have been known, give a characteristic lifetime τ_G of 2ps. In the stationary state [G] can be given by

$$[G] = (1/2)\Phi_{GP}\,\gamma_{SS}\,[S^*]^2\,\tau_G, \qquad (7.11)$$

which amounts to [G] = $6\times 10^{11}\,cm^{-3}$, using the values of Φ_{GP} = 0.1, α = $5\times 10^3\ cm^{-1}$ [7.13] and I_{ex} = 10^{21} photons $cm^{-2}s^{-1}$. At this density geminate pairs in the crystal are well separated from each other and cross recombination can be safely ruled out.

References

[7.1] E.A.Silinsh and H.Inokuchi,
Chem. Phys. 149 (1991) 373.

[7.2] A.J.Campillo, R.C.Hyer, S.L.Shapiro and C.E.Swenberg,
Chem. Phys. Lett. 48 (1977) 495.

[7.3] A.Braun, U.Mayer, H.Auweter, H.C.Wolf and D.Schmidt,
Z. Naturforsch 37a (1982) 1013.

[7.4] N.Karl,
in: Landort-Burnstein numerical data and fundamental relationships in science and technology, New series, Vol.17, Eds. O.Madelung, M.Schulz and H.Weiss (Springer, Berlin, 1985).

[7.5] L.Sebastian, G.Weiser, G.Peter and H.Baessler
Chem. Phys. 75 (1983) 103.

[7.6] N.Sato, H.Inokuchi, B.M.Schmid and N.Karl,
J. Chem. Phys. 83 (1985) 5413.

[7.7] C.L.Braun,
Phys. Rev. Lett. 21 (1968) 215.

[7.8] F.Hirayama, T.A.Gregory and S.Lipsky,
J. Chem. Phys. 58 (1973) 4696.

[7.9] V.P.Klochkov, E.G.Horsakova and E.B.Verkhovskii,
Opt. Spectrosc. (USSR) 62 (1987) 216.

[7.10] M.R.Topp, H.Lin and K.Chos,
Chem. Phys. 60(1980)47.

[7.11] B.Nickel and H.Karbach,
Chem. Phys. 148(1990)155.

[7.12] W.H.Melhuish,
J. Opt. Soc. Am. 52(1962)1256.

[7.13] L.B.Clark and M.R.Philpott,

J. Chem. Phys. 53(1970)3790.

[7.14] G.Klein, R.Voltz and M.Schott,
Chem. Phys. Lett. 16 (1972) 340.

[7.15] G.Klein,
in : Organic Molecular Aggregates, Eds., P.Reineker,
H.Haken and H.C.Wolf (Springer, Berlin, 1983), p149.

[7.16] R.C.Johnson and R.E.Merrifield,
Phys. Rev. B1 (1970) 896.

[7.17] H.Nishimura, T.Yamaoka, K.Hattori, A.Maysui and M.Mizuno,
J. Phys. Soc. Japan 54 (1985) 4370.

[7.18] R.W.Anderson,
in "picosecond Phenomena II ", Eds., R.M.Hochstrasser,
W.Kaiser and C.V.Shank (Springer, Berlin, 1980), p163.

[7.19] F.Laermer, T.Elsaesser and W.Kaiser,
Chem.Phys.Lett. 156 (1989) 381.

[7.20] Y.Hirata and T.Okada,
Chem.Phys.Lett. 187 (1991) 203.

[7.21] S.Tagawa, M.Washio, H.Kobayashi, Y.Katsumura and Y.Tabata,
Radiat. Phys. Chem. 186 (1983) 278.

8 Summary: Relaxation of higher excited states in aromatic hydrocarbon crystals

When aromatic hydrocarbon crystal is irradiated with light, excited states are populated and they decays through various channels. These decay processes can be studied by spectroscopic method, such as fluorescence emission, photoconductivity and external photoelectron emission. Relaxation processes of the lowest singlet exciton S^* have been studied extensively. They are fluorescence emission, nonradiative decay to the ground state and intersystem crossing into triplet exciton. Higher excited states undergo relaxation which may be different from S^* because energy of higher excited state is larger than that of S^*. Relationship with photoionization process is important when the higher excited state has enough energy for photoconduction and external photoemission. Here relaxation of higher excited state and photoionization process in aromatic hydrocarbon crystals are summarized below based on the experimental results obtained.

Singlet exciton, S^*, is populated by irradiation of light of the energy of 3-4 eV. The S^* decays with a lifetime of $\sim 10^{-8}$ sec. Higher excited states S^{**} can be populated by one-photon absorption with VUV excitation. Generally, a discharge lamp and a synchrotron radiation are used for such an experiment. These light sources are weak and time resolved measurement is difficult to made. Higher excited state is also populated by using multi-photon or multi-step excitaton. The S^* absorbs another photon and the S^{**} is populated. Generation and decay processes of higher excited states generated by photoabsorption of singlet exciton are illustrated in Fig. 8.1. The absorption spectrum of

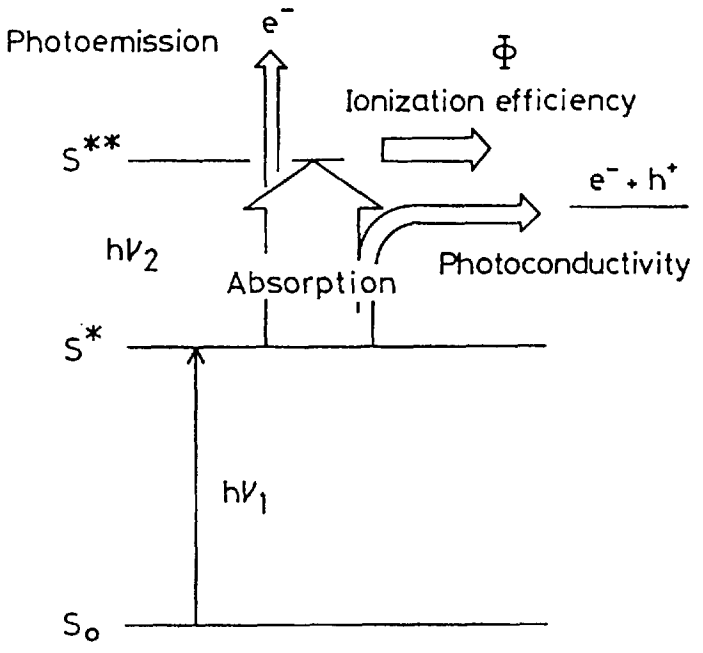

Fig. 8.1 Generation and decay processes of higher excited states generated by photoabsorption of singlet exciton.

S^* can be recorded through transient photoabsorption (§ 4.3). Observed spectra of anthracene, p-terphenyl and trans-stilbene crystals (§ 4.3) resemble to that in solution. This is due to weak intermolecular interaction of this class of material and shows that the S^{**} is a locally excited state of the constituent molecule. The number of S^{**} can be estimated from cross section of the absorption. Cross section of absorption is 1.8×10^{-17} cm^2 at 585 nm in anthracene, 1.8×10^{-17} cm^2 at 570 nm in p-terphenyl and 7.0×10^{-18} cm^2 at 590 nm in trans-stilbene (§ 4.4).

Higher excited states S^{**} generated by photoabsorption decay rapidly into the S^* through nonradiative transition. Only a small fraction of higher excited states contributes to photoconductivity and external photoelectron emission. These processes occur when excitation energy exceeds the threshold energies in each process. Threshold energy for external photoelectron emission can be determined from measurement of kinetic energy of electron emitted and of action spectrum of photoemission. VUV light is generally used for the measurement. Photoelectron emission can be also observed by photoionization of singlet and triplet excitons. Threshold energies for photoelectron emission via singlet exciton are 5.50eV in anthracene, 6.27eV in p-terphenyl and 5.30eV in naphthacene (§ 3.3). These values are not identical to thresholds for photoemission with VUV excitation. This shows that relaxation and stabilization occur in the lowest singlet exciton. Threshold energy for photoconductivity (band gap) can be estimated through study of photoconductivity and absorption spectrum of charge transfer state (§ 1). Band gap is difficlt to determine experimentally because extrinsic photoconductivity, such as

dissociation of S^* at crystal surface, easily affects the measurement. The band gap can be also determined by external photoemission of conduction electrons (charge carriers) (§ 3.5).

Measurement of photoconductivity is easily affected by presence of an impurity. Hence, the measurement should be made with purified material (§ 2). To avoid surface effect and high density excitaton absorption edge excitation and multi-photon excitation are useful (§ 5.1). When excitation is made in the absorption edge, a photocurrent which is proportional to the square of the exciting light intensity is observed. This is due to photoionization of singlet exciton. Possibility of the photocarrier generation by fusion of singlet excitons can be eliminated from kinetic analysis under high density excitation (§ 5.4). Cross sections of photoionization of singlet exciton with absorption edge excitation are 3.5×10^{-19} cm^2 at 420 nm in anthracene, 4.1×10^{-19} cm^2 at 340 nm in p-terphenyl and 3.3×10^{-19} cm^2 at 360 nm in trans-stilbene. Multi-photon excitation can be also available for the study of photoconductivity. In a p-terphenyl crystal photoconductivity due to direct two-photon absorption can be observed (Appendix 2).

The efficiency of photoionization of singlet exciton is a function of excitation energy. Action spectrum for photoconductivity by photoionization of S^* can be measured using two-color, two-step excitation technique (§ 5.5). One laser pulse ($h\nu_1$) generates singlet excitons and photocurrent due to photoionization of S^* can be observed by irradiation with another laser pulse ($h\nu_2$). Cross sections for the photoionization of singlet exciton are 4.0×10^{-21} cm^2 at 580 nm in anthracene, $2.8\times$

10^{-20} cm^2 at 570 nm in p-terphenyl and 4.9×10^{-21} cm^2 at 570 nm in trans-stilbene. Photocarrier yield is a function of electric field E and temperature T (§ 5.6). The efficiency of photoconductivity is a linear function of E with a finitte intercept. The efficiency exhibits thermally activated dependence on temperature. These features indicate that free charge carrier is generated by escape from the mutual Colombic potential. Quantitative interpretation of these dependences can be given by the Onsager model (§ 5.6). By Comparing the Onsager theory the initial separation r_0 between a parent cation and an electron emitted can be estimated. In an anthracene crystal it is 95Å with exciting energy of 6.1eV from the ground state and 85Å when excited at 5.1eV (§ 5.6).

Ionization efficiency Φ is important value for understanding ionization mechanism. In this class of material Φ is very small ($\sim 10^{-3}$). This indicates that the efficiency of photocarrier generation is dominated by geminate recombination. The efficiency can be estimated as a function of exciting energy. In the case of photocarrier geneation with two-color, two-step excitation ionization efficiency of the singlet exciton can be obtained as the ratio of the cross section for photoconductivity and for photoabsorption of singlet exciton (§ 6.2). The efficiency is insensitive to the exciting energy below the threshold energy E_{th} for external photoelectron emission and above E_{th} it increases steeply. The efficiencies is found to be 2.3×10^{-4} at 5.25 eV in anthracene, 1.6×10^{-3} at 5.88 eV in p-terphenyl and 7.0×10^{-4} at 5.70 eV in trans-stilbene (§ 6.2).

Ionization mechanism can be discussed from the results of

the efficiency of photocarrier generation as a function of exciting energy. There are two different modes for charge carrier generation, i.e., indirect process (ET) by electron transfer and direct photoionization (DI). Photoconduction is observed when exciting energy exceeds the band gap E_g. Below E_{th} electron transfer from higher excited state to neighbering molecule is dominant. The higher excited state is populated by light absorption and electron transfer occurs after a fast intramolecular vibration redistribution (IVR). Above E_{th} direct ionization occurs. The threshold energies are different for different modes of ionization. This is caused by different stabilization energy induced by electronic polarization of surrounding molecules. In the case of electron transfer mechanism both positive and negative charges are stabilized. In the case of direct ionization mechanism electron emitted from molecule moves very fast, so that electronic polarization of surrounding molecules cannot respond. Hence, only a cation is stabilized and threshold energy is higher than that for electron transfer mechanism (§ 6.3.2). Such a ionization mechanism is different from that in other condensed phase. This difference can be quantitatively understood by polarization energy and electron affinity of surrounding molecules (§ 6.4).

In aromatic hydrocarbon crystals singlet excitons can interact with each other (fusion or annihilation). When fusion of two singlet excitons occurs, ground state and higher excited state which has twice energy of S^* are generated. The rate constant of fusion has been determined through measurements of fluorescence as a function of exciting light intensity. In a p-terphenyl crystal the rate constant for the fusion is 7×10^{-9}

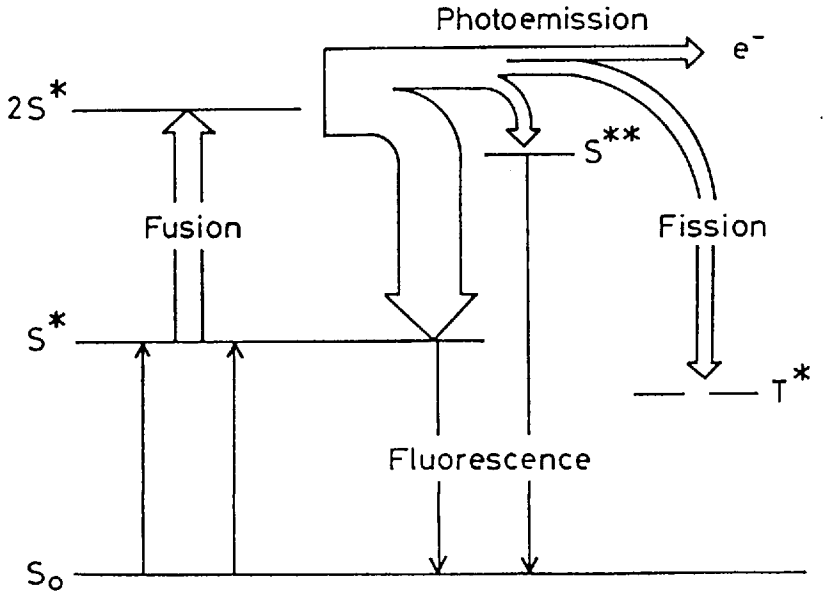

Fig. 8.2 Generation and decay processes of higher excited states generated by fusion of two singlet excitons.

$cm^3\ s^{-1}$ (Appendix 1).

When the energy obtained by fusion exceeds the threshold energy for external photoelectron emission, the emission of electron can occur. In this case action spectrum of the emission of electron is proportional to the square of the absorption coefficient (§ 3.4). When excitation is made with short light pulse, electron emission persisting after the light pulse can be observed (§ 3.4).

Most of higher excited states populated by the fusion are converted to heat and fluorescence from S^*. However, there are relaxation channels which are not present for the lowest excited state. Figure 8.2 illustrates the relaxation channels from higher excited states populated the fusion of two singlet excitons. The energy obtained by the fusion is larger than twice the energy of the triplet exciton. Hence, fission into two triplet excitons from the higher excited state is energetically possible. This process can be studied by measurement of magnetic field modulation of fluorescence (§ 7.3). Nonradiative decay from the higher excited state is a fast process, so that fluorescence emission from the higher excited states is inefficient. Fluorescence from S_2 and S_3 populated by the fusion in an anthracene crystal can be observed, which has quite low efficiency of the fluorescence ($\sim 10^{-6}$, § 7.2).

As discussed above, higher excited states in aromatic hydrocarbon crystals play an important role in photocarrier generation and have relaxation channels which are not possible with the lowest excited state.

Appendix 1 Absorption coefficient and rate constant of fusion of singlet excitons in a p-terphenyl crystal

Figure A-1 shows polarized absorption spectra in a p-terphenyl crystal near the energy range of absorption edge. A deuterium discharge lamp was used as a light source. The absorption spectra were recorded with a spectrophotometer (Hitachi, EPA-2A). Thickness of the sample flake was 10 μ m.

Decay kinetics of singlet excitons can be written by Eq. (3.1). Apparent quantum yield of fluorescence as a function of excitation light intensity was discussed in § 3.4, 5.4 and 7. Rate constant of the fusion of two singlet excitons γ_{ss} can be evaluated by the measurement of fluorescence intensity as a function of exciting light intensity. In the stationary state the fluorescence quantum yield is changed at the intensity I_c. It can be expressed as

$$I_c = 1/(\alpha \ \tau_s^2 \ \gamma_{ss}), \qquad \text{(A-1)}$$

where α is the absorption coefficient and τ_s is the lifetime of the singlet exciton. Figure A-2 shows fluorescence intensity as a function of the exciting light intensity (λ_{ex} = 338 nm). Polarization of the exciting light is parallel to the crystal b-axis. Experimental observation verifies above prediction. From these results the rate constant of singlet exciton fusion is found to be $\gamma_{ss} = 7\times 10^{-9}$ $cm^3 s^{-1}$ using the values of α = 150 cm^{-1} and τ_s = 2.1 ns [A-1].

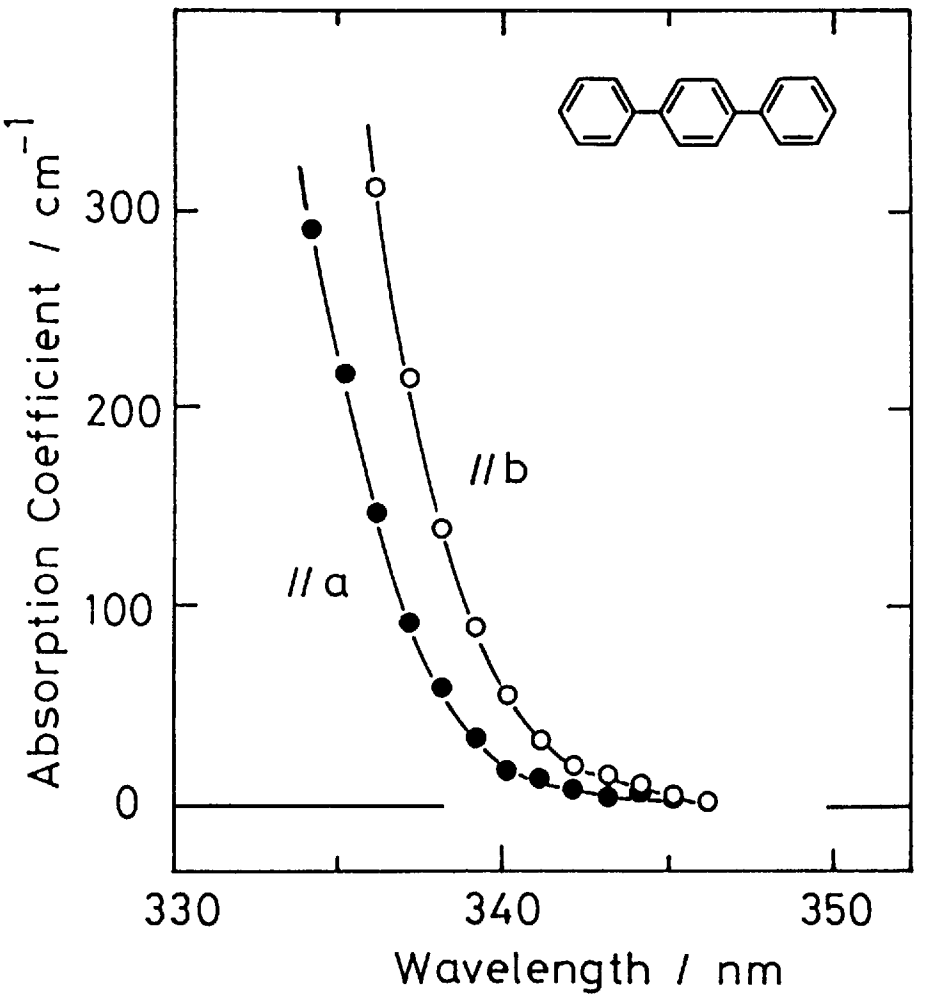

Fig. A-1 Polarized absorption spectra in a p-terphenyl crystal.

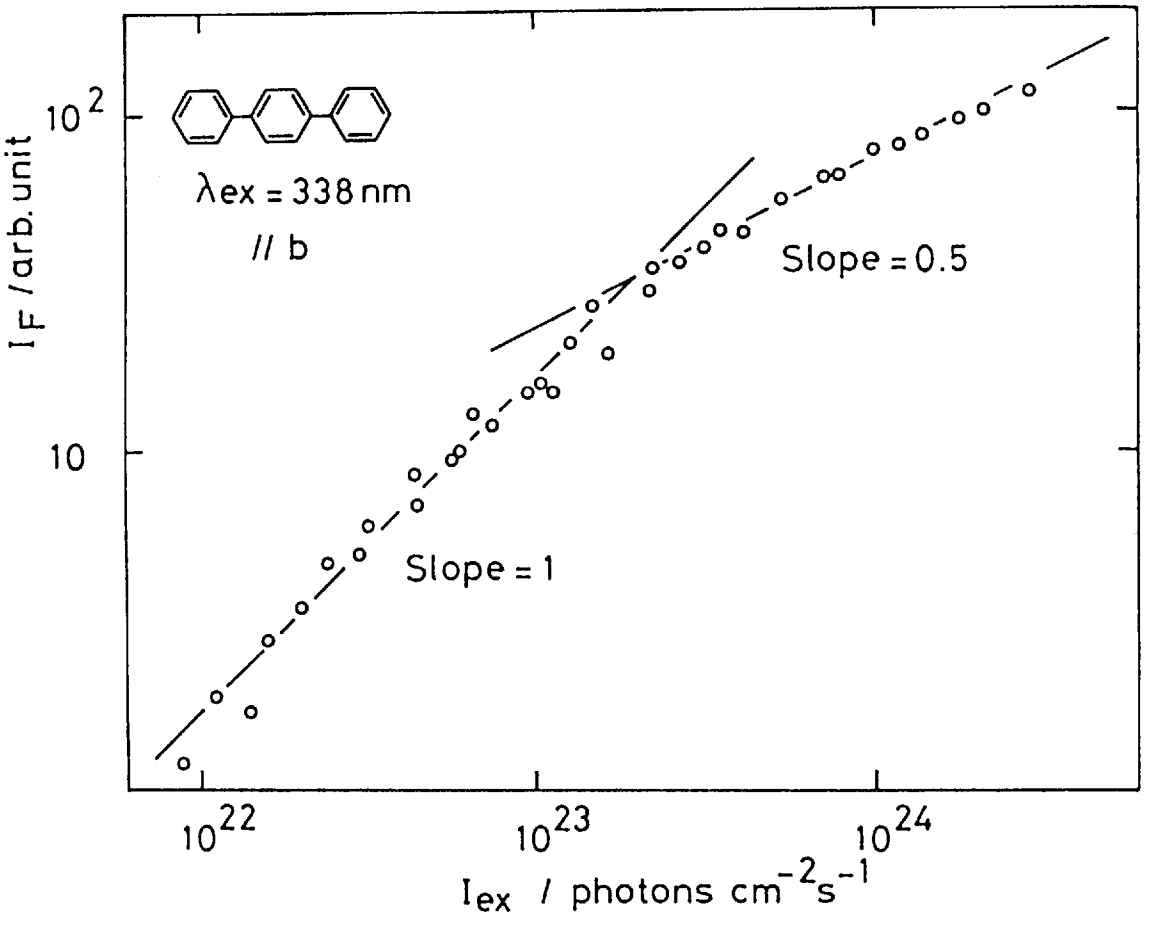

Fig. A-2 Fluorescence intensity (I_F) plotted against the exciting light intensity (I_{ex}) in a p-terphenyl crystal.

Appendix 2 Photoconductivity by one-color, two-photon excitation in a p-terphenyl crystal

As mentioned in § 5 photoconductivity is sensitive to the surface condition of sample specimens. In § 5.5 two-color, two-step excitation method was used to avoid such effects. One-color, multi-photon excitation method may be also effective.

Photoconductivity was measured with the same apparatus presented in § 5. Fluorescence was measured with a photomultiplier (Hamamatsu, R268) through a small double monochromator (Jobin-Yvon, H10D) and a band-pass filter (Hoya, U330).

[Carrier generation by one-color, two-photon excitation]

Figure A-3 shows the number of photogenerated carriers N as a function of exciting light intensity I_{ex} for λ = 420, 460, 480, 500 and 540 nm. It may be seen that N is proportional to I_{ex}^2 with λ = 420 and 460nm excitations and is proportional to I_{ex}^3 with λ = 500 and 540nm excitations. When excitation is made at λ = 480 nm both quadratic and cubed dependences are coexistent. Care was taken to keep the concentration of the carriers low so that the volume recombination of electrons and holes is unimportant. Volume recombination, when occurs, can be recognized by a deviation from a straight line as seen in Fig. A-3 at high I_{ex}.

Figure A-4 shows the intensity of the fluorescence F as a function of exciting light intensity I_{ex} for λ = 420, 480 and

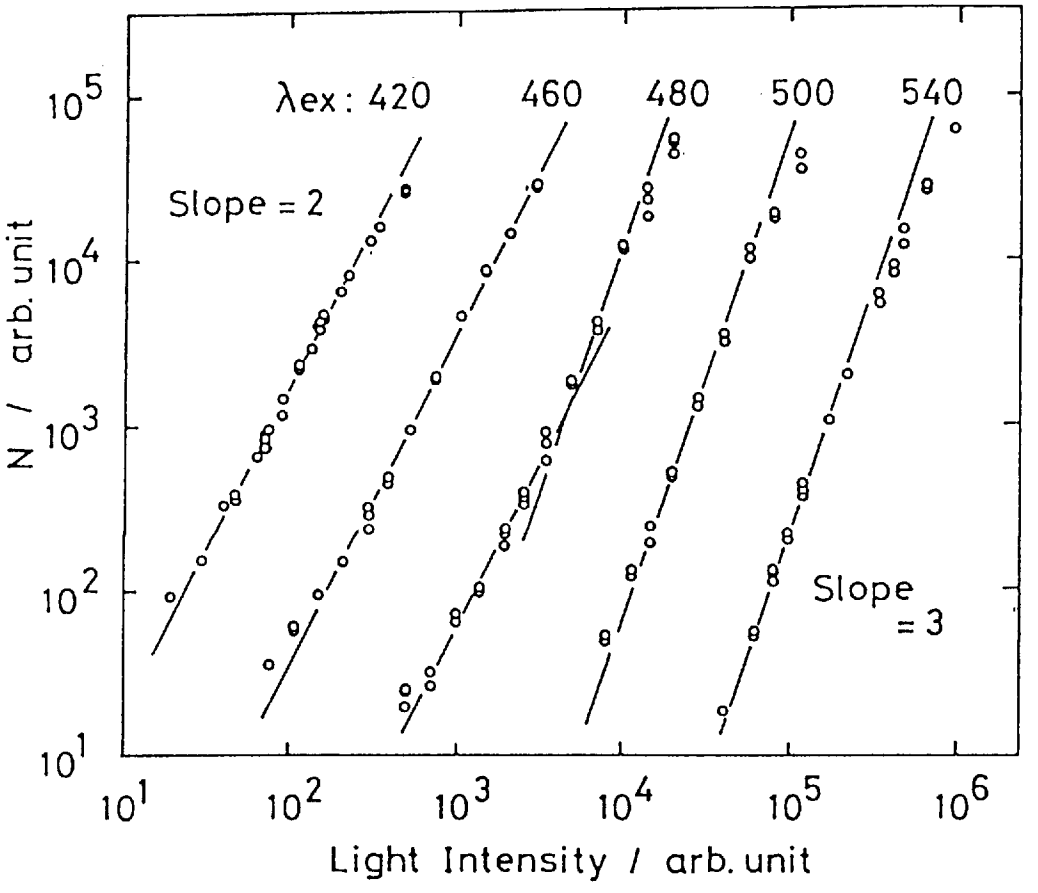

Fig. A-3 Observed photocurrent (N) versus exciting light intensity (I_{ex}). Wavelength of the exciting light are indicated (all in nm).

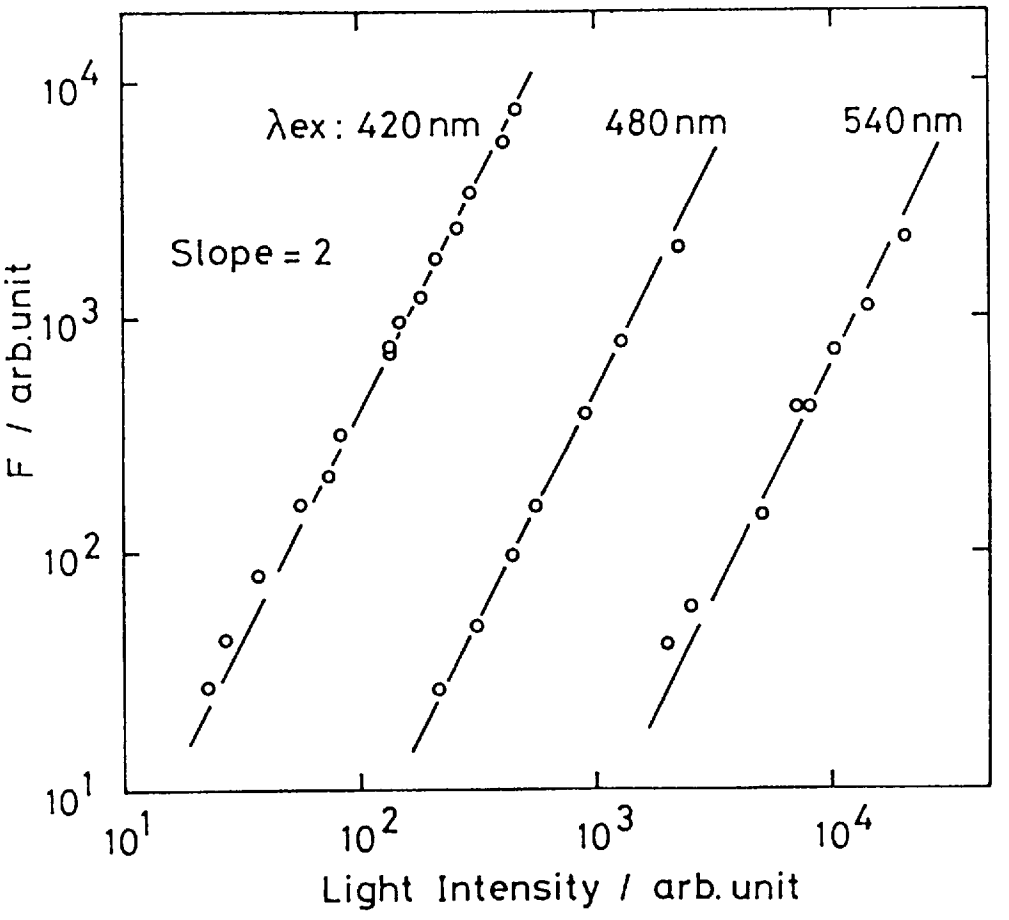

Fig. A-4 Fluorescence intensity (I_F) versus exciting light intensity (I_{ex}). Wavelength of exciting light are indicated.

540nm. It may be seen that F is proportional to I_{ex}^2. This indicates that singlet excitons can be populated only through two-photon absorption at these photon energies.

Figure A-5 shows the number of carriers generated by two-photon absorption N_{2P} and the intensity of the two-photon excited fluorescence F as a function of wavelength. Polarization dependence is small in both spectra. The relative (internal) ionization efficiency by two-photon excitation Φ_{2P} is defined as

$$\Phi_{2P} = N_{2P}/F. \qquad \text{(A-2)}$$

In Fig. A-5 Φ_{2P} is plotted as a function of exciting photon energy. The top scale is the two-photon energy. It may be seen that the ionization efficiency is constant between 5.3 eV and 6.4 eV. This indicates that the excess energy over the ionization threshold (energy gap) is not converted to the kinetic energy of the generated electrons and strongly suggests that the higher excited states relax rapidly to a lower-lying state which autoionizes:

$$S_0 \xrightarrow[2h\nu]{} S^{**}(v) \xrightarrow{R} S^{**} \xrightarrow{AI} e^- + h^+$$

where $S^{**}(v)$ is a higher excited state with vibrational excitation, R means relaxation and AI means autoionization. This is the behaviour which has been observed in exciton photoionization (two-color, two-step excitation). The absorption spectrum of a singlet exciton has a peak at 2.2 eV, which corresponds to the final state energy of 5.9 eV, whereas the two-photon absorption has a peak at 6.3 eV. Polarization is also different. These differences indicate that the nature of the final state of the two-photon excitation is not identical to that of the two-photon excitation. In spite of the difference of

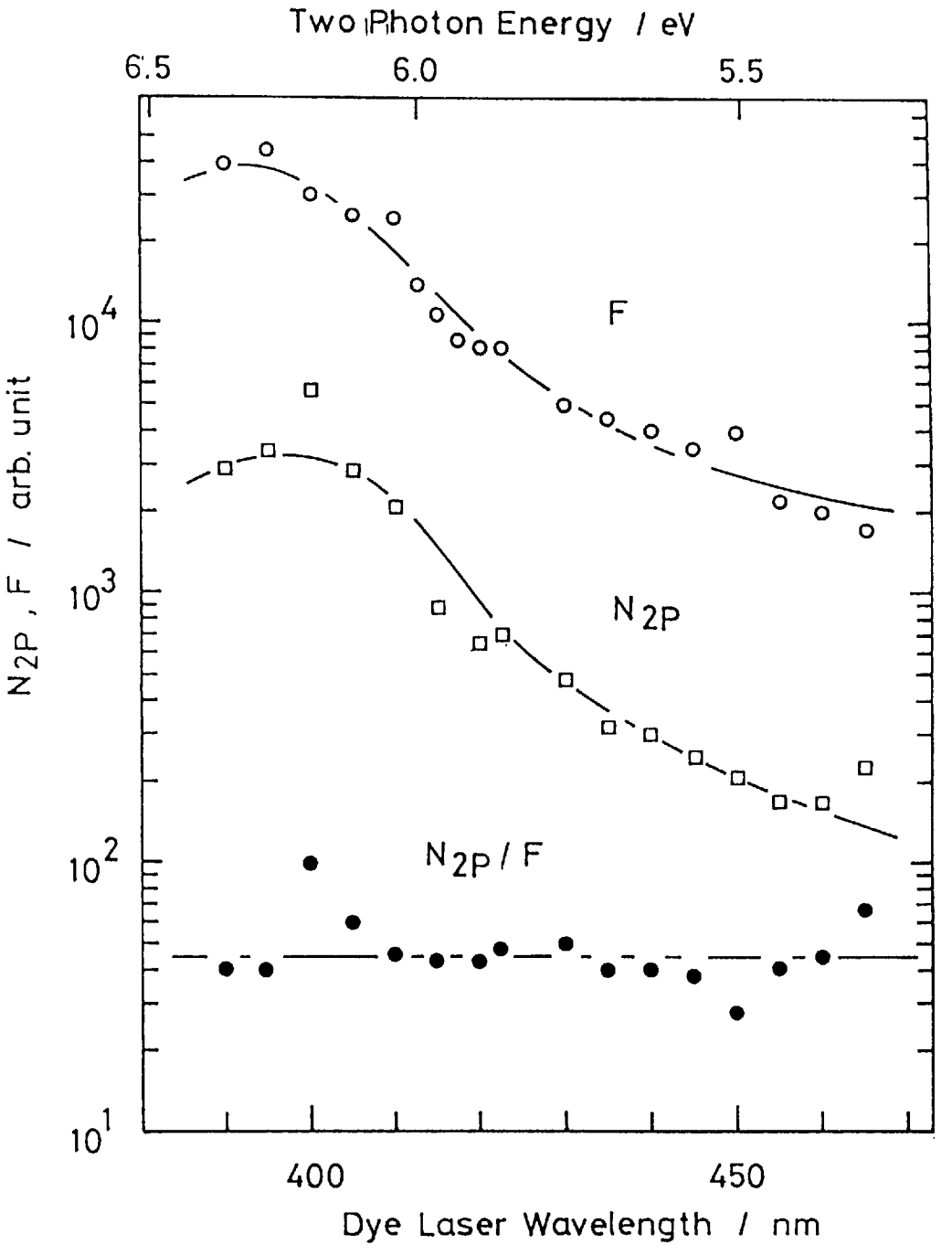

Fig. A-5 Excitation spectrum of two-photon fluorescence (F) and of two-photon excited photocurrent (N_{2P}). Relative ionization efficiency ($\Phi_{2P} = N_{2P}/F$) is also shown.

final states in the nature of the higher excited states generated by different excitation modes the behaviour leading to charge carrier generation is very similar: a fast relaxation and autoionization discussed in § 6 in detail.

The results with two different excitation modes are not completely identical, however, in p-terphenyl. In the case of two-step excitation the efficiency of the carrier yield begins to increase at 6.2 eV (see § 6). This has been ascribed to the opening of a new ionization channel, the direct photoionization of an exciton (see § 6). With two-photon excitation no corresponding increase has been observed up to 6.4 eV (Fig. A-5). The origin of this difference is unclear.

The number of carriers produced by a laser pulse was observed to increase with rising temperature (Fig. A-6). The activation energy depends on the excitation wavelength: 0.13 eV (λ_{ex}= 450 nm), 0.12 eV (430 nm), 0.105 eV (410 nm) and 0.105eV (390 nm). This could reflect the initial separation r_0 which varies with the photon energy. According to the Onsager theory the activation energy and the carrier yield are closely connected, both being determined by the initial separation r_0 between an electron and a hole. A large initial separation would lead to a small activation energy and a large carrier yield. Accordingly, the variation of the activation energy with excitation wavelength may seem to indicate the change in r_0. However, since no appreciable change has been observed in the carrier yield Φ_{2P} as the photon energy is changed, it is difficult to assume that the energy in excess of the energy gap is converted to the kinetic energy of an electron, or of a hole.

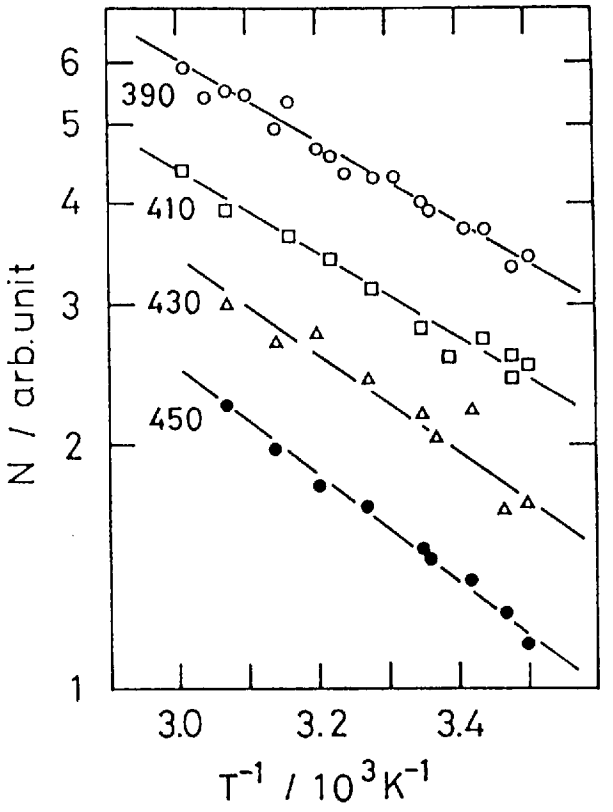

Fig. A-6 Observed photocurrent (N) versus reciprocal temperature. Wavelength of the exciting light are indicated (all in nm).

It seems probable that the temperature dependence observed with the number of carriers is caused by the change in the number of absorbed photons: reflection as well as two-photon absorption may change with temperature.

[One-color, three-photon excitation: phtoionization of singlet exciton generated by two-photon absorption]

Below the photon energy of 2.6 eV (λ = 480 nm) charge carriers are generated by a three photon process (Fig. A-3). There are two possible mechanisms for three-photon carrier generation;

(a) Direct three-photon ionization

$$S_0 \xrightarrow{3h\nu} e^- + h^+ .$$

(b) Photoionization of singlet exciton, generated by two-photon absorption

$$S_0 \xrightarrow{2h\nu} S^* \xrightarrow{h\nu} e^- + h^+ .$$

Figure A-7 shows the action spectrum of the three-photon photoconductivity N_{3P} and the excitation spectrum of the two-photon excited fluorescence F with excitation light polarized parallel to the crystal b-axis. With the polarization parallel to the a-axis the observed photocurrent is much smaller. The photoconductivity action spectrum has a shoulder at 560 nm, which coincids with the peak in the photoionization of the singlet exciton presented in § 5. Figure A-7 also shows the product of the two-photon absorption spectrum F and the singlet exciton

photoionization spectrum N_{2s}. The close similarity between the N_{3p} spectrum and the $F \times N_{2s}$ spectrum indicates that the three-photon photoconductivity is due to the photoionization of singlet exciton generated by two-photon absorption (2+1 mechanism). Polarization of the action spectrum for the photocurrent is consistent with this interpretation.

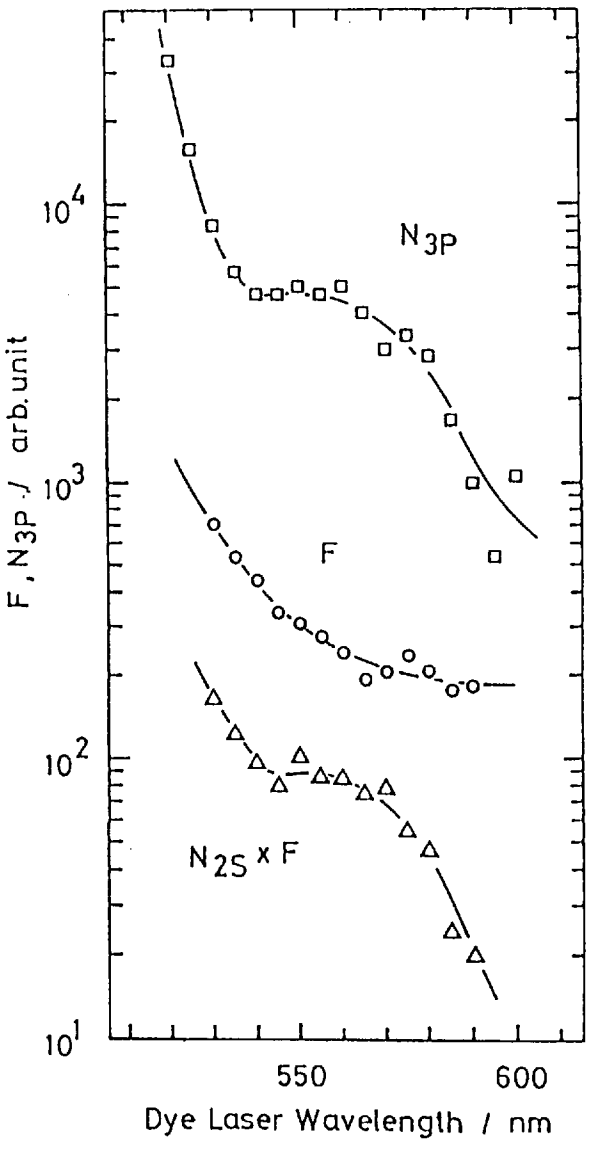

Fig. A-7 Action spectrum of photocurrent with three-photon excitation (N_{3P}) and excitation spectrum of two-photon fluorescence (F). For compaison the $N_{2S} \times F$ spectrum is also shown. The rather good coincidence indicates that the three-photon carrier generation (N_{3P}) is due to the photoionization of excitons generated by two-photon absorption.

References

[A.1] A.C.Jones, K.J.Styrcz, D.A.Elliott and J.O.Williams, Chem. Phys. Lett. 80 (1981) 413.

印　刷　　ナカバヤシ株式会社
〒174 東京都板橋区東坂下２－５－１
電　話（03）3558－1251
ＦＡＸ（03）3558－1260